THESIS FOR THE DEGREE OF DOCTOR OF PHILOSOPHY

A Theoretical Investigation in Heterogeneous Gold Catalysis

NOKO SIMON PHALA

B.Sc. (Chemical Engineering) – University of Cape Town

M.Sc. (Chemical Engineering) – University of Cape Town

April 2004

Catalysis Research Unit
Department of Chemical Engineering
University of Cape Town
Private Bag
Rondebosch, 7701
South Africa

Synopsis

Despite the nobleness of bulk gold metal in air, small supported gold particles have been shown experimentally to be active in a wide range of chemical reactions. The objective of this work was to study, theoretically, some of the fundamental aspects of the reactivity of gold catalysts. Using activation of CO, CO_2 and H_2 as a test case, periodic and cluster density functional theory (DFT) calculations, within the generalized-gradient approximation (GGA), were performed to investigate the change in nobility of gold from the extended surface to small clusters. Potential methanol synthesis intermediates were optimized on the Au(111) surface. It was found that the molecules that are stable as gas-phase species generally adsorbed weakly on the surface. Surface hydrogenation of CO-derived species appeared to be easier than surface hydrogenation of CO_2- derived species. On an Au_{13} cluster, the energetics of CO_2 adsorption and hydrogenation remain unfavourable.

The cluster-size dependency of hydrogen and carbon monoxide adsorption was investigated. It was found that small gold clusters (1 to 13 atoms in size) can bind both H and CO strongly. Due to the changes in the orbital spatial symmetries and the energies of the highest occupied molecular orbital (HOMO) and lowest unoccupied molecular orbital (LUMO) with cluster size in this small size range, the adsorption energies depend very strongly on the number of gold atoms present, i.e. each atom makes a difference. For H adsorption, there is a very marked oscillation in adsorption energies, with the clusters with an odd number of gold atoms (with lower LUMO energies) being generally more reactive than the even clusters, up to about 10 atoms when the HOMO-LUMO gap ceases to fluctuate strongly.

The role of the support material in activating gold atoms was studied. A hybrid quantum mechanics/molecular mechanics (QM/MM) electronic embedding technique was employed to model the ZnO(0001) surface of zincite. The QM region of the surface, treated by density functional theory, consisted of a total of 13 zinc and oxygen atoms for the zinc-vacant site, and 14 atoms for the bulk-terminated island site. It was found that

Au^0 and Au^+ could be stabilized at the zinc vacant site of this surface. The higher oxidation states are unstable with respect to auto-reduction by the ZnO surface (i.e. their LUMO energies were below the HOMO of a bare ZnO surface. However, gold hydroxyls, where gold has +1 to +3 oxidation states, can be stabilized at the vacancy. As zinc-substitutional impurities on the bulk-terminated island site, Au^+, Au^{2+} and Au^{3+} oxidation states can be stabilized. CO was used as a test molecule to probe the chemical reactivity of the gold atoms in different adsorption sites and oxidation states. It was found that supported Au^+ was more reactive than Au^0, Au^{2+}, or Au^{3+}. Furthermore, CO binds more strongly to supported Au^0 than the free Au^0 atom. This implies that the support does not simply disperse gold particles, but it also modifies their electronic properties. It was also found that the nucleation of gold atoms to clusters can be affected by the support. Supported charges Au clusters have shorter Au-Au distances than their gas-phase counterparts.

Acknowledgements

It gives me great pleasure to thank the people who have made this achievement possible. This list can never be complete. So, I would like to start by saying 'I thank all of you that I have known and got along fine with in my life so far'.

I wish to thank my parents, Mamorei and Mosebjadi, for bringing me into this wonderful universe. They have raised me to be who I am today, and for that I will always love them.

I would like to thank my brothers, Nape, Mphela and Nekwana; and my sisters, Rati and Nogana, for backing me up all the way. It is time for their own dreams to come true. To my uncles, grandparents, aunts, cousins, and friends, thanks for your support and encouragement.

The content of this work would not have existed if I was not introduced to the beauty of molecular modelling and catalysis by Prof. Eric van Steen (my supervisor), Prof. Jack Fletcher, and Dr Günter Klatt. Your inspirations, technical inputs, and constant interest during my studies helped me get this far. I would also like to thank the Catalysis Research Unit dwellers for creating a stimulating learning environment, and for their helpful work-hard, play-hard ethic, which I took great advantage off!

The second half of my thesis was made possible by a fruitful collaboration with the Royal Institution of Great Britain. I would like to thank Prof. Richard Catlow for inviting me to this prestigious institution for some quality learning. Drs Alexey Sokol and Sam French took me under their wing and improved my knowledge in the field of theoretical chemistry. For that, I thank them very much.

Finally, someone had to pay the bills. I greatly acknowledge the sponsorship from AngloGold, the University of Cape Town, The National Research Foundation, THRIP, The Catalysis Society of South Africa, and The Royal Institution of Great Britain.

List of Figures

List of Tables

Table of Contents

Chapter 1

INTRODUCTION AND SCOPE OF WORK

1.1. Background on Catalysis by Gold

Bulk gold is known to be chemically inert. It does not readily adsorb hydrogen and oxygen. However, it was pointed out in the 1970s that gold surfaces can catalyse the isotopic exchange reaction between hydrogen and deuterium at 200°C [Bond, 1972]. Furthermore, redistribution of an isotopic carbon tracer between CO and CO_2 was found to occur on Au/MgO and Au/Al_2O_3 catalysts at 200-400°C [Cha and Parravano, 1970]:

$$^{14}CO_2(g) + CO(g) = CO_2(g) + {}^{14}CO(g) \qquad (1.1)$$

The importance of gold particle size and metal-support interaction was emphasized in this work. Parravano [1970] also showed that the same gold catalysts could initiate the redistribution of an isotopic carbon tracer between benzene and cyclohexane in the same temperature range:

$$^{14}C_6H_6(g) + C_6H_{12}(g) = C_6H_6(g) + {}^{14}C_6H_{12}(g) \qquad (1.2)$$

Although this early work, and others, was ignored during the next decade, it clearly showed that when properly activated, gold can act as an oxygen or hydrogen transfer catalyst. It was the later work by Haruta et al. [1987] that sparked a renewed interest in the application of gold as a heterogeneous catalyst. It was shown that small gold particles on Fe_2O_3, Co_3O_4 and NiO, prepared by coprecipitation of a gold salt and a support-metal salt, were active for carbon monoxide oxidation at temperatures as low as –70°C. Subsequent work showed that small particles are highly active for both hydrogenation and oxidation reactions of industrial and environmental interest [Bond and Thompson, 1999; Haruta, 1997].

While debates are still ongoing regarding the origin of activity in small gold particles, it is clear that the choice of the support as well as control of the gold crystallite size is crucial for high catalytic activity.

1.2. Economic Drive for Gold Catalysis

The largest applications for gold are as an investment item and in jewellery. India is the largest consumer for the latter application. While platinum-group metals like platinum and palladium enjoy diversified applications, e.g. as autocatalysts and as catalysts in chemical industries, gold remain largely used for its nobility. This makes the gold price depend on a restricted group of consumers as well as geopolitical factors. South Africa is the world's largest gold producer, and will hence benefit from stabilised gold prices that may result from diversified applications for gold. Project AuTek, launched in South Africa in June 2000, is one such initiative. The objective is to exploit gold's properties with the hope of finding commercially viable uses for environmental and industrial applications. In the spirit of this initiative, the current work aims at exploring, theoretically, the potential for gold to act as a heterogeneous catalyst, in the light of recent findings.

1.3. Scope of Work

Catalysis by gold is a recent phenomenon, and most fundamental questions remain unanswered. A large volume of experimental work leaves no doubt that supported gold is indeed catalytically active, and it is reasonable to expect that industrial applications will be found as research continues. However, fundamental knowledge is lacking compared to that available for other noble metal catalysts. The objective of the current work is to study the fundamentals governing the reactivity of supported gold particles. This involves a critical review of the literature, with emphasis on work from which fundamental knowledge can be derived. Computational techniques, specifically quantum chemical methods, will prove to be useful in obtaining a fundamental insight in gold catalysis. The main work of this thesis is, hence, of theoretical nature. The electronic properties of gold surfaces and clusters (clean, modified or supported) were studied and evaluated in terms of known theories on metal-adsorbate bonding. Reaction-specific aspects were investigated by studying a

test reaction, methanol synthesis. It is hoped that this work will improve on fundamental knowledge in the gold catalysis literature, and will form a basis for design and synthesis of gold catalysts of more definitive character.

Chapter 2

CATALYTIC ACTIVITY OF GOLD: LITERATURE SURVEY

The high catalytic activity of gold is often attributed to the presence of small gold particles on the surface of a support. The mechanisms by which these nano-sized particles lose their nobility, with respect to bulk gold, are subject of many experimental and theoretical investigations. Elucidation of possible mechanisms from experiments is not trivial because the intrinsic size effects, the role of the support, and the mode of catalyst preparation all seem to play a very important role. Furthermore, the mechanism of the operation of these catalysts is clearly reaction dependent, illustrating that generalisations cannot be made on the basis of a single reaction.

2.1. Intrinsic Properties of Small Gold Particles

Creation of a surface implies that the surface atoms will have reduced number of nearest neighbours (coordination) relative to atoms in the bulk. The fraction of surface atoms increases sharply as the diameter of a particle decreases below about 5nm [van Heerdeveld and Hartog, 1969]. The fact that more and more coordinatively unsaturated metal atoms appear as the size decreases imply that a small particle is relatively unstable with respect to a transformation that will make the atoms increase their coordination. This intrinsic property of small particles yields the so-called size effects in the catalysis by metals. This is often referred to as a geometric effect even though the electronic structure is clearly the causal link between structure and reactivity.

Ercolessi et al. [1991] studied the melting point of small gold particles via molecular-dynamics simulations. The melting temperatures of 1077 °C, 707 °C, 547 °C and 227 °C were calculated for Au_{bulk}, Au_{879}, Au_{477} and Au_{219} clusters respectively, suggesting that small gold particles have much lower melting temperatures than bulk gold. These findings were in line with earlier experimental findings by Buffat and Borel [1976], where the melting point of 2 nm particles was found to approach room temperature. This phenomenon implies that strong contact with the support is necessary for thermal stability of these nanoparticles in practical applications to prevent them from agglomerating to larger particles. The internal energy of gold increases with decreasing cluster size, as has also been found theoretically and experimentally for Mo and W nanocrystals [Jiang et al., 2002].

Catlow et al. [1997] quotes Häberlen et.al 's an ab initio study of Au_{55} clusters where the icosahedral (exposing {111} faces) and the cuboctahedral (exposing both the {111} and the {100} faces) shapes had binding energies of 3.59 eV and 3.55 eV respectively. If the activation energy of transition between these two structures is low, then interchange between the two structures may occur. This is a significant point in the discussion of the reactivity of small gold clusters, as the electronic properties of the surface atoms may be different in the two morphologies.

Grönbeck and Andreoni [2000] studied the electronic structure of Au_2 to Au_5 clusters by density functional theory (DFT) employing the BLYP functional. Au_2 and Au_4 clusters had HOMO-LUMO gaps (the difference in energies between the highest occupied molecular orbital (HOMO) and the lowest unoccupied molecular orbital (LUMO)) of 1.8 and 0.9 eV respectively, while the gaps for Au_3 and Au_5 clusters were lower at 0.2 and 0.3 eV respectively. This points to a fluctuation in the HOMO and LUMO energies within this size range. The fluctuation of the frontier orbital energies, especially the HOMO, has also been obtained for Pd clusters up to Pd_{13} [Efremenko and Sheintuch, 1998; Roques et al., 2001]. For neutral Au_2 to Au_{10} clusters, the HOMO-LUMO gap is largest for Au_2, Au_6 and Au_8 clusters [Häkkinen and Landman, 2000]. Gold clusters below about 7 atoms generally prefer planar structures [Häkkinen and Landman, 2000; Grönbeck and Andreoni, 2000; Wang et al., 2002; Wu et al., 2002]

For sufficiently large clusters (up to Au_{147}), the binding energy per atom, ionization potential and the electron affinity fall onto smooth curves and appear to approach bulk values, although the HOMO-LUMO gap for Au_{147} clusters is about 0.3 eV [Häberlen et al., 1997]. Density of states (DOS) calculations showed that for the Au_2 cluster, the d_z^2 orbitals were mixed into the HOMO, making this level only 20% s-character [Grönbeck and Andreoni, 2000]. In contrast, the HOMO of the Au_5 cluster was already 50% s-character. The HOMO of Pt_2 to Pt_5 clusters was mostly of d-character. It is noticeable that the electronic structure of the Au_2 cluster begins to resemble that of its catalytically useful neighbour, Pt. The lowest energy structures of the small gold clusters were planar, in agreement with second order Møller-Plesset (MP2) calculations for Au_2 to Au_6 clusters [Bravo-Pérez et al., 1999]. Very strong s-d hybridisation has been reported for Au_{147} clusters (~31% d at the HOMO) [Härbelen et al., 1997]. From a chemical point of view, a very important reactivity measure may be position of the centre of the d-band relative to the Fermi level [Ruban et al., 1997], since this is where maximum coupling of adsorbate states with d-states will occur. The further the position of the d-band centre from the Fermi level, the higher the Pauli repulsion between a molecule and a surface, because the resulting antibonding orbital from the interaction between filled orbitals will not rise above the Fermi level. This model has been used to explain bulk gold's intrinsic nobility [Ruban et al., 1997; Hammer and Nørskov, 1995].

Small gold crystallites have different properties to those of bulk gold. Small metal crystallites are typically found in catalysts. This enhances the dispersion and thus the exposure of surface atoms, which may enhance the performance of these catalysts.

2.2. Standard Preparation of Gold Catalysts

The catalytic activity of gold depends, in addition to the size of gold particles and the nature of the support, on the mode of preparation of the catalysts [Bond and Thompson, 1999]. Starting from $HAuCl_4$ as a precursor, the pH of the solution affects the relative proportions of $AuCl_4^-$, $Au(OH)Cl_3^-$, $Au(OH)_2Cl_2^-$, $Au(OH)_3Cl^-$, $Au(OH)_4^-$ and $Au(OH)_3$ species and hence the mode of interaction of gold with the support material [Chang et al., 1998]. $Au(OH)_3$ is insoluble and hence precipitates onto a suspended support material (deposition-precipitation method), producing small crystallites dispersed onto the support after drying (and calcination). Alternatively, the support can be made in situ from a salt (usually a nitrate) of the oxide metal. Upon raising of the solution pH, the co-precipitation of the carbonate of the oxide-metal and $Au(OH)_3$ occurs, forming the final catalyst after calcination. Clearly the coprecipitation route will result in incorporation of some Au particles into the support, making them, in some cases, inaccessible to catalysis. It is argued that calcination prevents this from happening [Bond and Thompson, 2000]. Small particles may, however, still remain as impurities in the bulk of the oxide support.

2.3. Structural and Electronic Properties of Gold on Support Materials

It is useful to examine the interactions between Au atoms/clusters and oxide surfaces in order to build up the understanding of the role of supports in gold catalysts. Unfortunately, studies of this nature are very few, which is probably why the support role is still not well understood.

The deposition process of Au particles onto MgO (100) surfaces was studied by Kubo et al. [1997] by molecular dynamics (MD). Depositing 20 Au atoms onto the surface, one atom at a time at 180 m/s, resulted in the formation of a hemispherical Au cluster at 27°C. At higher temperatures or higher deposition rates, some Au atoms were repelled from the surface. In the presence of point defects on the MgO (100) surface,

the first atom got trapped in the defect, after which other atoms came in contact with the trapped atom and eventually formed a hemispherical cluster around the defect. Transmission electron microscopy (TEM) studies on Au/Al_2O_3 revealed a similar usefulness of defects in the nucleation of gold atoms [Carrey et al., 2002]. Increasing the temperature of the supported cluster on the defect MgO (100) surface resulted in aggregation to a spherical particle. The presence of steps stabilised the Au clusters on MgO (100). Unfortunately, the more important electronic effects could not be obtained from MD simulations. Density functional theory calculations, within the generalized gradient approximation (GGA-DFT), have shown that Cu_1 to Cu_{13} clusters on MgO (100) prefer the on-top oxygen site [Musolino et al., 1998]. The Cu-O interactions decreased, and consequently the Cu-Cu interactions increased, with increasing cluster size. XPS studies have shown that a strong interaction between Cu and O atoms leads to Cu^+ species formation at the interface, with comparable binding energies to Cu in Cu_2O [Jonnard et al., 1998]. It is a reasonable assumption that gold atoms may behave similarly on this surface. Contrary to this, calculations show that the high CO oxidation activity of Au nanoclusters deposited on MgO may be attributed to the fact that the MgO support transfers electron density to the Au clusters [Heiz and Schneider, 2000], making the gold cluster anionic.

The adsorption of Cu, Ag and Au atoms onto TiO_2 (110) surface were studied by DFT by both the cluster and the periodic slab approaches [Giordano et al., 2001]. Cu adsorbs preferentially on the oxygen atoms in the TiO_2 (110) surface. An electron density shift from Cu to oxygen is predicted. DOS curves indicated that the Cu 4s states lies above the Fermi level, indicating the depopulation of the 4s electron shell. The situation with Ag was found to be similar to that with Cu, except that the former had longer oxygen to metal distances (~ 3 Å). For Au, however, the extent of charge transfer between Au and O was not as large as with Cu and Ag, although the Au atoms also preferred the O sites over the Ti sites on the titania surface. Lopez and Nørskov [2002a] studied coverage effects on the electronic structure of Au adsorbed onto TiO_2 (110) via DFT employing the slab model. The O and Ti sites were favoured for low and medium coverages (0.17 and 0.33 monolayers (ML)) respectively, while for higher coverages (1.00 to 2.00 ML) several sites were occupied. The position of the d-band centre relative to the Fermi level was lower for Au on TiO_2 (110), relative to its value for free Au (up to 1.0 ML). This suggests inertisation of the Au atoms on

the perfect TiO_2(110) on these surfaces. This may seem to contradict the fact that Au/TiO_2 catalysts are among the most active catalysts [Bond and Thompson, 2000]. However, the TiO_2 surface considered in this simulation was perfect. Defects may play an important role. For >1.0 ML, there were no significant changes in the relative position of the d-band, and the structure of the adsorbed gold atoms changed to 3D. Scanning tunnelling microscopy studies (STM) and DFT calculations by Wahlström et al. [2003] have shown that Au atoms bind very strongly on the oxygen vacancies of the titania rutile support. Furthermore, each vacancy was found to bind on average about 3 Au atoms. The gold-titania interaction on the stoichiometric surface was found to be very weak. Nucleation of Au atoms is favoured on the vacancy site of TiO_2 anatase(101), while standing geometries are preferred on the stoichiometric surface [Vittadini and Selloni, 2002].

2.4. Oxidation of Carbon Monoxide

The oxidation of carbon monoxide is the most widely studied gold-catalysed reaction, and is consequently the main subject of many reviews [e.g. Bond and Thompson, 1999 and 2000]. The contradictory nature of literature results is emphasised in these reviews. Selected studies will be discussed with the aim of capturing the essential chemistry of Au (supported or bare) as studied either by CO oxidation or via CO or O_2 adsorption studies.

2.4.1. Adsorption of CO and Oxygen onto Au Surfaces

CO was found to adsorb onto an Au(100) surface with an initial heat of adsorption of -58 kJ/mol [McElhiney and Pritchard, 1976]. The surface potential measurements indicated the absence of monolayer coverage between 81 K and 260 K. No ordering of CO on the surface was revealed by low energy electron diffraction (LEED). Similar adsorption properties and energetics were obtained for the Au(332) surface [Ruggiero and Hollins, 1996]. CO has been shown to reconstruct a perfect Au(110) surface to a (2 x 1) structure upon adsorption [Jugnet et al., 2002]. It has been found experimentally that the initial heat of CO adsorption onto Au particles in the size range 1.8 to 3.1 nm, supported on TiO_2, increases with a decreasing gold particle size from -52 to -76 kJ/mol [Meier and Goodman, 2004]. For a 0.5ML Au/TiO_2 system,

the initial heat of CO adsorption was almost constant between 0% and 35% coverage at -52 kJ/mol, and changed sharply with increasing coverage above 35% and reached a value of -29 kJ/mol at about 83% coverage.

Experiments by Wallace and Whetten [2000, 2002] have shown that CO adsorbs on anionic gold clusters (Au_N^-, N=4-19). No adsorption is observed on the gold dimer or trimer anion. Wu et al. [2002] studied, theoretically, CO adsorption onto gold clusters (anionic, neutral and cationic clusters) from the monomer to the hexamer. Au_n^+ clusters bind CO the strongest, followed by neutral and then anionic clusters. CO adsorption strength decreases with increasing cluster size for Au_n^+ clusters, and increases with cluster size for Au_n^- clusters. For the neutral clusters, the CO adsorption strength goes through a maximum at n=5 as n increases. For CO bonding onto Au clusters supported on TiO_2 anatase (101), the CO adsorption is stronger when the cluster carries a positive charge [Vittadini and Selloni, 2002].

Through ultraviolet photoelectron spectroscopy (UPS) and thermal desorption spectroscopy (TDS) studies, it has been shown that an Au(110)-(2 x 1) surface binds atomic oxygen at 300K and gives rise to β_1 (gold oxide – Au_2O_3) and β_2 (chemisorbed oxygen) oxygen species [Gottfried et al., 2003a and 2003b]. Under a CO static pressure of 1 x 10^{-6} mbar, evolution of CO_2 occurred at temperatures below 100 K. In an oxygen plasma, a thermally unstable 4 nm layer of Au_2O_3 could be formed over an Au(111) surface [Koslowski et al., 2001].

Mavrikakis et al. [2000] found, from DFT slab calculations, that the stepped Au(211) surface was more reactive towards atomic O and CO than the Au(111) surface. Furthermore, a stretched Au(111) surface was more reactive than an unreconstructed Au(111) surface. Atoms on steps have a reduced coordination relative to other surface atoms. Such low coordination atoms are abundant in small metal particles. DFT calculations show that the O_2 dissociation barrier is 215 kJ/mol on Au(111) and 90 kJ/mol on Au(211), again demonstrating the effectiveness of low coordination atoms [Liu et al., 2002]. In general, atoms with a low coordination have higher lying d-states [Liu et al., 2002; Lopez and Nørskov, 2002b]. A stretched Au(111) surface binds O_2 to a better extent than the unstretched surface [Xu and Mavrikakis, 2003]. In real

catalysts, stretching can be caused by lattice mismatch between Au particles and the support.

Nakatsuji et al. [1997] have suggested on the basis of cluster unrestricted Hartree-Fock (UHF) and MP2 calculations that a superoxide species, O_2^-, can be formed on Cu_2, Ag_2 and Au_2 clusters. This species could interact with ethylene to yield ethylene oxide, with high barriers to total oxidation. Electron transfer from Au_2 to molecular oxygen, a step critical for superoxide formation, was found to be a difficult process. The binding energy of O_2 onto anionic gold clusters is stronger than binding onto neutral clusters [Yoon et al., 2003; Franceschetti et al., 2003]. For the anionic clusters, the binding energy is larger for the even numbered clusters. This is in agreement with experimental work by Wallace and Whetten [2002], who showed that only the even-numbered gold anions had reactivity towards O_2.

It seems unlikely that the CO and O_2 activation sites will be similar on a supported gold catalyst. CO prefers neutral to cationic sites, while O_2 activation could be happening on anionic centres or the support. Surface oxygen vacancies of TiO_2 trap electrons, which can facilitate the adsorption and dynamics of O_2 on this surface [Wahlström et al., 2004]

2.4.2. Effect of Particle Size and Morphology on the Activity of Gold Catalysts

Pioneering work by Haruta et al. [1989] indicated that Au particles of diameters smaller than 10 nm (preferably below 5 nm) supported on α-Fe_2O_3, Co_3O_4 and NiO and prepared by coprecipitation method were very active for CO oxidation at temperatures as low as –70 °C. An Au/Al_2O_3 catalyst of similar gold particle size and prepared in the same manner had a higher light-off temperature, indicating that size is not the only key factor determining reactivity.

Work by Haruta et al. [1993] and Bwambeda et al. [1997] on Au/TiO_2 catalysts clearly showed that the smaller supported particles have a much higher intrinsic activity than larger particles (see Figure 2.1). Turnover frequencies were calculated

assuming hemispherical particles, which were seen on TEM photographs [Haruta et al., 1993].

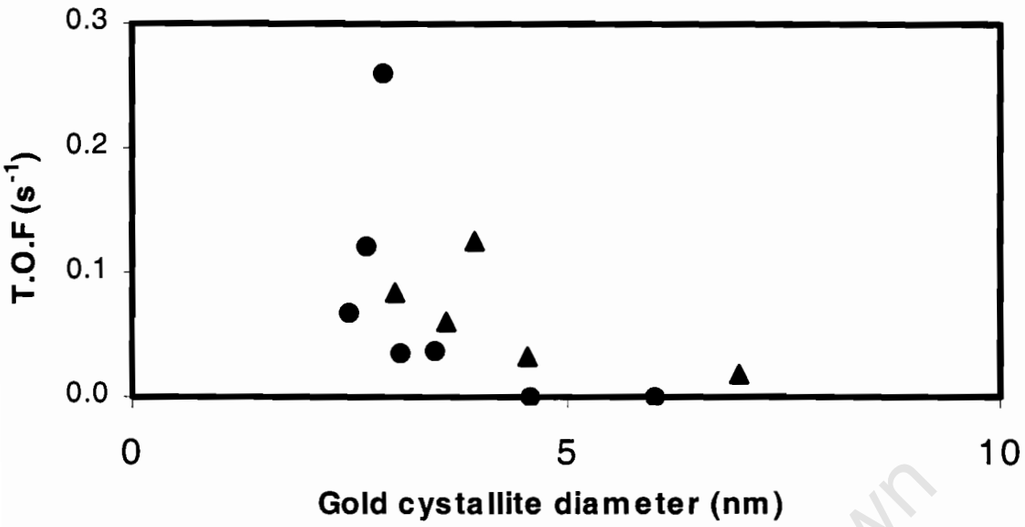

Figure 2.1: Turnover frequencies, based on surface gold atoms, for the oxidation of CO on Au/TiO_2 as a function of the mean Au crystallite diameter [Haruta et al., 1993; Bwambeda et al., 1997]. (circle) 27°C and (triangle) 0°C. All catalysts were prepared by the deposition-precipitation technique.

Valden et al. [1998] prepared Au nanoparticles on crystalline $TiO_2(110)$ and found that a HOMO-LUMO gap opens on the Au particles below 3.5 nm, or 300 atoms per cluster. The authors suggested that the presence of this gap might be related to the onset of activity of small particles. This is not yet a satisfactory explanation of their results, because in their experiments the HOMO-LUMO continued to increase as the particle size decreased, while the catalytic activity went through a maximum. The size range at which CO oxidation goes through a maximum is similar to the size range that was found to yield the highest CO adsorption energy in an experimental study of CO adsorption on Au/TiO_2 [Meier and Goodman, 2004]. Heiz and Schneider [2000] have found that for Au supported on MgO the catalytic activity commences at Au_8, and

attributed this to the charge transfer from the support to the gold cluster. It is, therefore, believed that negatively charged surface atoms of small clusters might render the clusters very active [Okumura et al., 2001]. This may be related to the ease with which anionic gold clusters bind oxygen easily by donating an electron to it [Yoon et al., 2003; Häkkinnen and Landman, 2003]. Coadsorption of CO and O_2 onto gold anions at room temperature results in CO_2 evolution. This will be true if O_2 activation is rate limiting. It may not be true if the support can easily activate O_2. Guzman and Gates [2004] have observed a correlation between the CO oxidation rate and the amount of Au present as Au^+ in Au/MgO catalysts, i.e. the larger the fraction of Au^+, the more active the catalyst. However, both Au^+ and Au^0 needed to be present in a working catalyst.

The previous discussion of particle size effects was limited to cases where one considers the small particles themselves to have higher intrinsic activity. However, changing the size of a crystallite will result in a change in its shape (and proportion of given crystallographic planes) in order to keep the surface energy at its minimum, as known from the Wulff theorem [Graoui et al., 1998]. Morphology effects on reactivity can, therefore, be expected if different morphological structures have different intrinsic activity.

$Au/Mg(OH)_2$ catalysts with an average gold diameter of 0.6 nm (Au_{13}), containing cuboctahedral and icosahedral clusters, were found to be active for CO oxidation at –70°C [Cunningham et al., 1988]. As the average cluster size increased, the turnover frequency decreased, and this correlated with an increase in the relative fraction of cuboctahedral particles from 42% to 93%. This led to the conclusion that the icosahedral particles were more active than cuboctahedral particles. Icosahedral particles expose {111} planes, while the cuboctahedral particles expose both the {100} and the {111} planes. It may be thought then that the {111} planes are the active sites. However, it is still difficult to distinguish between size and morphology effects from these experiments (and many other). Clearly, theoretical work is needed to gain more insight.

2.4.3. Effect of Catalyst Pre-treatment on Activity of Au Catalysts

Park and Lee [1999] studied the effect of pre-treatment conditions on the CO oxidation activity of Au catalysts prepared via the deposition-precipitation method. Using TiO_2, Fe_2O_3 and Al_2O_3 as supports, it was found that the CO oxidation activity decreased with increasing calcination temperature (in air) from 100 to 400°C. By X-ray photoelectron spectroscopy (XPS), it could be shown that the proportion of oxidized gold decreased with increasing calcination temperature. For the Au/Fe_2O_3 catalysts, Au_2O_3 was being changed to Au^0 as the calcination temperature increased. Water vapour seemed to suppress the reduction of oxidized gold. In the case of Au/Al_2O_3 catalysts, $Au(OH)_3$, Au_2O_3 and Au^0 were found to co-exist at low calcination temperatures. Increasing the calcination temperature resulted in a change in the gold phase from $Au(OH)_3$ through Au_2O_3 to Au^0. An oxidative calcination (air) was found to be more effective than reductive (H_2) pre-treatment for Au/TiO_2 catalysts. On the basis of these results, it can be concluded that oxidised gold particles play a role in CO oxidation.

For Au/ZnO catalysts prepared by coprecipitation, however, the CO oxidation activity at ambient temperature increased with calcination temperature (in O_2/Ar) until an optimum temperature of 240°C was reached [Wang et al., 2003]. The CO oxidation reaction was carried out in the presence of water vapour, which, as noted above, prevents over-reduction of gold particles to metallic gold. The initial increase can, therefore, be attributed to creation of Au^0, which must co-exist with oxidised gold for optimum activity. Margitfalvi et al. [2002] varied the $Au^{\delta+}/Au^0$ ratio in $Au/Mg(OH)_2$ catalysts by controlling the amount of ascorbic acid added during preparation. It was found that an optimum $Au^{\delta+}/Au^0$ ratio existed for CO oxidation. The catalysts were prepared by impregnation.

Clearly, the pre-treatment conditions affect the final surface composition of the catalyst (most notably the Au^+/Au^0 ratio). The as-prepared surface composition might depend on the type of support material, due to the anticipated differences in metal – support interactions when using different oxides.

2.4.4. Active Sites, Active Species and Reaction Mechanisms

A superoxide species, O_2^-, was found to form on the ZnO surface of Au/ZnO catalysts upon introduction of molecular oxygen in an electron paramagnetic resonance (EPR) study [Hao et al., 2001]. The interaction of O_2^- with CO pulses at room temperature resulted in the evolution of CO_2. In an in situ FTIR study, CO adsorption onto Au/ZnO produced a band at 2106 cm^{-1}, assigned to CO bonded to Au particles [Boccuzi et al., 1996]. An isolated band at 1577 cm^{-1} was assigned, on the basis of comparison with CO on Cu/ZnO spectrum, to CO bonded to both an Au atom and a Zn cation. Upon introduction of O_2, the CO bands showed a blue shift to 2116 cm^{-1} and 2133 cm^{-1}. These were attributed to CO bonded to Au^+. This was accompanied by appearance of signals in the carbonate region (1700 – 1000 cm^{-1}) and the CO_2 region (2400 – 2250 cm^{-1}). Coadsorption of ^{12}CO -$^{18}O_2$ and ^{12}CO -$^{16}O_2$ produced bands of the same frequency in the carbonate region, indicating that lattice oxygen (probably from the support), is involved in the carbonate formation. Similar effects were observed for Au/TiO_2, except that for the Au/TiO_2 catalyst a CO stretch at 2186 cm^{-1} was observed and assigned to CO bonded to Ti^{4+} sites [Boccuzi et al., 1996, 2002]. The mean diameters of Au in the Au/ZnO and Au/TiO_2 catalysts were 5 nm and 2-4 nm respectively. In a similar study on Au/Fe_2O_3, the decrease in activity of the catalysts with time could be correlated to a decrease in the intensity of the band at 2159 cm^{-1}, assigned to Au^+ [Minicó et al., 1997]. On Au/ZrO_2, Boccuzzi et al. [1998] found a higher Au^+ content on the used (and hence lower activity) samples than fresh ones. It seems, again, that both Au^0 and Au^+ are required for activity, and not an excess of the one or the other. For the Au/Fe_2O_3 catalyst, the involvement of lattice oxygen (from the support) is highly likely due to the ease with which the Fe^{3+}/Fe^{2+} redox can occur [Gupta and Tripathi, 2001].

On the basis of selective CO oxidation experiments on $Au/\gamma\text{-}Al_2O_3$, Costello et al. [2002 and 2003] proposed a mechanism that seems to fit most of the experimental data on CO oxidation. The authors proposed that both Au^0 and Au^+ are required for activity, with the Au^+ component existing as a hydroxyl, Au–OH. The proposed reaction scheme is shown in Figure 2.2. This mechanism could explain why a reaction -deactivated $Au/\gamma\text{-}Al_2O_3$ catalyst could be regenerated by treatment with H_2 or H_2O at

room temperature [Costello et al., 2002]. The deactivation of the catalyst was thought to occur through carbonate formation via the reaction:

$$Au\text{-}CO_3H + Au\text{-}OH = Au\text{-}CO_3\text{-}Au + H_2O \qquad (2.1)$$

Bond and Thompson [2000] proposed a similar active-site model on the basis of their comprehensive review of the literature on CO oxidation. While the proposed pathway can explain most of the literature findings on CO oxidation, it should be noted that the chemical involvement of the support cannot be entirely excluded due to the ease with which some oxides can transport lattice oxygen (for example Fe_2O_3). A possible role of the support needs to be built into the mechanism to make it truly complete. In Haruta's mechanism [Haruta, 1997], the support helps in activation of O_2.

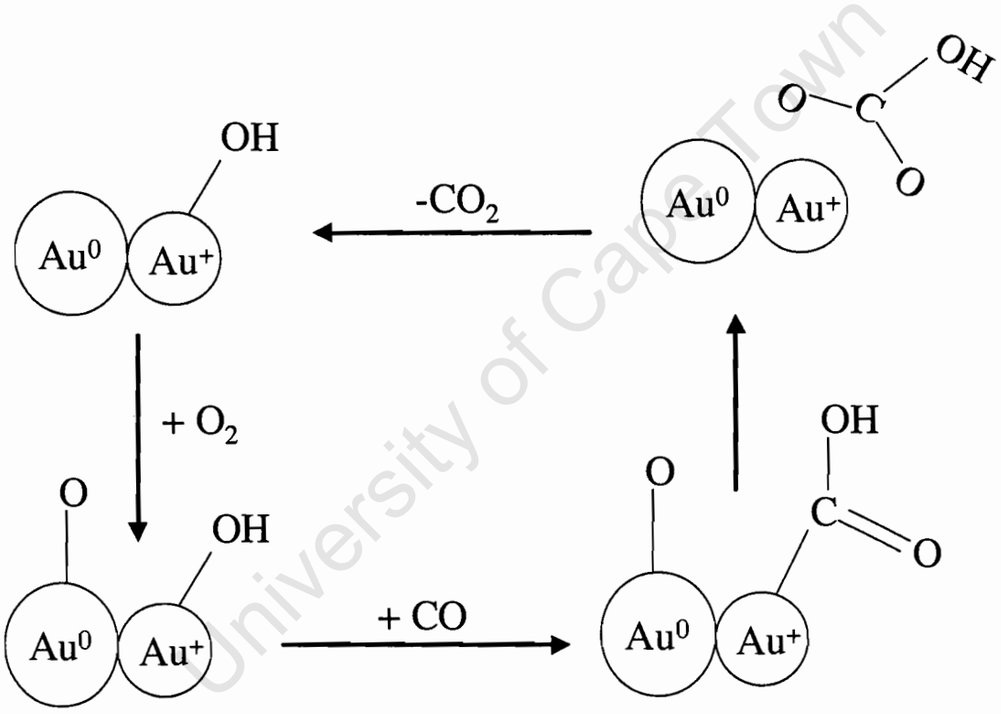

Figure 2.2: Proposed mechanism for CO oxidation over gold catalysts [Costello et al., 2003].

CO oxidation on clean Au surfaces has also been investigated theoretically by DFT. Lopez and Nørskov [2002b] studied some of the elementary steps of CO oxidation in an array of Au_{10} (3,7) clusters (each in a cell) and concluded that the reaction barrier was less than 39 kJ/mol and hence the reaction should occur at room temperature or below. Liu et al. [2002] found a minimum barrier of 44 kJ/mol along a reaction route that involves direct CO and O_2 coupling to yield an unsymmetrical O-O-CO intermediate on stepped Au surfaces. While O+CO coupling was found to proceed with a barrier of about 24 kJ/mol, O_2 dissociation still required 90 kJ/mol (on Au(211)) and may only proceed on metallic gold at temperatures above room temperature. This justifies Haruta's assumption that the O_2 dissociation could be support-assisted [Haruta, 1997] (in the absence of anionic gold). It seems that the main reaction limiting step in CO oxidation is the activation of molecular oxygen. Molina and Hammer [2003] and Liu et al. [2003] studied, via DFT, the role of the support in CO oxidation over gold supported on MgO and TiO_2 respectively. Sites at the Au-MgO interface were found to stabilize a CO-O_2 peroxolike reaction intermediate, while the Au-TiO_2 interfacial sites were found to be active for O_2 adsorption. The support promotion can be direct (adsorbates bonding to both Au atoms and the support-metal atoms) or indirect (the support modifies electronic properties of the Au atoms at the interface).

2.5. Epoxidation of Propene

The direct epoxidation of propene to propylene oxide (Reaction 2.2) is not carried out industrially due to the lack of a suitable catalyst.

$$CH_3CHCH_2 + 0.5O_2 = CH_3CH(O)CH_2 \qquad (2.2)$$

In the presence of hydrogen, propene can be oxidised very selectively to propylene oxide (PO) over Au catalysts using TiO_2, titanium silicate (TS-1) or TiO_2/SiO_2 as supports [Nijhuis et al., 1999]. At 50 - 125°C, the PO selectivity (based on propene converted) exceeds 99%, although the yields are disappointing at below 2%. A gold sponge, bare titania, Au/γ-Al_2O_3 and Au/SiO_2 all showed no epoxidation activity. Since PO formation in the absence of hydrogen was not possible, the authors

suggested that a hydrogen peroxide-like intermediate was involved in the synthesis, based also on the fact that TS-1 itself can produce PO if H_2O_2 was used as an oxidant. Since H_2O_2 synthesis is theoretically possible over gold and silver surfaces [Olivera et al., 1994], the mechanism in which the role of Au was to provide H_2O_2 from H_2 and O_2 was proposed. H_2O_2 was thought to spillover to the support and interact with propene to produce PO (in an unspecified manner). In other studies, pure $Au(OH)_3$ was found to react with propene/H_2/O_2 mixtures to form PO with 60% selectivity at room temperature, even though the reaction was probably more stoichiometric than catalytic [Stangland et al., 2000]. Deactivation was linked to reduction of $Au(OH)_3$ to Au^0. Other workers have used more complex mixed titania-silica oxides like Ti-MCM as supports [Uphade et al., 2000, 2001]. Although the complexity of these oxides makes it difficult to understand the catalytic action, PO yields improve to near 5%.

2.6. Oxidation of Volatile Organic Compounds

Scirè et al. [2001 and 2003] and Minicò et al. [2000 and 2001] have shown that gold on reducible oxides like Fe_2O_3 and Ce_2O_3 prepared via deposition-precipitation or coprecipitation is very effective for combustion of volatile organic compounds in excess oxygen, including alcohols, acetone and toluene. For ethanol conversion, the main selective oxidation product at low temperatures (below 200°C) is acetaldehyde, with CO_2 being produced at higher temperatures [Minicò et al., 2000 and 2001]. Oxidation of non-alcohols produced only CO_2. A Mars-van Krevelen mechanism was proposed for the oxidation of volatile organic compounds [Minicò et al., 2000]. The implied involvement of lattice oxygen is in harmony with the fact that ethanol and methanol adsorb onto metal oxide surfaces to produce various partial oxidation products via methoxy and ethoxy intermediates [Idriss and Seebauer, 2000 and Badlani and Wachs, 2001]. The role of Au in Au/Fe_2O_3 and Au/Ce_2O_3 catalysts was thought to be the lowering of the reduction temperature of the oxide, thus increasing the mobility of the support surface oxygen. Temperature programmed reduction (TPR) studies have confirmed that the Fe_2O_3 to Fe_3O_4 transition temperature is lowered by up to 140°C by the presence of gold [Minicò et al., 2000; Ilieva et al., 1997]. The concentration of surface hydroxyls increases with gold addition, as evidenced by infrared (IR) [Ilieva et al., 1997]. Similarly, gold promotes Ce_2O_3 [Scirè

et al., 2003] and V_2O_5 [Andreeva et al., 1998] supports by lowering their reduction temperatures.

Gold on a less reducible oxide, Al_2O_3, was found to be active for combustion of n-hexane, 2-propanol and benzene [Centeno et al., 2002]. Activity data for the bare alumina support was not presented, making it difficult to gain mechanistic insight. Other volatile organic compounds like Freon-12 (CCl_2F_2) and methyl chloride (CH_3Cl) could be decomposed on Au/Al_2O_3, although the reaction here might be occurring exclusively on the hydroxylated alumina surface [Aida et al., 1990].

2.7. Methane Oxidation

Comparison of supported gold catalysts for methane oxidation indicated that the activity fell in the order: $Au/Co_3O_4 > Au/NiO > Au/MnO_x > Au/Fe_2O_3 >> Au/CeO_x$ [Waters et al., 1995]. The Au/Co_3O_4 catalyst started showing activity at temperatures between 200 and 250°C. XPS analysis on a possible correlation between Au oxidation state and catalytic activity was inconclusive. The fact that the oxides of Co and Ni themselves are active oxidation catalysts further complicates the efforts to rationalise the observed trend.

Addition of Au to MgO was shown to change the selectivity of MgO support from oxidative coupling (forming C_2 hydrocarbons) to complete oxidation to CO_2 at 750°C [Blick et al., 1998]. The C_2 yield decreased with an increase in Au loading. The CH_4 conversion also decreased with Au addition. The authors suggested that Au blocked the O^{2-} vacancies on the MgO surface, which are thought to be responsible for coupling activity. Au atoms generally prefer defect sites on the MgO surface for nucleation [Kubo et al., 1997].

2.8. Water-gas Shift and Methanol Synthesis

The water gas-shift reaction is a well established process:

$$CO + H_2O = CO_2 + H_2 \qquad \Delta H_{25°C} = -41 \text{ kJ/mol} \qquad (2.3)$$

Fe_2O_3 is a high temperature water-gas shift (WGS) catalyst that operates via an Fe^{3+}/Fe^{2+} redox [Rhodes et al., 1995]. Au can lower the temperature at which $Fe^{3+} \rightarrow Fe^{2+}$ reduction takes place [Ilieva et al., 1997]. It was, therefore, expected that Au/Fe_2O_3 catalysts would be active for the water-gas shift reaction at low temperatures [Andreeva et al., 1996]. The activity of coprecipitated Au/Fe_2O_3 catalysts at low temperatures is comparable to that of the commercial catalyst, $CuO/ZnO/Al_2O_3$ [Andreeva et al., 1996]. Sakurai et al. [1997] has since shown that Au/TiO_2 catalysts were equally or more active that Au/Fe_2O_3 and $CuO/ZnO/Al_2O_3$ catalysts [see Table 2.1]. Au/ZnO catalysts are also active, although their activity is lower than for all the other catalysts tested. Au/CeO_2, Au/ZrO_2 and Au/Co_3O_4 are also active WGS catalysts [Tabakova et al., 2000; Andreeva, 2002].

Table 2.1: Catalytic activity of supported gold catalysts for the water-gas shift reaction [Haruta et al., 1997][a].

Catalyst[b]	Diameter of metal particles[c] [nm]	Rate at 100°C [mol s^{-1} g_{cat}^{-1}]	TOF[f] at 100°C [s^{-1}]	E_{Act}[g] [kJ/mol]
Au/TiO_2 (DP,3.4%)[d]	4.4	1.0×10^{-7}	7.9×10^{-4}	46
Au/TiO_2 (DP, 5%)[d]	-	1.4×10^{-7}	-	45
Au/TiO_2 (DP,10%)[d]	4.4	3.0×10^{-7}	9.2×10^{-4}	31
Au/TiO_2 (Cop,33%)[d]	2.8	6.4×10^{-8}	5.6×10^{-5}	47
Au/Fe_2O_3(Cop,5%)	3.3	2.2×10^{-8}	9.1×10^{-5}	52
Au/Al_2O_3 (Cop,5%)	3.7	3.4×10^{-8}	1.1×10^{-4}	24
Au/ZnO(Cop,5%)	4.9	9.0×10^{-9}	5.7×10^{-5}	34
$Cu/ZnO/Al_2O_3$[e]	13.4	1.2×10^{-7}	2.0×10^{-4}	53

[a]Feed gas: 1% CO, 2% H_2O, balance He; GHSV = 12 600 ml hr^{-1} g_{cat}^{-1}; pressure = 1 bar.

[b]DP = deposition-precipitation, Cop = coprecipitation

[c]Calculated from XRD by using Scherrer's equation

[d]Magnesium citrate was added during preparation

[e]Commercial catalyst, with 42atom%Cu by XRF analysis

[f]Turnover frequency

[g]Activation energy

Owing to the difference in redox and acid/base properties of the supports tested, it is not clear how the reaction takes place. Fourier-transform infrared (FTIR) studies on Au/Fe_2O_3 and Au/TiO_2 catalysts have shown that CO and H_2O adsorption sites can be found on the support, metal-support interface and the metal [Boccuzzi et al., 1999]. Au/CeO_2 catalysts leached with a cyanide solution are just as active as unleached samples (activity expressed per total surface area of the catalyst) [Fu et al., 2003]. Since leaching removes all Au^0 particles and leaves behind only Au^{+1} and Au^{+3} (as evidenced by XPS), this result suggests that Au^0 species might be spectators and the reaction proceeds either on cationic gold or on the ceria support.

In Frost's theory, any metal which does not dissociate CO and forms a Schottky barrier in the region of 0.45 eV with the support oxide should make the metal/oxide combination active for methanol synthesis [Frost, 1988]. In his theory of methanol synthesis, the active sites are the oxygen vacancies in the support. The enthalpy of formation of these defects will decrease if a Schottky barrier is formed between the metal and the support (valence electrons can flow to the metal Fermi level instead of the oxide conduction band). Although the theory has been disputed [e.g. Shaw et al., 1992], it led to the prediction that Au/ThO_2 can be an active methanol synthesis catalyst. It has since been shown that gold supported on ZrO_2, ZnO, TiO_2, Fe_2O_3 and other oxides forms active methanol synthesis catalysts via both CO and CO_2 hydrogenations [Sakurai et al., 1993, Sakurai and Haruta, 1995 and 1996, and Baiker et al., 1991 and 1993]. Tables 2.2 and 2.3 list the activity of various gold catalysts for CO and CO_2 hydrogenation at 250-400°C respectively [Sakurai and Haruta, 1995]. The catalysts were prepared by coprecipitation and had a gold loading of 5 wt%, except for the titania supported catalyst, which was prepared by deposition-precipitation and had a gold loading of 2 wt%. For CO_2 hydrogenation (Table 2.2), the CO_2 conversion at 300°C is similar on all catalysts (~25%), so methanol selectivities can be compared. The methanol selectivity decreases in the order: $Au/ZnO > Cu/ZnO/Al_2O_3 \approx Cu/ZnO > Au/Fe_2O_3 >> Au/TiO_2$. The commercial $Cu/ZnO/Al_2O_3$ catalyst is still the most active at the typical methanol synthesis temperature of 250°C. The inferiority of the Au/TiO_2 catalyst is also seen for CO hydrogenation, where the ZnO based catalysts (with Au or Cu) are very active (see Table 3). Clearly the sites responsible for WGS and methanol synthesis are not similar

on all catalysts, because Au/TiO_2 and Au/Fe_2O_3 are superior to Au/ZnO in the WGS [Haruta et al., 1997]

Table 2.2: Activity of gold catalysts for CO_2 hydrogenation [Sakurai and Haruta, 1995][a].

Catalysts	d_{Au}[b] [nm]	SA[c] [m^2/g]	T[°C]	CO_2 conv [%]	Product Selectivities[d] [%]		
					MeOH	**CO**	**CH_4**
Au/ZnO	3.5	41.0	250	8.2	48.8	51.2	0.0
			300	24.5	21.2	78.8	0.0
			400	37.7	1.1	98.4	0.5
Au/Fe_2O_3	3.3	32.8	250	18.4	29.3	69.6	1.1
			300	25.3	14.2	78.3	7.5
			400	38.3	0.8	67.1	32.4
Au/TiO_2	3 - 4	41.0	250	18.6	6.5	75.3	18.3
			300	25.6	1.2	58.6	39.8
			400	38.8	0.3	47.6	52.4
Cu/ZnO	-	49.1	250	17.2	37.2	62.8	0.0
			300	25.3	16.6	83.0	0.01
			400	39.0	1.3	97.9	0.8
$Cu/ZnO/Al_2O_3$ (commercial)	-	54.2	250	22.8	51.3	48.7	0.0
			300	26.6	17.3	82.7	0.4
			400	38.1	1.3	94.2	3.4

[a]Reaction conditions: $CO_2/H_2/Ar$ = 23/67/10, total pressure = 50 atm, GHSV=3000 ml/ h/g_{cat}.

[b]Calculated by using Scherrer's equation

[c]BET surface area of the catalyst

[d]Rest contained mainly C_2 to C_3 hydrocarbons, and unspecified products

Table 2.3: Activity of gold catalysts for CO hydrogenation [Sakurai and Haruta, 1995][a].

Catalysts	d_{Au} [b] [nm]	SA[c] [m^2/g]	T[°C]	CO conv [%]	Product Selectivities[d] [%]		
					MeOH	**CO_2**	**CH_4**
Au/ZnO	3.5	41.0	250	3.7	70.3	29.7	0.3
			300	9.3	81.7	10.8	4.3
			400	17.5	4.0	47.4	42.3
Au/Fe_2O_3	3.3	32.8	250	9.8	16.3	54.1	13.3
			300	79.6	2.5	54.4	20.7
			400	88.8	0.1	52.0	18.7
Au/TiO_2	-	41.0	250	17.2	0.6	52.3	40.7
			300	65.3	0.2	53.3	34.5
			400	88.4	0.0	46.9	38.9
Cu/ZnO	-	49.1	250	2.5	72.0	24.0	0.8
			300	10.3	81.6	11.7	3.9
			400	17.5	4.0	47.4	38.3
$Cu/ZnO/Al_2O_3$	-	54.2	250	28.5	89.5	8.1	0.4
(commercial)			300	26.0	45.3	36.5	3.1
			400	26.3	2.7	49.8	30.8

[a]Reaction conditions: $CO/H_2/Ar$ = 30/60/10, total pressure = 50 atm, GHSV=3000 ml / h /g_{cat}.

[b]Calculated by using Scherrer's equation

[c]BET surface area of the catalyst

[d]Rest contained mainly C_2 to C_3 hydrocarbons, and unspecified products

For Au/ZnO catalysts, Sakurai and Haruta [1996] have shown that the methanol formation rate from CO_2 and H_2 is higher for smaller gold particles on the support (see Figure 2.3). Although no active sites were proposed, it was thought that the gold-oxide interface plays a crucial role in the synthesis.

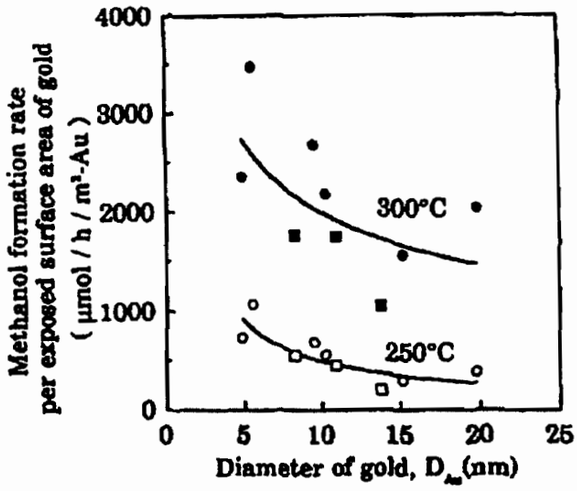

Figure 2.3: The aerial rate of methanol synthesis as a function of the mean diameter of the gold particles in Au/ZnO catalysts. The mean diameters were determined by TEM (●, ❍) and XRD (■, □) [Sakurai and Haruta, 1996]. $CO_2/H_2/Ar$ = 23/67/10, total pressure = 50 atm, GHSV=3000 ml/ h/g_{cat}.

FTIR studies on methanol synthesis over Au/ZrO_2 catalysts by Baiker et al. [1991] showed peaks that were assigned, on the basis of previous work on Pd/ZrO_2 and Cu/ZrO_2, to methoxy ($-CH_3O$), formaldehyde (CH_2O) and, carbonate (CO_3^{2-}). Bonding sites were not identified, making mechanistic conclusions impossible. A theoretical study of methanol synthesis intermediates on single Au atoms resulted in a proposal for a CO_2 hydrogenation pathway given in Figure 2.4 [Phala et al., 2003]. The relative energies indicate the stability of the intermediate with respect to decomposition to CO_2 and H_2. CO_2 is adsorbed on a gold cation and then, by successive hydrogenations, transformed into formate, formaldehyde, hydroxymethyl and finally methanol. A hydroxymethyl species appears to be more stable than a methoxy species. Furthermore, the relative energies of the intermediates on Au were similar to those on Zn, suggesting that migration of reaction intermediates between the metal and the support can, in principle, happen on Au/ZnO catalysts. These results clearly need to be expanded to include other possible active site models. Methanol synthesis is a good 'test' reaction, and a detailed knowledge of its mechanism on gold-based catalysts will eventually lead to the understanding of other reactions like

water-gas shift and CO oxidation, due to the similarity of the intermediates involved in these reactions.

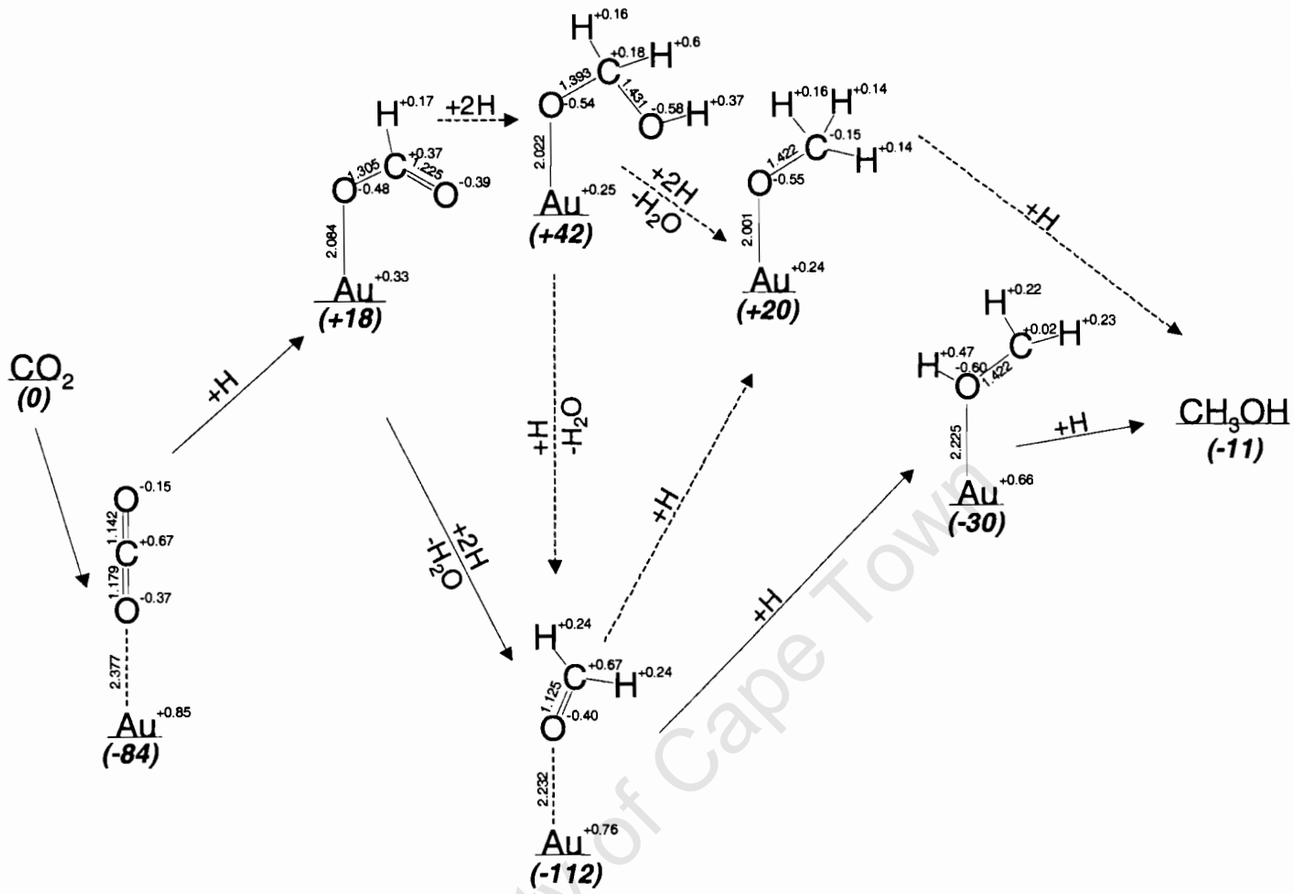

Figure 2.4: Energetics of various species bonded to gold atoms [Phala et al., 2003]. Relative energies, in kJ/mol, are shown in parenthesis, while metal charges are shown as superscripts. Low energy route is indicated by the solid arrows.

2.9. Other Hydrogenations/Dehydrogenations

Bond and Sermon [1973] reported that Au/SiO_2 and Au/Al_2O_3 catalysts prepared by the impregnation method were active for the hydrogenation of 1-pentene to n-pentane and the cis-trans isomerisation of pent-2-ene at 100°C. The activity was, however, much lower than that of Pt catalysts. In active Au catalysts, small particles were found. This led to the proposal that those small Au particles somehow 'behave' like Pt by losing electrons to the support. Au catalysts are active for H_2/D_2 exchange reaction at 150-300°C with activation energies of 40-60 kJ/mol [Bond and Thompson, 1999]. It is clear from the review by Bond and Thompson [1999] that H_2 dissociation is rate limiting in most Au catalysed hydrogenations. Reactions with H_2 or D_2 show different propene hydrogenation activities (may be a kinetic isotope effect), and alkadiene partial hydrogenations are totally selective with zero reaction orders of hydrocarbon and first in hydrogen at an activation energy of 37 kJ/mol. Au/ZnO and Au/ZrO_2 have been reported to be active for the selective hydrogenation of unsaturated aldehydes, with preference for the C=O bond over the C=C bond [Hutchings, 2002]. The catalysts pre-treated with sulphur showed higher activities. Dehydrogenation of methylcyclohexane to toluene and benzene has been reported on $Pt\text{-}Au/\gamma\text{-}Al_2O_3$ catalysts prepared by impregnation at temperatures in the range 150-500°C [Rouabah and Fraissard, 1993]. Although Au particles below 1 nm have been observed in the active catalysts, it is unclear if Au is playing a role at all – given that Pt is a very active metal.

2.10. Reduction of Nitric Oxide

Gold catalysts can catalyse the reduction of NO by CO, H_2 or C_3H_6 very efficiently [Bond and Thompson, 1999; Ueda and Haruta, 1999]. As with other gold catalysed reactions, the preparation method and the choice of support are crucial. For NO reduction by H_2 in the presence of oxygen, precious metal catalysts show the activity order: Pt > Rh > Pd > Au,Ru > Ir when using Al_2O_3 and TiO_2 as supports [Ueda and Haruta, 1999]. Performance data for selected gold catalysts tested for NO reduction by C_3H_6 is shown in Table 2.4, where it is clear that Au/ZnO is the most active catalyst below 300°C, followed closely by Au/ZrO_2. The $NO/H_2/CO$ reaction in

Au/NaY zeolite catalyst has been shown to produce both Au^0-NO and Au^+-NO bands in FT-IR [Salama et al., 1996].

Table 2.4: NO conversion to N_2 over supported gold catalysts [Ueda and Haruta, 1999].

Catalyst[a]	Au loading [wt%]	d_{Au}[b] [nm]	NO Conversion to N_2 [%][c] 200°C	250°C	300°C	350°C	400°C	450°C	500°C
Au/MgO	0.85	5.1	8.6	12.6	20.2	42.5	37.7		
Au/Al_2O_3	0.28	4.9	4.2	6.8	12.2	34.1	50.7	39.4	
Au/TiO_2	0.76	3.3	5.5	8.1	18.4	30.4	18.9		
$Au/\alpha\text{-}Fe_2O_3$	0.79	3.4	6.1	12.3	7.8	3.1	1.7		
Au/ZnO	1.2	3.5	24.4	49.2	35.1	23.5	14.0		
Au/ZrO_2	0.84	3.8	12.3	32.4	24.5	17.4	8.2		
Al_2O_3	-	-				0.5	1.2	1.8	2.6

[a]All catalysts prepared by deposition-precipitation method, except for Au/ZnO which was prepared by co-precipitation.

[b]Crystallite size of gold was calculated by using Scherrer's equation from XRD data.

[c]NO reduction by propene (with N_2O) as another reaction product. Reaction conditions: 0.1 vol% NO, 0.1 vol% C_3H_6, 5.0 vol% O_2, and 10.0 vol% H_2O in He. Space velocity = 20 000 ml h^{-1} g_{cat}^{-1}.

2.11. Hydrochlorination of Ethyne

The initial rate for the hydrochlorination of ethyne, CH≡CH by HCl to vinyl chloride over metal chlorides supported on carbon increases with an increase in the standard electrode potential of the metal, $M^{n+} + ne \rightarrow M$ [Hutchings, 2002]. Au cations have an electrode potential higher than that of Hg^{2+} and Pd^{2+} (the commonly applied catalysts) and was thus predicted (and confirmed experimentally) to be a catalyst of choice for this reaction. A cause-effect explanation for this correlation is not available, but it has been found via ^{197} Au Mössbauer spectroscopy that deactivation of the gold catalysts was correlated with reduction of Au^{3+} through Au^+ to metallic gold.

2.12. Conclusions and Fundamental Key Questions

The literature work on catalysis by gold is vast and often contradictory. The selected reviewed work clearly shows that modifying gold (by changing its size or morphology), changes its chemical reactivity .The direction of the change depends on the nature of the reaction being catalysed. The mode of catalyst preparation is important as it controls the final dispersion of gold particles and their interaction with the support. The support can play a chemical role for some reactions. While the above might seem like a conservative generalisation, the fact that nothing beyond can be said illustrates a clear need of fundamental knowledge on this subject. It is the goal of this study to fill some areas of this gap and stimulate further work in that direction. Leading to the hypothesis that forms the basis of this work was the following key questions:

'What happens when the crystallite size of supported gold is decreased?'

An increase in number of atoms with less than bulk coordination is expected from a statistical viewpoint. This should intuitively make a gold surface active. However, this also leads to increased binding of the particles to the support. There should, therefore, be a change in electronic nature of gold particles with size, and those changes should necessarily imply increased reactivity for smaller particles. On the basis of surface energy arguments, it is expected that the relative proportion of crystallographic planes will change with size to continue minimising the total surface energy. Most notably, the crystal planes that expose the closed packed (111) phase should be dominant. Therefore, the chemical reactivity of this surface may also feature in catalysis by a bare metallic surface.

'What is the nature of the interaction between gold and the support material?'

Depending on the kind of support, modification of electronic properties of gold particles in contact with support should make them react differently. Do atoms at the metal-support interface necessarily differ in reactivity to those of a free particle? Since most oxide surfaces are oxygen-terminated, an electron transfer process at the gold/oxide interface can make interfacial gold atoms cationic. Electrostatic

interactions could then favour chemisorption of molecules onto cationic gold atoms. It is therefore important to investigate the nature of the metal-support interaction, particularly with emphasis on the nature of the gold atoms that are bound directly to the support. This is probably the most reaction and support sensitive aspect of catalysis by gold. It is clear that addressing these fundamental questions is not an experimentally trivial task, due to the empirical nature of experiments. It is for this reason that high-level quantum chemical methods were employed in this study.

Chapter 3

MOLECULAR MODELLING METHODS IN HETEROGENEOUS CATALYSIS

Catalytic processes are largely developed by empirical methods. This is due to the difficulty associated with obtaining molecular-scale understanding of the catalytic action from empirical experiments. With the development in computing power, most of the fundamental aspects of catalysis are amenable to computation. Interatomic potential-based methods, also known as molecular mechanics methods, can be used to tackle systems containing many thousands of atoms. However, these methods suffer from the lack of transferability, in that parameters for the potentials are generally only adequate for a given molecular system. At the forefront of various computational techniques lies the sophisticated quantum chemical methods, which make it possible to interpret chemical reactions on the basis of the electronic structure of the constituents involved. When applied to catalysis, these methods can be used to study the electronic structure of the catalytic surface and adsorbates, and to explain the observed or the anticipated functioning of a catalytic system. The information obtained is very useful for the understanding of the reaction and consequently the development of more selective catalysts. In certain cases, the high level quantum chemical methods are combined with parameter-based molecular mechanics methods.

3.1. Basics of Molecular Mechanics

The ultimate goal in molecular mechanics (MM) is to describe the energetics of a molecular system in terms of the nuclear coordinates only, without much regard to the motion of the electrons. Force field or inter-atomic parameters are employed to describe various interactions, and the energy of the total system is minimised with respect to the nuclear coordinates. These parameters are generally derived from experiment or quantum chemical calculations on a smaller system. A typical molecular mechanics force field describing the total energy, V, of a polyatomic system consisting of N particles at positions r may have the form [Leach, 2001]:

$$V(r^N) = \sum_{bonds} \frac{k_i}{2}(l_i - l_{i,o})^2 + \sum_{angles} \frac{k_i}{2}(\theta_i - \theta_{i,o})^2 + \sum_{torsions} \frac{V_n}{2}(1+\cos(nw-\gamma))$$
$$+\sum_{i=1}^{N}\sum_{j=i+1}^{N}(4\varepsilon_{ij}[(\frac{\sigma_{ij}}{r_{ij}})^{12} - (\frac{\sigma_{ij}}{r_{ij}})^{6}]) + \sum_{i=1}^{N}\sum_{j=i+1}^{N}\frac{q_i q_j}{4\pi\varepsilon_o r_{ij}} \qquad (3.1)$$

The form of first term is the familiar Hooke's Law description of the stretching of two bodies connected by a spring. In this case, it represents the change in energy as the bond length, l_i, varies from its reference value, $l_{i,o}$. k_i is a constant for each bond, i. This *harmonic* representation of bond-stretching energetics is only accurate at short deviations from the reference bond length. The true potential has the form of a Morse potential. Higher order terms, e.g. cubics, can be added to make the bond-stretching description more accurate. The second term in 3.1, also *harmonic*, similarly describes the energetics as the bond angles, θ_i, deviate from their reference value, $\theta_{i,o}$, as an angle between three atoms is bend. The third term describes the energetic cost of changing a torsion angle, w. n (called multiplicity) is the number of energy minima in the potential energy as the torsion angle, w, is changed from 0 to 360°. The phase factor, γ, determines where the torsion angle passes through its minimum value. The fourth term is the non-bonded *Lennard-Jones 12-6 function* that models the van der Waals interaction. If not calculated between two molecules, the atoms in on-bonded interactions have to be separated by at least three bonds. Hydrogen bonding is sometimes represented by a *10-12 Lennard-Jones function*.

Van der Waals interactions are sometimes represented by the popular Buckingham potential:

$$V = A\exp(-r/\rho) - \frac{C}{r^6} \qquad (3.2)$$

This potential is attractive at very short distances, an undesirable artefact.

The last term in 3.1 is the well known Coulomb interaction between non-bonded charged atoms (or molecules). When one models the Coulomb interaction between two charge distributions, the interaction energy can also be expressed in terms of contributions from charge-charge, charge-multipole and multipole-multipole interactions. Note that the forcefield parameters that determine the bonded interactions (bond stretching, angle bending and torsional terms) will include the electrostatic interactions between those bonded atoms. The functional form of the forcefield presented above is the most basic, and usually the inter-atomic potentials are adapted to suit particular problems of concern.

3.2. Molecular Mechanical Modelling of Ionic Solids

Although zeolites, metals, and other bulk solids are easily amenable to molecular mechanics modelling using appropriate potential forms and parameters, the discussion here will be limited to ionic solids, which are commonly used as supports for metal catalysts. In ionic solids, e.g. oxides, there is a substantial charge localisation on the atoms in the material. The Born model divides the interaction energy between any two atoms in a polyatomic system as a sum of the long range Coulomb interactions and a repulsive short-range term:

$$V(r^N) = \sum_{i=1}^{N} \sum_{j=i+1}^{N} \left(\frac{q_i q_j}{4\pi\varepsilon_o r_{ij}} + \frac{A}{r_{ij}^{\ n}}\right) \qquad (3.3)$$

The parameters, A and n, are obtained from experimental data. For oxides, the simplest choice of ionic charge, q, would be the formal oxidation states of the charges concerned. More generally, the partial charges (which may be non-integral) are chosen to reproduce the electrostatic potential around a given region.

In the Born model, the ions are assumed to have zero polarisability. While this may be reasonable for cations, it may lead to serious errors for the case of anions, e.g. O^{2-}. The valence electrons around an anion are not static but move back and forth between the anionic core and the atom surroundings depending on the external field. The shell model, proposed by Dick and Overhauser [1958], takes polarisation into account by treating the anion as a massive core connected to a mass-less shell by a spring. Both the core and the shell are assigned partial charges (total charge equals the charge of the anion). The core-shell interaction energy is then described by a harmonic potential similar to the bond stretching term. Different ions in the solid interact only through the shells. The cores of ions that have not been represented via a shell model will interact with ions through core-shell interactions. This useful treatment of ionic solids is already implemented in some standard molecular mechanics software, e.g. MARVIN [Gay and Rohl, 1995] and GULP [Gale, 1997].

It turns out that in practice there is no single 'best' potential form and usually a combination of various form may be desirable. For example, Whitmore et. al [2002] employed a mixture of the Buckingham potential, polynomial potentials, spring potential and a Lennard-Jones potential to model the surface structure of $ZnO(10\bar{1}0)$ surface with high accuracy. The Zn core-O shell interactions had different parameters for different ranges in both the Buckingham and polynomial potentials.

Molecular mechanics is generally not suited to the problem of bond making/breaking, due to the fact that electron dynamics and interactions are not treated explicitly. For this reason, molecular mechanical methods find use mostly in determination of equilibrium structures of materials. To study the electronic structure of molecules/solids and hence energetics of catalytic processes, quantum mechanical methods are much more useful.

3.3. The Schrödinger Equation

The wave-particle nature of elementary particles was recognised in the 1920s. The motion of a particle through space can be described by a wavefunction, Ψ, from which other properties of the particle can be obtained. The product of the

wavefunction and its conjugate at a particular point in space represents the probability of finding the particle there. The time-independent Schrödinger equation is solved to obtain the energy of the system:

$$\left(-\frac{\hbar}{2m}\nabla^2 + V\right)\psi(r) = E\psi(r) \tag{3.4}$$

In Equation 3.4, V represents the external field and E represents the energy of the particle (or the system if Ψ is the *total* wavefunction). ∇^2 represents the second-derivative operator with respect to the x,y and z coordinates. The first term in the bracketed terms is, therefore, the kinetic energy operator. The bracketed term of Equation 3.4 is typically replaced by H, called the Hamiltonian operator. $\hbar$ is Planck's constant divided by 2π.

If the wavefunction is known, the energy of the system can be obtained by integrating both sides of Equation 3.4 over all space:

$$E = \frac{\int \psi^* H \psi d\tau}{\int \psi^* \psi d\tau} \tag{3.5}$$

In Equation 3.5, $d\tau$ implies that integration is over all space, and consequently the denominator on the right hand side equals unity for a *normalised* wavefunction. The normalisation ensures that the particle is somewhere in space. This normalisation is often referred to as a boundary condition. Another boundary condition, which is often imposed on possible solutions to the Schrödinger equation, is that any two wavefunctions of the same system must be orthogonal, i.e they have a zero overlap:

$$\int \psi_a \psi_b d\tau = 0 \tag{3.6}$$

In chemistry, the simplest molecule for which the Schrödinger equation can be solved exactly is H_2^+. For polyatomic systems, approximate solutions to the Schrödinger equation have to be utilized.

3.4. The Atomic Orbitals and Molecular Orbital Theory

3.4.1. The Born-Oppenheimer Approximation

In a polyelectronic (or polyatomic) system, the nuclei travel much slower than the electrons due to the large mass of the nuclei compared to the electrons. It can, therefore, be assumed that the electrons will instantaneously adjust to any change in spatial arrangement of the nuclei. This is the so-called Born-Oppenheimer Approximation, and it allows decoupling of the nuclear and electronic motions. The practical problem is therefore reduced to the calculation of the electronic Schrödinger equation for a given spatial arrangement of the nuclei. The total energy is then given by the sum of the quantum mechanical electronic energy and the classical nuclear-nuclear interaction. The electronic energy will include the potential energy due to electron-electron and electron-nuclear interactions.

3.4.2. Atomic Orbitals

As a consequence of the boundary conditions, the energies that can be assumed by an electron in a one-electron atom are not arbitrary, but quantized. The mathematical form of the wavefunctions corresponding to the energies gives rise to the known s, p, d and f orbitals. These functions also define the angular momenta of the particles that they describe. The angular momentum numbers, l, equal 0,1,2 and 3 for the s, p, d and f electron shells respectively. A graphical picture of the orbitals (up to the d orbitals), useful when interpreting chemical bonding, is given in Figure 3.1. In Figure 3.1, the difference in shading denotes the difference in the sign of the wavefunctions at different points in space. The spherical symmetry of the s-orbitals can be seen. It should be noted that physically only the square of the wavefunctions is meaningful (as it gives probabilities), and the diagrams are just empirical aids to facilitate interpretation of chemical phenomena. The analytical expressions for the orbitals are commonly referred to as the Slater-Type Orbitals (STOs), and are exemplified by expressions for the 1s, 2s and $2p_z$ orbitals given in Table 3.1.

Table 3.1: Analytical expressions for the 1s, 2s and $2p_z$ Slater-Type Orbitals[a].

$\phi_{1s}(r)$	$\frac{1}{\sqrt{\pi}}\zeta^{3/2}e^{-\zeta r}$
$\phi_{2s}(r)$	$\frac{1}{\sqrt{3\pi}}r\zeta^{5/2}e^{-\zeta r}$
$\phi_{2p,z}(r)$	$\frac{1}{\sqrt{\pi}}\zeta^{5/2}e^{-\zeta r}\cos\theta$

[a] ζ is known as the orbital exponent, and there are special rules for determining its value [Leach, 2001].

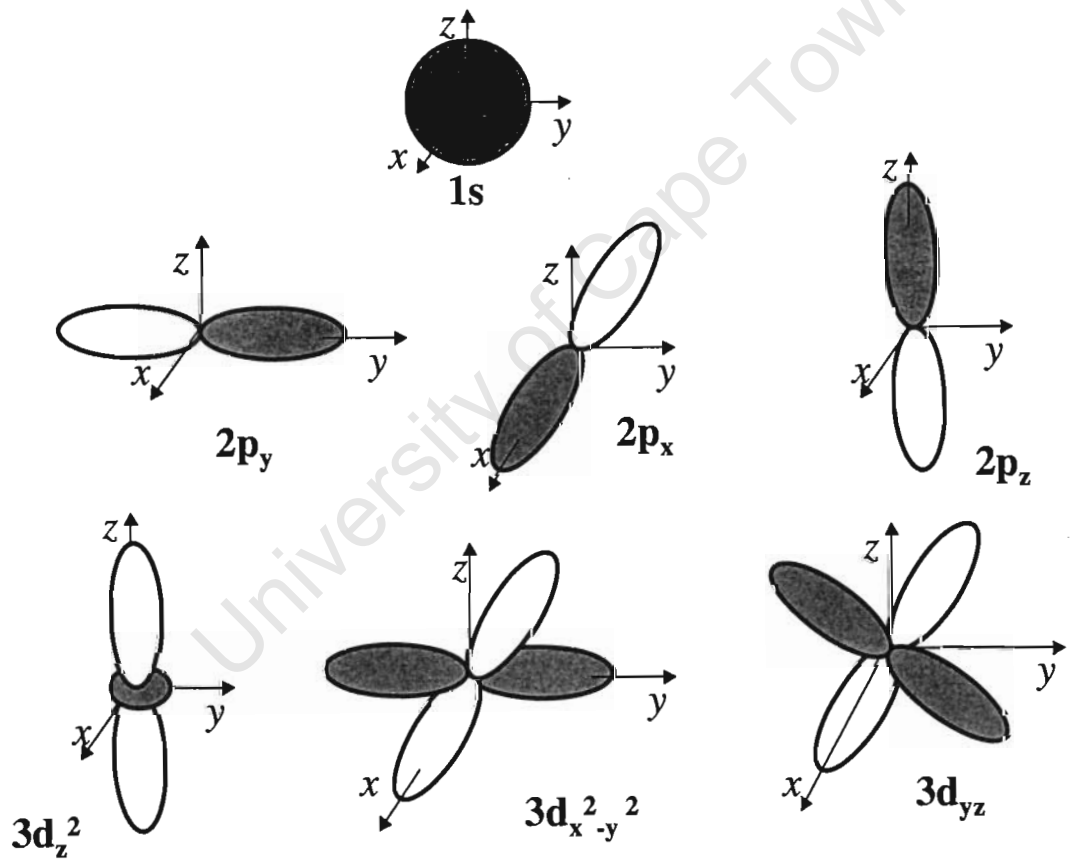

Figure 3.1: Schematic diagram showing the symmetry of the s, p and d orbitals. Note that the $3d_{yz}$ orbital lies on the yz planes and the wavefunction is zero along the x, y and z axes. Similarly, the $3d_{xz}$ and the $3d_{xy}$ lie on the xz and xy planes respectively.

3.4.3. The Linear Combination of Atomic Orbitals (LCAO) Method

The total Hartree-Fock electronic energy of a polyelectronic system, with 2 electrons per orbital, is related to the orbital energies of individual electrons via the equation:

$$E = \sum_{i}^{occ}\left[2\varepsilon_i - \sum_{j\neq i}^{occ}(2J_{ij} - K_{ij}) \right] \qquad (3.7)$$

where ε_i is the energy of orbital i, obtained from molecular orbital (wavefunction), φ_i; J_{ij} is the classical Coulomb repulsion between pairs of electrons; and K_{ij} is the *non-classical* exchange term, brought about by the fact that electrons of the same spin tend to avoid each other, as two electrons in an orbital must have opposite spins. The summations are taken over all occupied orbitals. The total orbital energy is simply the sum of the energies of the up-spin (alpha) and the down-spin (beta) electrons in a spin-unrestricted calculation.

In the LCAO approach, the molecular orbitals, φ_i, are expressed as a linear combination of basis functions, ϕ_i, and the problem is reduced to solving the coefficients of the expansion that give the lowest energy. The basis functions can, in principle, be the STOs described earlier. Using the STOs in molecular systems turned out to be difficult, due to the fact that some of the integrals become almost impossible to evaluate, especially when orbitals are centered around different nuclei. This led to the use of the so-called Gaussian Type Orbitals (GTOs), whose usefulness arose from the ease with which Gaussian functions can be manipulated algebraically. When two Gaussian functions are multiplied together (could be centered on different nuclei), the resultant function is still a Gaussian.

As an example, the following function has the symmetry of an s atomic orbital;

$$g_s = (\frac{2\alpha}{\pi^3})^{3/4} e^{-\alpha r^2} \qquad (3.8)$$

There are other Gaussian functions whose symmetry resembles the p and d functions.

The atomic orbitals in molecules are consequently replaced by GTOs as basis functions, to be used in the LCAO calculation of the total electronic energy and wavefunction. A *minimal basis* set contains the minimum number of functions required to accommodate all the filled orbitals in each atom. STO-nG basis sets are minimal basis sets in which *n* Gaussian functions are used to represent each orbital. The radial exponents of the Gaussians are not allowed to vary in size during a calculation. This implies that the same size Gaussians are used for atoms of different sizes. This makes the minimal basis sets unsuitable for large molecules. A *double zeta* basis set doubles the number of functions in the minimal basis set, thereby increasing the accuracy.

Core orbitals, unlike valence orbitals, do not affect bonding in a molecule. Therefore, a minimum number of basis functions can be retained for the core orbitals, and only doubled for the valence orbitals. Such basis sets are known as the *split-valence* double zeta basis sets. An example of such a basis set is the 3-21G basis set, where three Gaussians are used to represent the core orbitals, with the valence orbitals also represented by three Guassians: two for the 'contracted' part and one for the 'diffuse' part. The accuracy can be increased further, with an increase in computation cost, by adding *polarisation* functions (e.g a p orbital for hydrogen and a d orbital for first- and second-row elements). A 6-31G basis set with an added polarisation function is written 6-31G*. The basis sets can further be improved by adding *diffuse* functions, which account for existence of electron density very far from the nucleus, e.g anions and molecules with lone pairs. The presence of '+' in the basis set representation indicates the presence of a diffuse function. These types of functions are employed in ab initio codes such as GAMESS US [Schmidt et al., 1993] and GAUSSIAN [Frisch et al., 1995]. It is sometimes desirable in publications to describe fully the number of atomic functions used in the creation of a basis set for a particular atom. For example, the notation {12s7p2d/6s4p1d} for an oxygen basis set means that 12s, 7p and 2d atomic functions were contracted to form a basis set that contained 6s, 4p and 1d functions that formed a basis set to represent the $1s^2 2s^2 2p^4 3d^0$ electronic configuration for an oxygen atom. A disadvantage of using small analytical basis functions arises from their inadequacy in calculating interaction energies between two species, A and B. Basis set superposition error (BSSE) occurs as a result of the fact that the basis set of molecule A, can describe the approaching molecule B, and vice versa. As a result,

in the complex AB each molecule A or B is being described by a larger basis set that in its isolated form. For accurate interaction energies, the significance of BSSE has to be checked, or large basis sets (e.g. triple zeta basis with valence and polarisation functions (TZVP)) have to be used. BSSE is typically smaller in programs that employ numerical basis sets, for example the density functional theory (DFT) code DMol^3 [Delley, 1990 and 2000]. In this case, the basis sets are not given as analytical functions but as values on an atom-centred spherically symmetrical mesh, with a defined cutoff radius. In the counterpoise correction method, the entire basis set is included in all calculations to estimate BSSE [Leach, 2001].

3.4.4. Relativistic Effects

The non-relativistic Schrödinger equation uses the rest mass of an electron. According to relativity theory,

$$m = \frac{m_0}{\sqrt{(1-\frac{v^2}{c^2})}} \tag{3.9}$$

where, for a given particle, m_0 is the rest mass, m is the actual mass, v is the velocity of the particle and c is the speed of light. Therefore, the non-relativistic Schrödinger equation assumes by definition that the velocity of light is infinite. For atoms with heavy nuclei, the core electrons travel at very high velocities to remain in orbit (due to the large nuclear charge). Consequently, their mass is significantly different from their rest masses. The atom is therefore slightly contracted in a relativistic treatment, because the Bohr radius is inversely proportional to the electron mass:

$$a_o = \frac{4\pi\varepsilon_0\hbar^2}{mZe^2} \tag{3.10}$$

Also the higher s electrons, e.g. the 6s electrons, occasionally visit the nuclear neighbourhood and, while there, reach high velocities. Another essential characteristic that is not captured by the non-relativistic Schrödinger equation is the coupling between the orbital angular momentum of the electron (l) and its spin angular momentum, s. The total angular momentum of an electron is, therefore, given by j =

$l+s$. Since s = +/- ½, a p shell (l=1) , for example, would split into $p_{1/2}$ and $p_{3/2}$ subshells. Similarly, a d shell (l=2) becomes $d_{3/2}$ and $d_{5/2}$ subshells. This spin-orbit splitting is seen experimentally and cannot be predicted from the spin-independent non-relativistic Schrödinger equation. Calculations that include mass-velocity corrections in the Hamiltonian but only average-out the spin-orbit interaction effects are known as scalar-relativistic calculations. The best known fully relativistic theory of electronic structure is the Dirac equation. This equation is, however, difficult to solve, and is not implemented in standard quantum chemistry packages.

3.4.5. Effective Core Potentials (Pseudopotentials)

Effective core potentials (ECPs), or pseudopotentials, can be employed to indirectly account for relativistic effects in heavy atoms. The chemically inert core electrons are replaced by a pseudopotential (or an effective core potential) which assumes a zero value outside the core region of the atom. The pseudopotential approximation basically states that the valence electrons interact with some sort of an average potential in the core of the atom. Therefore, the core electrons are not included in the calculation, and only the basis set for the valence electrons is needed for calculation. The potential term in the Hamiltonian is modified by the ECP, and the Hamiltonian then acts on the wavefunction of the valence electrons only. For each electron in the valence region, its angular momentum will determine how it interacts with the core region. The form of the pseudopotentials is usually such that its parameters depend on the angular momenta (s, p, d or f). In selecting the pseudopotential parameters, the ultimate goal is to reproduce the total-valence energies obtained from highly-accurate (often quasi-relativistic) all electron wavefunctions with the pseudo-orbital energies outside the core region, defined by some cut-off radius. The reference data for the choice of parameters may also come from experiment. The charge of the pseudo-orbitals inside the core region may be the same or different from that of the all-electron valence orbitals, depending on whether the pseudopotential is norm-conserved or ultrasoft.

3. 5. Density Functional Theory

Inherent in the Hartree-Fock method is the assumption that each electron moves in an average field created by the other electrons. Therefore, the fact that electrons have highly correlated motions is only partially taken into account. This makes Hartree-Fock theory unsuitable for the study of systems with high concentration of electrons, like transition metals. While a few methods exist for taking into account the electron correlation much more accurately, e.g. the Moller-Plesset Pertubation Theory, the Configuration Interaction (CI) Method, Coupled-Clusters with Singles and Double Exitations (CCSD) or with CCSD with pertubative triple excitations (CCSD(T)), they remain computationally expensive for treatment of most problems in heterogeneous catalysis. The most useful method, at least from a surface science point of view, is the Density Functional Theory (DFT).

The basic idea in DFT is that the ground-state total energy of a system depends on its electronic density, ρ. The constituents of the total energy can be written:

$$E(\rho) = T_0(\rho) + U(\rho) + E_{xc}(\rho) \tag{3.11}$$

where T_0 represents the kinetic energy, U the classical Coulomb interaction between all particles of the system, and E_{xc} is the exchange-correlation energy. The kinetic and Coulomb energies are not very different from their Hartree-Fock meaning. The exchange-correlation energy principally contains all the other interactions that are required to reproduce the total energy exactly. The form of this exchange-correlation energy functional is not known exactly, and different DFT functionals basically differ in their representation of this term. The derivative of the exchange-correlation energy with respect to the electron density gives the exchange-correlation potential:

$$\mu_{xc} = \frac{\partial E_{xc}[\rho]}{\partial \rho} \tag{3.12}$$

which will be added to the potential in the Hamiltonian operator:

$$\left(-\frac{\hbar}{2m}\nabla^2 + V(r) + \mu_{xc}(r)\right)\psi_i(r) = \varepsilon_i \psi_i(r) \tag{3.13}$$

The Schrödinger equation can be solved for the one-electron orbitals, also called the Kohn-Sham orbitals, from which the electron density, ρ, at any given point, r, can be calculated:

$$\rho(r) = \sum_{i=1}^{N} |\psi_i(r)|^2 \qquad (3.14)$$

Solving the DFT equations is an iterative procedure starting from 'guess' wavefunctions, even though in principle the wavefunctions are not necessary for evaluation of 3.11. The self-consistent field (SCF) procedure in DFT consists essentially of (i) choosing an initial set of coefficients to expand basis sets, (ii) constructing a set of molecular orbitals (wavefunctions), (iii) using the trial set of molecular orbitals to construct the electronic density according to Equation 3.14, (iv) using the obtained density to calculate the Coulomb and the exchange-correlation potentials, a new set of molecular orbitals and the electronic density. The procedure is repeated until the input and output densities agree to some tolerance value. This is then the density used to evaluate the total energy (see Equation 3.11).

A few suggested forms of the exchange-correlation energy can be found in literature [Leach, 2001 and Wimmer and Freeman, 2000]. When the exchange-correlation energy at a point, r, depends only on the local density, ρ(r), then the DFT method is said to be 'local', giving rise to the name local density approximation (LDA). If the exchange-correlation energy depends also on the gradients of the density, then the method is said to be 'gradient-corrected', giving rise to the gradient generalized approximation (GGA). Pure GGA fails in describing the adsorption of oxygen molecules on gold clusters [Ding et al., 2004], overestimating adsorption energies by 0.2-0.4 eV. Hybrid functionals perform better. For calculation of reaction barriers, the LDA underbinding of core electrons results in underestimation of the barrier heights relative to GGA estimations [Hammer et al., 1993].

3.6. Extended Hückel Theory

Extended Hückel Theory (EHT) was developed in the 1960s as an alternative theory to the computationally expensive ab initio based methods [Hoffmann, 1963]. In this theory, the coupling between two STOs is calculated from the simple expression:

$$H_{ij} = 0.5K(H_{ii} + H_{jj})S_{ij} \quad (3.15)$$

where H_{ij} is the coupling energy, H_{ii} are the experimentally derived orbital energies and S_{ij} is the overlap (which is not necessarily zero since the orbitals in question would not necessarily be orthogonal). K is a constant that was initially set to 1.75. The simplicity of this method makes it possible to study hundreds of atoms in a fraction of the time that would be required with DFT or *ab initio* methods. EHT is not reliable at all for quantitative determination of energeties, but the trends derived from such calculations can be useful in uncovering the chemistry involved in a catalytic process. Examples of EHT-based software are the freely YAeHMOP [Landrum and Glassey, 2001] and CACAO [Mealli et al, 1998]. The validity of EHT results should always be checked with more sophisticated methods like DFT.

3.7. The Solid State Physics Approach

With current computational techniques, the surface of a solid can be studied by considering it as a slab of finite thickness, and infinite in the other two dimensions. The 'infinity' problem is tackled by assuming that the constructed lattice is periodic, and therefore only a unit cell of the complex with periodic boundary conditions is employed for calculations. The 'surface' is created by employing a vacuum region in the z-direction, large enough to minimise interaction between cells in this direction. For any position in a lattice with vectors **a**, **b** and **c**, represented by the general vector:

$$\mathbf{r} = (x\mathbf{a}, y\mathbf{b}, z\mathbf{c}), \quad (3.16)$$

the electronic wavefunctions have to satisfy Bloch's theorem:

$$\psi(\mathbf{r}+\mathbf{T}, \mathbf{k}) = e^{i\mathbf{k}.\mathbf{T}}\, \psi(\mathbf{r},\mathbf{k}) \quad (3.17)$$

where **k** is an index (called a wavevector, which has components in the x, y, and z directions) that characterises the wavefunction, and **T** is a translation by integer multiples of the lattice vectors, thereby mapping position **r** into an equivalent position on another unit cell. The wavefunction, ψ, would typically be a linear combination of atomic basis functions, and a **k** value determines how the these atomic orbitals combine with each other. Some **k** values will give combinations that result in a wavefunction of low resultant energy, while other combinations give the total wavefunction that result in a high total energy. A graph of energy versus **k** is called a band structure. The real space vectors, **a**, **b**, and **c**, for a unit cell can be converted to reciprocal space vectors, **a***, **b***, and **c***, using some mathematical relations. Different values of **k** will correspond to different points in the reciprocal lattice defined by the reciprocal space vectors. A unit cell in reciprocal space (also called k-space) is called the first Brillouin zone, and it is the cell usually considered to calculate the band structure of a solid.

While localised basis sets can still be used for construction of the wavefunctions in periodic systems, the non-atom centred *plane waves* are generally preferred for their inherent periodic nature and, hence, mathematical simplicity. The wavefunctions are expanded in a set of these plane waves:

$$\psi(\mathbf{r}, \mathbf{k}) = \sum_j c_j \; e^{i(\mathbf{k} + \mathbf{G}_j) \cdot \mathbf{r}} \qquad (3.18)$$

where **G** is a lattice vector in reciprocal space.

The larger the number of plane waves, the more accurate the calculations. In general, the core electrons in an atom require an even larger number of plane waves due to their high kinetic energy (meaning the wavefunctions have high curvature). This computational difficulty is eliminated by using pseudopotentials for core electrons whose kinetic energy is above a certain cutoff. Pseudopotentials can either be norm-conserving (meaning the electron density of the valence electrons in the core region is reproduced exactly) or ultrasoft. The former requires large cutoff energies. This methodology is implemented in various commercial solid state software, like CASTEP [Segall et al., 2002]. The solid state approach usually gives surface

chemisorption results that can be directly compared with experiment. In CASTEP, the k-point grid for the Brillouin-zone integrations are chosen according to a scheme developed by Monkhorst and Pack [1976] and extended by Froyen [1989]. Each point in a specially generated grid of k-points in the Brillouin zone is given a weight equal to the inverse of the number of points. The grid is reduced to the irreducible part of the zone by examining each pair of points to check if they are related by an element in the point-group symmetry. Should a given pair of points be related by symmetry, one of the points is removed and its weight is added to the weight of the remaining point.

3.8. Cluster vs Periodic Approaches in Catalysis Research

Catalytic processes involve the interaction between a molecule and a surface. If it is assumed that such interactions are local, then the cost of the computation can be reduced by using only a few atoms (from a single atom up to ~50 atoms) to model the surface. The few atoms are typically chosen to represent what is thought to be the 'active site'. The calculations will then proceed in the conventional quantum chemical sense as if the molecule-surface complex were a 'supermolecule'. The usefulness of the results will, therefore, depend on the proper choice of the active site. The cluster approach has been widely used to study the energetic details of elementary steps in catalytic processes, and also to study the effect of modifiers on such processes. The full methanol partial oxidation pathway has, for example, been studied over the Cu(111) surface using Cu_{22} clusters [Illas et al., 2001]. The promotional role of potassium in CO_2 chemisorption onto a platinum surface was explained by studying $Pt_{16}CO_2$, $Pt_{16}KCO_2$ and $Pt_{16}K_3CO_2$ clusters.

There are, however, a few cautionary points that must be mentioned about the cluster approach. Firstly, the fact that the cluster chosen to represent the surface will be finite brings about the edge effects that might not exist in a real surface, where the adsorbate molecule may not 'feel' the presence of edges. The seriousness of this problem depends on the system being studied, because for very small dispersed metal particles (less than ~2 nm) the edge effects exist in reality and are sometimes *required* for high catalytic activity due to reduced coordination of the corner atoms [Van Hardeveld and Hartog, 1969]. The second problem with the cluster approach is the use of discrete metal orbitals which are localised on atoms. This is inconsistent with the accepted

notion of bonding in the metallic state, where the orbital energy levels are continuous. Furthermore, the electrons in a solid are generally delocalised and not centred around specific nuclei. For very small metal particles, the discreteness of energy levels and the localisation of electrons is a reality, therefore the cluster approach remains satisfactory.

As with the cluster approach, the solid state approach has its cautionary notes. For example, while particles above ~5 nm might behave like a bulk surface, the electronic properties of small metal particles may differ significantly from those of the extended surface, thus changing the surface reactivity. Therefore, the choice between the cluster and the solid state approaches depends on the system being studied and the properties of interest, and to understand all the relevant physics and chemistry of a surface, it is much more fruitful to employ both methodologies.

3.9. Locating Transition States

For a detailed understanding of the kinetics of an elementary step, it is important to know the barrier between the reactants and the products. A local minimum on the potential energy surface is characterized by a zero first derivative of the energy with respect to all the coordinates, and a positive second derivative. The highest energy point along a shortest route joining the two energy minima is a transition state. DMol^3 [Delley, 1990 and 2000] and CASTEP [Segall et al., 2002] use the so-called the synchronous transit method. The method is described in detail by Govind et al. [2003]. Basically, a number of single-point energy calculations are performed on a set of linearly interpolated structures between the reactant and the products. The highest energy point is the linear synchronous transit (LST) estimate for the transition state. The LST-obtained structure is then refined once in a direction orthogonal to the LST path. Based on this structure, a quadratic interpolation connecting the reactant and product is defined, and a QST maximum is determined and refined. An energy maximum, or transition state, is found when the first derivative of the energy with respect to the coordinates fall below a certain tolerance value. The LST/QST-calculated maxima from CASTEP calculations cannot really be confirmed as true transition states because second derivatives cannot be calculated.

3.10. The QM/MM Embedding Method

Solids such as zeolites and oxides are still difficult to treat via a either QM or MM methods alone. This is because a large number of atoms are required to reproduce the electric properties of the material. In response, various quantum mechanics/molecular mechanics (QM/MM) hybrid methods have been developed to address this problem. In this method, a portion of the crystal ('the active site') is treated via a high level QM method, while the crystal remainder is treated by MM using interatomic potentials. The active site can, for example, be a vacancy on an oxide or an area where an adsorbate interacts with the oxide. The advantage of this method is that the long-range steric effects as well as electrostatic influence of the crystal on the active site are taken into account. Various methods differ in the way in which the interface region between the QM and MM regions are described, as well as whether polarisation of ions in the MM region is allowed or not. In the most recent QM/MM embedding method by Sherwood et al. [2003], the potential into which the active site is embedded consists of the system remainder combined with pseudopotentials located at the QM/MM boundary. This is a physically more reasonable method of coupling the MM to the QM region than methods employing 'guest' atoms (like hydrogens) at the boundary as link atoms [Sherwood et al., 1997]. The pseudopotentials, generally placed on the cations, ensure that electrons in the QM region remain localised in this region. For ionic solids, the anions in the MM region are represented via the shell model. The total energy is then simply the sum of the QM and MM contributions, which are calculated self-consistently allowing for ionic relaxations. As the cluster is generally finite, point charges are added around the QM/MM cluster to reproduce exactly the electrostatic potential at the QM region. The computational chemistry software, Chemshell, is used as an interface between the QM software (e.g. GAMESS-UK), and the MM software (e.g. GULP). The theory is described in detail by Sherwood et al. [2003], Sokol et al. [2003] and Bromley et al. [2003]. Briefly, the total energy is given by:

$$E^{Total} = E^{QM} + E^{MM} \tag{3.19}$$

In addition to the short range interactions within both the QM and MM regions, the two regions also interact with each other. The QM region responds to the field of the

MM region electronically, while shells in the MM region allow this region to respond to the electron density in the QM region.

The energy in the QM region is given by:

$$E^{QM} = \int \Psi [H^{QM} + V^{short} + V^{long}] \Psi d\tau + U_{NN} + U_N^{long} \quad (3.20)$$

where H^{QM} is the many electron Hamiltonian of the QM region, V^{short} is the short-range potential of the immediate environment around the QM cluster (commonly represented by pseudopotentials at the interfacial region), V^{long} is the long-range Coulomb potential for the crystal remainder, U_{NN} is the Coulomb interaction between the nuclei in the QM region, while U_N^{long} is the Coulomb interaction between nuclei in the QM region and those of the crystal remainder.

The energy of the MM region, E^{MM} is simiply the sum of the classical interactions of the ions in the MM region, evaluated from forcefield or interatomic potentials. Most importanty, the polarisable shells are represented by harmonic and quartic terms:

$$E_i^{shell} = (1/2)k^2r^2 + (1/12)k^4r^4 \quad (3.21)$$

where r is the shell-core separation.

Since computational costs limit relaxation of the solid ions to a certain radius from the QM centre during calculations, polarization energy corrections must be added to the total energy in 3.19 to account for long-range polarisation of the crystal by charge species introduced at the QM region. Integration of the electrostatic energy of the crystal from a distance R to infinity yields, for surfaces, the correction term:

$$W_p = -\frac{q^2}{2R}\frac{\varepsilon - 1}{\varepsilon + 1} \quad (3.22)$$

where q is the polarising charge in the QM region and ε is the static permittivity of the dielectric.

This method has been found appropriate for the study of metal-support interactions, where the metal and a section of the support are selected as the QM region, and embedded into an MM-treated lattice. Nasluzov et al. [2001 and 2003] propose similar models for treating both ionic and covalent solids.

Chapter 4

ELEMENTARY STEPS IN CO_X (X=1,2) HYDROGENATION TO METHANOL ON A GOLD SURFACE: PERIODIC AND CLUSTER DFT STUDIES

The energetics of CO and CO_2 hydrogenation to methanol on gold surfaces were studied via periodic and cluster DFT calculations. On a slab model of the Au(111) surface, CO hydrogenation appears to be much easier than CO_2 hydrogenation. The use of a cluster model yields CO_2 hydrogenation energetics that are similar to the surface results. Hydrogen addition to an oxygen atom seems more favoured than addition to a carbon atom. Adsorption of CO and H_2 is more facile on the cluster model, suggesting that nanosized gold particles or stepped surfaces may be beneficial in gold-catalysed CO hydrogenation.

4.1. Introduction

The applications of elemental gold in heterogeneous catalysis are significantly fewer than those of its neighbour in the periodic system, platinum, and its coinage-group partners, copper and silver. This is due to its bulk state resistance to oxidation, which led to little initial interest in exploring its catalytic properties. However, recent research indicates that gold nanoparticles supported on certain metal oxides are highly active for a large number of reactions that are important in both pollution control and chemical synthesis, for example the conversion of synthesis gas (syngas) to methanol [Bond and Thompson, 1999]. In most cases, e.g. for CO oxidation, the high activity of small particles is not a simple surface area effect because the turnover frequency based on surface atoms increases sharply below a gold crystallite diameter of 5 nm [Bond and Thompson, 1999 and Haruta, 1997]. Periodic DFT calculations have shown that stepped Au surfaces (e.g. Au(211) and Au(221)) can bind CO and O much more strongly than the Au(111) surface [Liu et al., 2002; Mavrikakis et al, 2000]. The barriers to both the CO + O_2 coupling reaction and O_2 dissociation are lower on the stepped surfaces [Liu et al., 2002]. Atoms on steps have lower coordination and higher-lying d-states than atoms on a planar surface, making them much more reactive in agreement with the d-band centre model [Ruban et al., 1997]. Statistically, the proportion of low coordination atoms increases as the crystallite size decreases. A recent DFT study, however, has shown that CO oxidation on the planar Au(111) surface has a lower barrier than on Cu(111) and Pt(111) surfaces [Kandoi et al., 2004]. There is also an interest in the interaction gold surfaces with adsorbates that may be involved in synthesis gas conversion [e.g. Gomes and Gomes, 2000a and 2000b].

Currently, methanol synthesis from syngas (a mixture of CO, CO_2 and H_2) is usually carried out using copper catalysts. A number of theoretical studies have been undertaken to elucidate the reaction mechanism [Hu and Nakatsuji, 1999; Kakumoto and Watanabe, 1997; Morikawa et al., 2001 and French et al., 2001]. Studies on the reverse reaction, methanol decomposition, on are also relevant [Greely and Mavrikakis, 2002a and 2002b; Gomes and Gomes, 2001; Desai et al., 2002].

Frost [1988] proposed that any metal with a large enough workfunction to form a Schottky barrier with a semiconducting oxide (e.g. ZnO) will increase the methanol productivity of the oxide, on the assumption that methanol synthesis occurs on the oxygen vacancies. Although this theory is not without controversy [Shaw et al., 1992], it resulted in a prediction that gold and silver, like copper, should be active for methanol synthesis since they have comparable workfunctions. Baiker et al. [1993] reported that Au/ZrO_2 had some activity for CO_2 hydrogenation to methanol at temperatures between 130°C and 250°C at 17 bar pressure. The methanol selectivity was, however, lower than that obtained for Cu/ZrO_2 and Ag/ZrO_2 catalysts, which is thought to be due to Au/ZrO_2's high activity for the reverse water-gas shift reaction. Carbonate, formate and formaldehyde were identified on the catalyst surface by IR studies. Sakurai and Haruta [1995 and 1996] have shown that Au/ZnO, Au/Fe_2O_3 and Au/TiO_2 catalysts are active for methanol synthesis from both CO/H_2 and CO_2/H_2 mixtures. Of all tested metal oxide supports, ZnO resulted in the highest methanol selectivity (comparable to copper-loaded ZnO), and the methanol synthesis activity per surface gold atom increased with a decrease in gold crystallite size. These results indicate that the nature of the support is of importance in gold-catalysed methanol synthesis. In a previous theoretical study, the route: CO_2 – HCOO – H_2CO – H_2COH – H_3COH was identified as a thermodynamically viable route to methanol from CO_2 on a single Au atom [Phala et al., 2003]. This study was undertaken at the B3LYP//HF level using single metal atoms as active sites. In the work presented here, the pathways for both CO and CO_2 hydrogenation, including reaction barriers, were computed on a slab model of an Au(111) surface. The Au(111) surface was chosen since it is expected that large (>5 nm) Au particles might adopt this closely packed structure to minimise their surface energy. Energetically demanding steps on this surface were identified, and possible coordination effects are discussed with reference to calculations on an Au_{13} cluster as a model for a gold nanoparticle.

4.2. Computational Details

4.2.1. Periodic Calculations

All slab calculations reported in this chapter were performed with the PW91-GGA density functional [Perdew and Wang, 1992] as implemented in the CASTEP program [Segal et al., 2002]. Mavrikakis et al. [2000] have shown that the reactivity of an Au(111) slab does not change significantly as the number of gold layers increases from 2 to 6. Previous studies on methanol decomposition over Pt(111) have shown that the reaction energetics remain within DFT accuracy as the number of layers increase from 3 to 6 [Desai et al., 2002]. The influence of the third-layer onwards is expected to be significant for adsorbates bonded to a hollow site of a reactive metal [Watson et al., 2001]. This is especially true for the fcc hollow site, which requires at least three metal layers to model. In this work, a two-layer Au(111) slab consisting of a total of 6 Au atoms per unit cell was chosen as a surface model. This corresponds to an adsorbate coverage of 0.33 monolayers (ML), at which equivalent atoms in adjacent unit cells are ~5 Å apart. However, non-equivalent oxygen atoms of the bidentately bonding species like dioxomethylene (see Figure 4.2) were found to be only 3.2 Å away from each other in adjacent unit cells. This might lead to significant energy changes for the bidentate species as the coverage is decreased. Experimentally, CO adsorption energy on 0.5ML Au/TiO_2 remains unchanged with coverage up to 35% coverage, after which the adsorption energy decrease sharply with coverage [Meier and Goodman, 2004]. Vanderbilt ultrasoft pseudopotentials [Laasonen et al., 1993] were used to describe the ionic cores. The Brillouin zone was sampled by a 3x3x2 Monkhorst-Pack grid of k-points (9 special k-points). The total energy per gold atom for a frozen two layer Au(111) surface was calculated to be 917.21, 917.80, 917.94 and 918.0 eV using cutoff energies of 240, 280, 300 and 320 eV respectively. A plane-wave cutoff energy of 300 eV was subsequently used. Convergence with respect to the number of k-points was checked by way of comparison with the 5x5x2 and 6x6x3 Monkhorst-Pack grids for the reaction and activation energies of the hydrogenation of formate to dioxomethylene, all of which agreed to within 3 kJ/mol. A vacuum region of 8 Å separated the slabs, and the adsorbates were introduced on one side of the slab. Starting configurations for the adsorbates were chosen such that the bonding atoms satisfied their gas-phase bonding valence (i.e. 2 for oxygen and 4

for carbon). As will be shown, this proved to be a reasonable approximation for most adsorbates were alternative bonding sites were selected. Greely and Mavrikakis [2002b] obtained similar obedience of gas-phase bond order rules and coordination for adsorbates and transition states in methanol decomposition on Pt(111). For hydrogen, the bridge position was selected based on gas-phase cluster studies. The Au-Au distance was constrained to the experimental bulk value of 2.88 Å [Maeland and Flanagan, 1964] during the calculations since we expect reconstruction of the already closed packed Au(111) surface in vacuum to be minimal; proper modelling of surface reconstruction would require a large number of layers to account for bulk steric constraints, which was not feasible with the resources that were available. Although fixing the surface metal – metal bond distances to their experimental bulk values is common in the literature [e.g. Greely and Mavrikakis, 2002b], it will lead to strain on the lattice and may lead to significant errors in the calculations. Strongly bound adsorbates, on the other hand, can induce reconstructions or even vacancies on the Au(111) surface [Molina and Hammer, 2002]. Smearing (0.1 eV thermal occupation) was used to facilitate SCF convergence, with the total energies subsequently extrapolated to k_BT= 0.0 eV. Transition states were determined via the complete linear and quadratic synchronous transit (LST/QST) method [Halgren and Lipscomb, 1977] implemented in CASTEP, which also refines the transition state via the conjugate gradient method. Since Au has a filled d-shell, spin polarisation is not expected to have a major influence on its metallic properties; indeed, it was found that the reaction and activation energies for the spin-polarised formaldehyde to methoxy calculation at a single k-point differed from those of the spin-unpolarised calculations by at most 3 kJ/mol. All calculations were consequently performed for spin-unpolarised systems. The Broyden-Fletcher-Goldfarb-Shanno (BFGS) algorithm was used in CASTEP for geometry optimisations. The energy and gradient convergence tolerances were set at $2x10^{-6}$ eV/atom and 0.05 eV/Å respectively.

4.2.2. Cluster Calculations

To investigate coordination effects, the reaction enthalpies of selected elementary steps were computed on an Au_{13} cluster using the DMol^3 software [Delley, 1990 and 2000]. A cuboctahedral Au_{13} cluster has a diameter of about 0.6 nm, a size range that has been encountered in some gold catalysts [Cunningham et al., 1998]. Both the Au(111) surface and the Au_{13} cluster used in the calculations are shown in Figure 4.1. The Au_{13} cluster exposes on-top, bridged, and hollow sites. For fair comparison with the periodic calculations, the PW91 density functional [Perdew and Wang, 1992] was used in the cluster calculations as well. Effective core potentials (ECPs) were used for the Au atoms. A numerical basis set of double-zeta quality with additional polarisation on all atoms (DNP) with a basis set cutoff radius of 5.5 Å was employed. The quality of the DNP basis set is similar to the 6-31G** gaussian basis set, but it is generally more accurate. The band gap is an important electronic parameter determining the reactivity of small molecules. Band gaps calculated for CO, CO_2, H_2CO and CH_3OH with DMol^3 and CASTEP agreed to within 0.3 eV, implying that the difference in energetics results largely from the difference in electronic structures of the Au(111) versus Au nanoparticle systems, rather than from the differences in basis sets and periodicity. All adsorbate degrees of freedom were fully relaxed during geometry optimisations. However the Au-Au distance was constrained to its bulk experimental value of 2.88 Å [Maeland and Flanagan, 1964]. The Broyden-Fletcher-Goldfarb-Shanno (BFGS) algorithm is used in DMol^3 for geometry optimisations. The energy and gradient convergence tolerances were set at $2x10^{-5}$ a.u and $4x10^{-3}$ Ha/Å respectively.

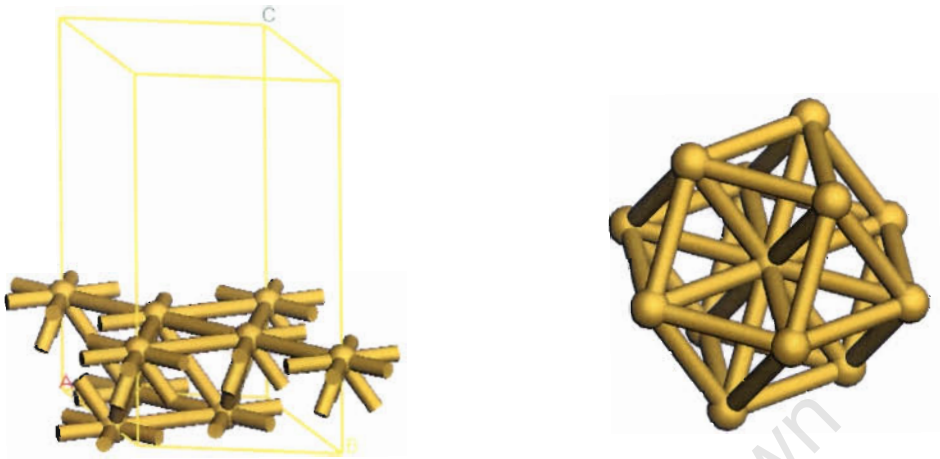

Figure 4.1: Au(111) slab model showing the unit cell (left) and cluster model of an Au_{13} gold nanoparticle (right).

4.3. Structural Features of Potential Methanol Synthesis Intermediates

Most of the calculations were performed on the Au(111) surface in order to determine the intrinsic reactivity of this surface. The CO_x hydrogenation pathways considered in this study are shown in Figure 4.2. Stationary structures from CASTEP geometry optimisations for potential methanol synthesis intermediates are shown in Figure 4.3.

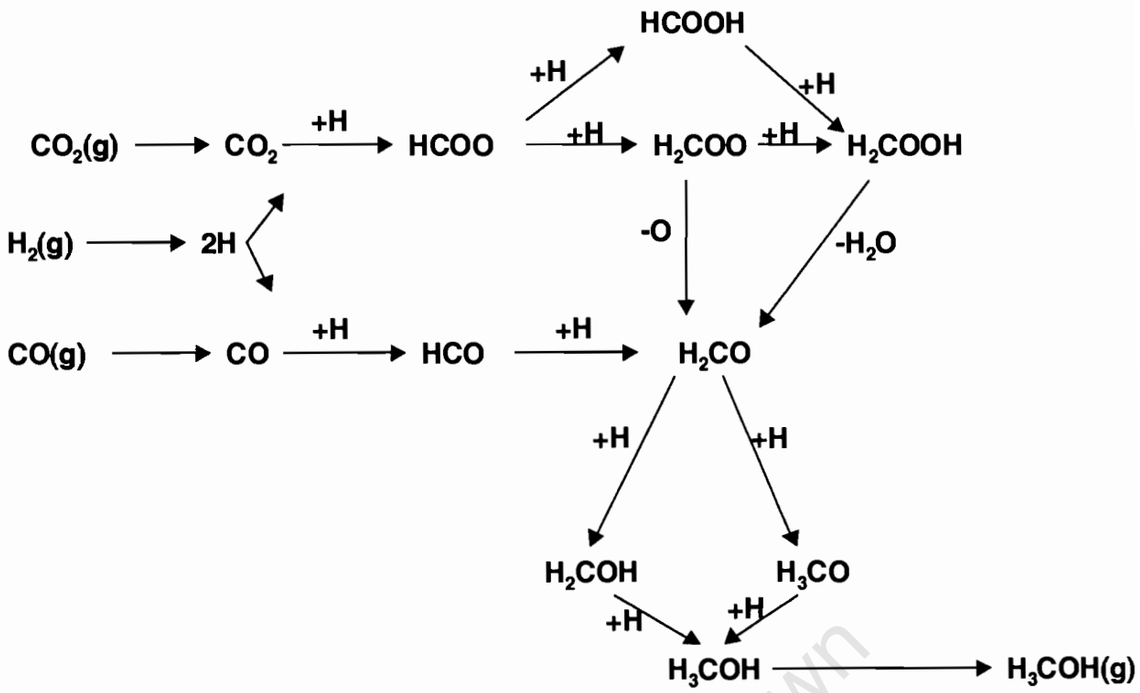

Figure 4.2: CO and CO_2 hydrogenation pathways considered in this study.

Based on cluster model calculations, **hydrogen** was bonded in a bridge-tilted mode to the Au(111) surface. The Au – H distance was 1.80 Å in the optimised structure. The hydrogen was found to lie at a shallow potential well with respect to migration to the hcp hollow site and the on-top site. At the hcp hollow site, the Au – H distance was 1.88 – 1.89 Å, and hydrogen was a mere -2 kJ/mol more stable than at the bridge site, well within DFT accuracy. At the on-top site, the hydrogen is 9 kJ/mol less stable than at the bridge site, and the Au – H distance is 1.59 Å. Other periodic DFT calculations established that H binds preferentially to the hollow sites on Cu(111) and Au(111) surfaces [Kandoi et al., 2004; Greely and Mavrikakis, 2002a], while the chemisorption strengths are similar among the three adsorption sites on Pt(111) [Kandoi et al., 2004; Desai et al., 2002]. **Carbon monoxide** can be stabilized in a tilted-bridge mode, with an Au – C bond length of 2.21 Å. The CO chemisorption energy was identical (agreement to less than 1 kJ/mol) to that for CO bonded on the hcp hollow site and on-top sites, where the Au – C distances were 2.26 and 2.23 – 2.37 Å respectively. CO, like H, appears to be fairly mobile on the surface. At the on-top configuration, the C – O bond axis is tilted slightly to an angle of 35° with respect to the surface normal. At the bridge mode, the C – O bond length is elongated to 1.17 Å, compared to the 1.14 Å calculated for a free CO molecule, which can be rationalised by the principle of bond order conservation around the carbon atom [Shustorovich, 1986; Sellers, 2003]. Greely and Mavrikakis [2002a and 2002b] report preference for the fcc/hcp hollow sites for CO on Cu(111) and fcc hollow site on Pt(111). However, the bridge site is only 7 kJ/mol less stable on Cu(111). It is also reported that the all the {111} faces of Au, Cu and Pt bind CO at the fcc hollow site, but the CO moves to the on-top position when coadsorbed with O [Kandoi et al., 2004]. The 3-fold hollow site is also preferred on Pd(111) by both CO and H [Desai et al., 2002]. Another study pointed out that site preference issue on Pt(111) may depend on the value of the CO band gaps calculated with different DFT functionals [Gil et al., 2003]. **Formyl** bonds on-top an Au atom. When formyl was located at a bridge position and then optimised, the formyl species migrated to an on-top position upon relaxation. This seems to follow the gas-phase bond valency principle employed when choosing starting geometries. On M_{10} clusters, Gomes and Gomes [2000b] found that the formyl carbon was much closer to the Pt surface (1.50 Å) than to Cu (1.91 Å) and Au (2.16 Å) surfaces, and formyl was coordinated in a bridge configuration. The calculated Au - C distance of 2.13 Å in the current work is similar to their

calculations, despite the difference in adsorption sites. On-top coordination of formyl is predicted on Pt(111) slab, with the C – O and Pt – C distances of 1.21 and 2.02 Å respectively [Greely and Mavrikakis, 2002b]. In general, clusters and extended surfaces are not expected to bind molecules similarly due to their different electronic structure. **Carbon dioxide** is only weakly physisorbed to the Au(111) surface. Its C – O bond lengths of 1.17 Å are identical to those calculated for a free CO_2 molecule. Kandoi et al. [2004] also found that CO_2 was very weakly adsorbed on Au(111), Cu(111) and Pt(111) surfaces, and the CO_2 molecule was over 3.6 Å from the surface.

Formate coordinates in a bidentate fashion on-top two bridging Au atoms. The C – H bond lengths for formate and all other intermediates stay within the 1.08 to 1.14 Å range. This is the same geometry as the one obtained on a Cu_{22} model of the Cu(111) surface [Gomes and Gomes, 2001]. The bonding mode of **dioxomethylene** corresponds to that of formate. **Formic acid** interacts with the surface at an O - Au distance of 2.67 Å, indicative of physisorption. **Oxycarbinol** binds to a surface gold atom via a single O atom at a decreased distance of 2.19 Å, compared to formic acid. The starting geometry prior to the optimisation was a bidentate bonding mode. The extra hydrogen atom on the carbon atom reduces the C – O bond order in accordance with the above-mentioned principle of valence conservation around the carbon atom, and hence makes the terminal oxygen more reactive. When the starting geometry of oxycarbinol was with the bonding oxygen on a bridge site, the optimised structure had an oxygen on-top an Au atom (at an Au – O distance of 2.29 Å) but tilted to a bridge site. The structure was 14 kJ/mol higher in energy than the one shown in Figure 4.3. Like CO_2, **formaldehyde** does not bond chemically to the Au(111) surface. The nearest Au-formaldehyde distance of 3.58 Å is indicative of a physisorbed species. This feature of formaldehyde bonding is also observed on Cu(111) surfaces [Greely and Mavrikakis, 2002a; Gomes et al., 2001; Gomes and Gomes, 2001]. Formaldehyde can, however, be stabilised on Pt(111) and Pd(111) surfaces [Greely and Mavrikakis, 2002b; Desai et al., 2002]. Coadsorbed oxygen atom can increase the stability of this intermediate [Gomes et al., 2001]. In the current work, dissociation of formic acid to formaldehyde and atomic oxygen left the formaldehyde still bonded to the surface adjacent to the O atom. Formaldehyde can be considered as a possible CO_x hydrogenation or methanol decomposition/oxidation product on Au(111). **Methoxy** could be stabilized on-top an Au atom. However, it was found that this species, like H

and CO, is fairly mobile on the surface. Two other methoxy species were obtained, which were at most 3 kJ/mol more stable than the on-top position (well within DFT accuracy): a methoxy species on-top an Au atom but tilted to the hollow site (obtained from an hcp hollow starting geometry) as well as a bridge-bonded species. DFT calculations based on M_7 clusters predict that the hollow site is favoured on Au, Ag and Cu surfaces [Gomes and Gomes, 2000a]. For Cu, this conclusion seems to agree with periodic DFT calculations [Greely and Mavrikakis, 2002a] and experimental surface science studies [Johnston et al., 2003]. On Au_7, the binding energy of methoxy on four adsorption sites were within 30 kJ/mol of each other [Gomes and Gomes, 2000a]. Desai et al. [2002] calculated that on Pd(111) and Pt(111) surfaces methoxy prefers the hollow and bridge sites respectively. Greely and Mavrikakis [2002b] predict the on-top site as being the preferred one on Pt(111). It may be that, as calculated for Au(111), the methoxy species sits at a shallow potential well on the Pt(111) surface as well. **Hydroxymethyl**, another possible methanol precursor, again coordinates on-top a gold atom. A starting geometry with hydroxymethyl at the bridge site resulted in a desorbed state of hydroxymethyl, which was 53 kJ/mol higher in energy than the adsorbed state. Hydroxymethyl bonds on-top at Pt(111) and Pd(111) surfaces [Desai et al., 2002]. **Methanol** is weakly adsorbed on Au(111), a fact that desirably facilitates product detachment during methanol synthesis. Weak bonding of methanol occurs also for copper [Johnston et al., 2003; Gomes and Gomes, 2001] and silver [Sun et al., 2000] surfaces. Although methanol seems to bond to the Pt(111) surface via an oxygen atom, the methanol-Pt interaction is weak, with a Pt – O distance of 2.59 Å [Desai et al., 2002].

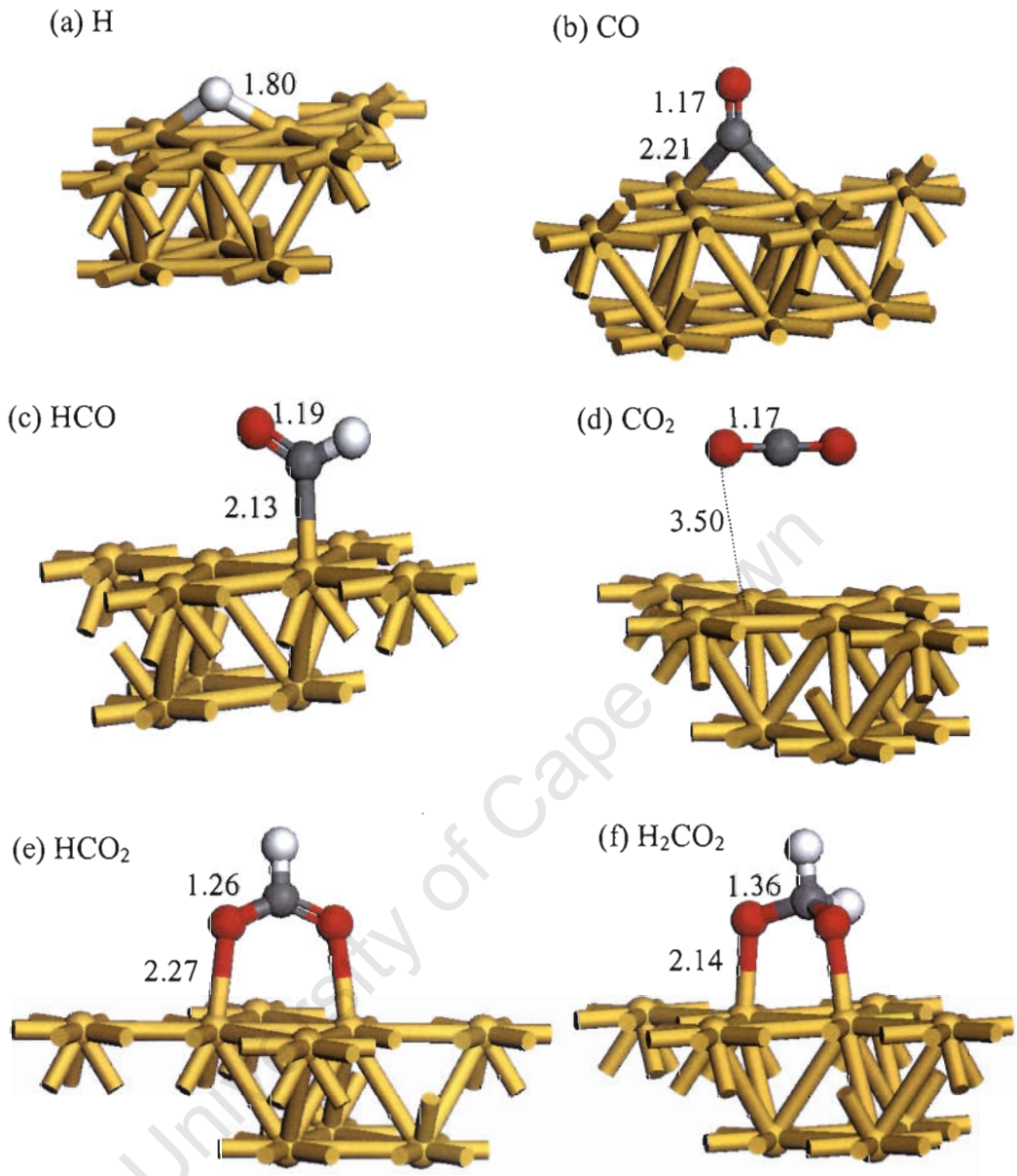

Figure 4.3: Geometries for potential methanol synthesis intermediates on the Au(111) surface: (a) Hydrogen, (b) carbon monoxide, (c) formyl, (d) carbon dioxide, (e) formate, (f) dioxomethylene, (g) formic acid, (h) oxycarbinol, (i) formaldehyde, (j) methoxy, (k) hydroxymethyl and (l) methanol. All distances in Å. Figure continues on next page.

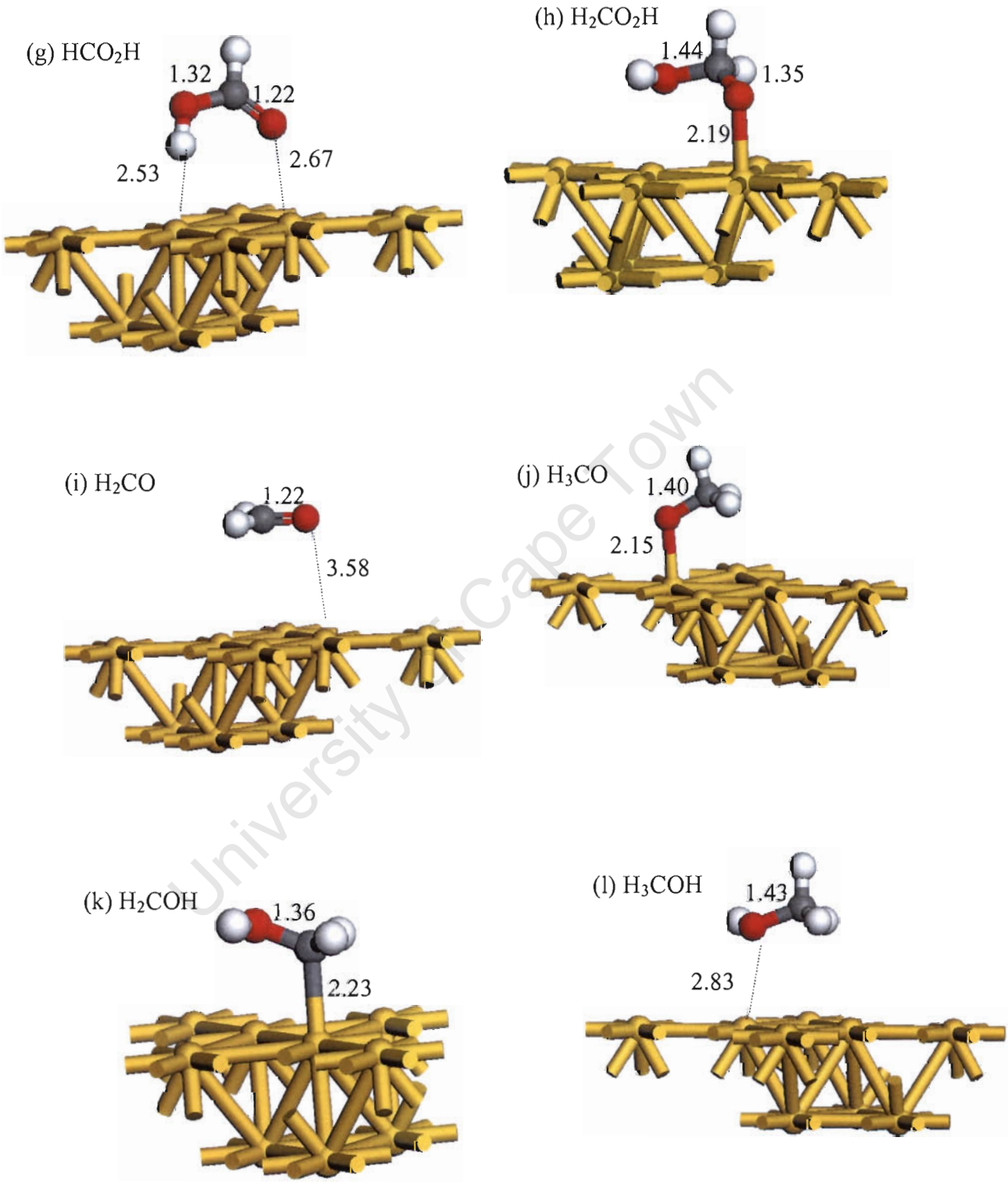

Figure 4.3 Continued

4.4. Methanol Synthesis on an Au(111) Surface

4.4.1. Activation of Syngas Molecules

A schematic of the energetics of the chemisorption of syngas molecules on Au(111) is given in Figure 4.4. Adsorbed species, A*, B* are initially at infinite distance from each other, and subsequently move to neighbouring positions, denoted as A*+ B*. The majority of the species remained in the optimised positions even when coadsorbed with hydrogen. Only hydrogen was switching between the on-top and bridge sites when coadsorbed with other species. Since it has been stated that hydrogen is fairly mobile on the surface, the coadsorption energies that will be reported are mainly due to orbital interactions between the adsorbed species at close distances, and not due to species being adsorbed at non-optimum sites.

The dissociation of hydrogen on Au(111) is endothermic (+60 kJ/mol) and has an activation energy of 129 kJ/mol. These values are in reasonable agreement with the calculations by Kandoi et al. [2004], who calculated an activation energy of 109 kJ/mol and a reaction energy of 41 kJ/mol for hydrogen dissociation on Au(111) using a three layer slab and 0.25ML coverage. The authors also found that hydrogen dissociation is exothermic on Cu(111) and Pt(111) surfaces, and essentially barrier-less on Pt(111). The two hydrogen atoms in the dissociated state have a repulsive coadsorption energy of 27 kJ/mol. Kandoi et al. [2004] calculated a coadsorption energy of 29 kJ/mol. Stobiński et al. [1996, 1997] report a H_2 desorption energy of 57 to 63 kJ/mol on Au films, which is close to the value of 129 – 60 = 69 kJ/mol implied by these calculations. A barrier of 129 kJ/mol is quite high for methanol synthesis to commence easily on an Au(111) surface.

The chemisorption energy of CO on an Au(111) surface is -13 kJ/mol, which is lower than the experimental value of -55 kJ/mol reported on an Au(332) surface [Ruggiero and Hollins, 1996]. Au nanoparticles (1.8 to 3.1 nm in size) on titania give adsorption energies of between -52 and -76 kJ/mol [Meier and Goodman, 2004]. On an Au(100) surface, which is thought to reconstruct to a (5x20) structure, the CO chemisorption energy is -58 (±3) kJ/mol [McElhiney and Pritchard, 1976]. Periodic DFT

calculations by Mavrikakis et al. [2000] give a CO adsorption energy of -64 kJ/mol for an Au(211) surface and -17 kJ/mol on a frozen two layer Au(111) surface (these authors used 54 k-points, a cutoff energy of 408 eV and a 0.25ML coverage). The adsorption energy on a four-layer Au(111) slab was calculated to be -23 kJ/mol for a frozen slab, and -29 kJ/mol when reconstruction of the top two layers was allowed [Mavrikakis et al., 2000]. Including only two layers in this work, and not allowing for reconstruction contribute to the weaker CO binding calculated. Kandoi et al. [2004] calculated a CO adsorption energy of -39 kJ/mol on Au(111). These calculations seem to reasonable agree that a clean Au(111) will not strongly bind the CO molecule. The low coordination gold atoms on the stepped or reconstructed surfaces bind CO more strongly, due to the presence of higher lying d-states [Liu et al., 2002]. CO adsorption energy is calculated to be -168 to -175 kJ/mol on Pt(111) [Kandoi et al., 2004; Greely and Mavrikakis, 2002b; Desai et al., 2002], -76 to -93 kJ/mol on Cu(111) [Kandoi et al., 2004; Greely and Mavrikakis, 2002a], and -191 kJ/mol on Pd(111) [Desai et al., 2002].

Recombination of CO and H to formyl (HCO) will require migration of H towards CO. At the coadsorbed state, the total energy of the CO + H system is 26 kJ/mol higher than if adsorbed CO and H were at infinite separation. This coadsorption or proximity energy will add to the overall activation energy for coupling between CO and H species. CO_2 does not seem to chemisorb onto an Au(111) surface. The adsorption energy of only -4 kJ/mol is indicative of physisorption. This implies that CO_2 hydrogenation will not commence easily on a clean Au(111) surface, unless alternative CO_2 activation sites are provided (e.g. on the support or non-zero-oxidation state metal sites). The weak interaction between CO_2 and the {111} surfaces of Au, Cu and Pt is estimated to be around -9 kJ/mol [Kandoi et al., 2004]. Direct coupling between gas-phase CO_2 and adsorbed hydrogen is the only alternative for methanol synthesis from CO_2 on Au(111), i.e. CO_2 insertion onto a metal-hydride. The energy required to form the coadsorbed state, CO_2 + H, is 12 kJ/mol, understandably small because CO_2 is not close to the surface and the H-CO_2 interactions are therefore very small. However, it may be enough to push CO_2 back into the gas phase.

The results discussed in this section imply that chemisorption of syngas on Au(111) is not strong enough to enable easy subsequent reactions to methanol to proceed. Since this reaction occurs at reasonable rates on Au/ZnO and Au/ZrO_2 catalysts [Baiker et al., 1993; Sakurai and Haruta, 1995 and 1996], the sites responsible for the initial activation of syngas molecules are, therefore, not the Au(111) faces of large metallic gold particles.

4.4.2. CO Hydrogenation to Methanol on Au(111)

Figure 4.5 shows the energetics of CO hydrogenation to methanol on Au(111). The reaction between H and CO to HCO is exothermic by 77 kJ/mol, with an intrinsic activation energy of only 20 kJ/mol. Typically, coadsorption energies were in the range of 0-30 kJ/mol. Recombination of formyl and hydrogen to formaldehyde (H_2CO) is exothermic by 93 kJ/mol, with an activation energy of 32 kJ/mol. Desai et al. [2002] calculated that the reverse reaction sequence, i.e hydrogen abstraction from formaldehyde to formyl and the CO, are all exothermic on Pt(111) and Pd(111) surfaces. Greely and Mavrikakis [2002a] calculated that the methanol decomposition steps on Cu(111) were endothermic. This means that the CO to formaldehyde route is more favoured on Au(111) and Cu(111) than Pt(111) and Pd(111) surfaces. Consequently, Au and Cu should be better methanol synthesis catalysts.

Overall, the transformation of CO to H_2CO on Au(111) occurs with very low reaction barriers. The problematic steps in CO hydrogenation are represented by initial CO adsorption and H_2 dissociation, in turn due to the inability of the Au(111) surface to activate these molecules very efficiently.

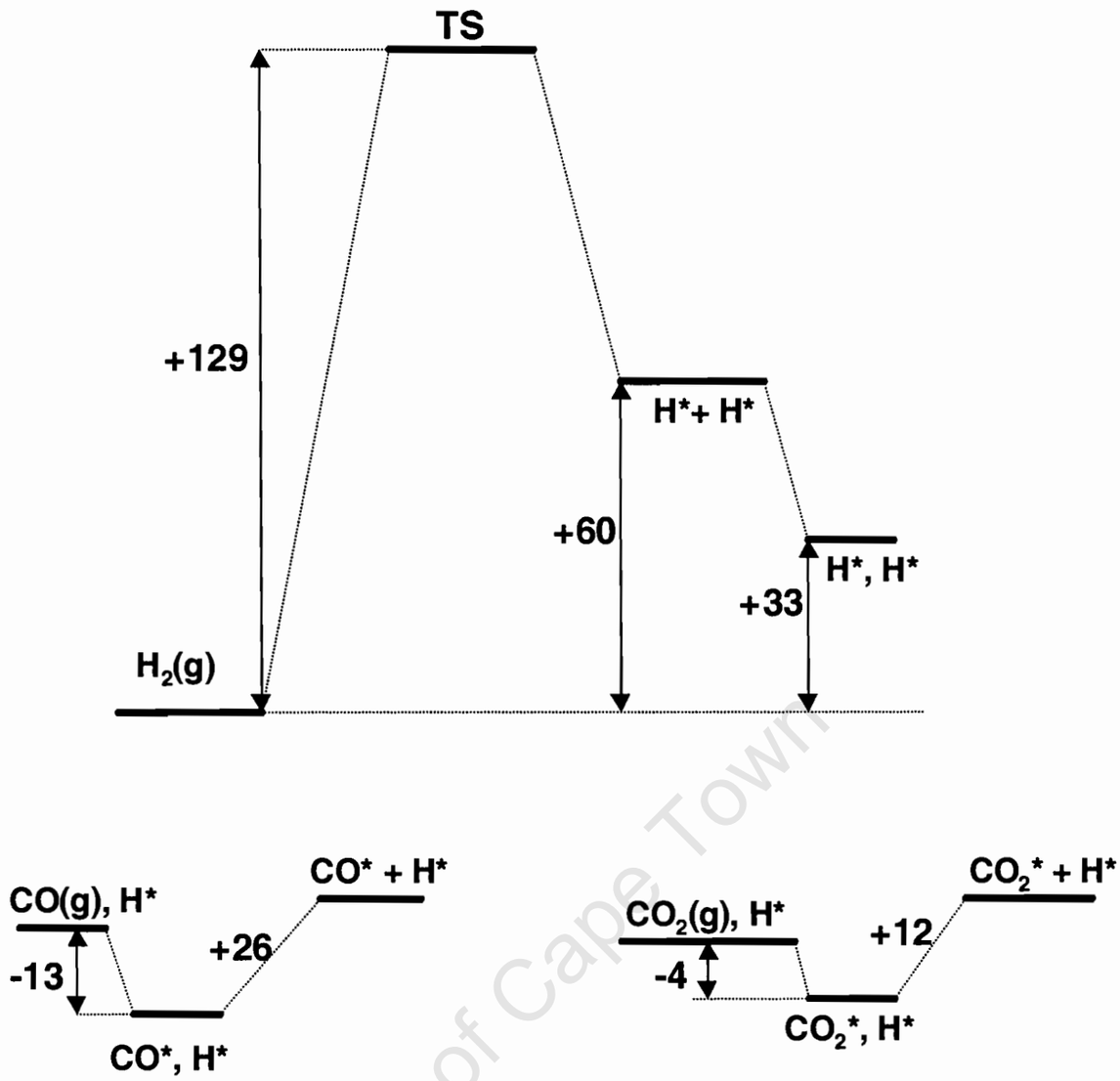

Figure 4.4: Energetics of activation of H_2, CO and CO_2 on Au(111). All energies are in kJ/mol. An asterisk denotes an adsorbed species. A*, B* indicates the energy of A and B at a large separation, while A* + B* indicates the energy of coadsorbed A and B.

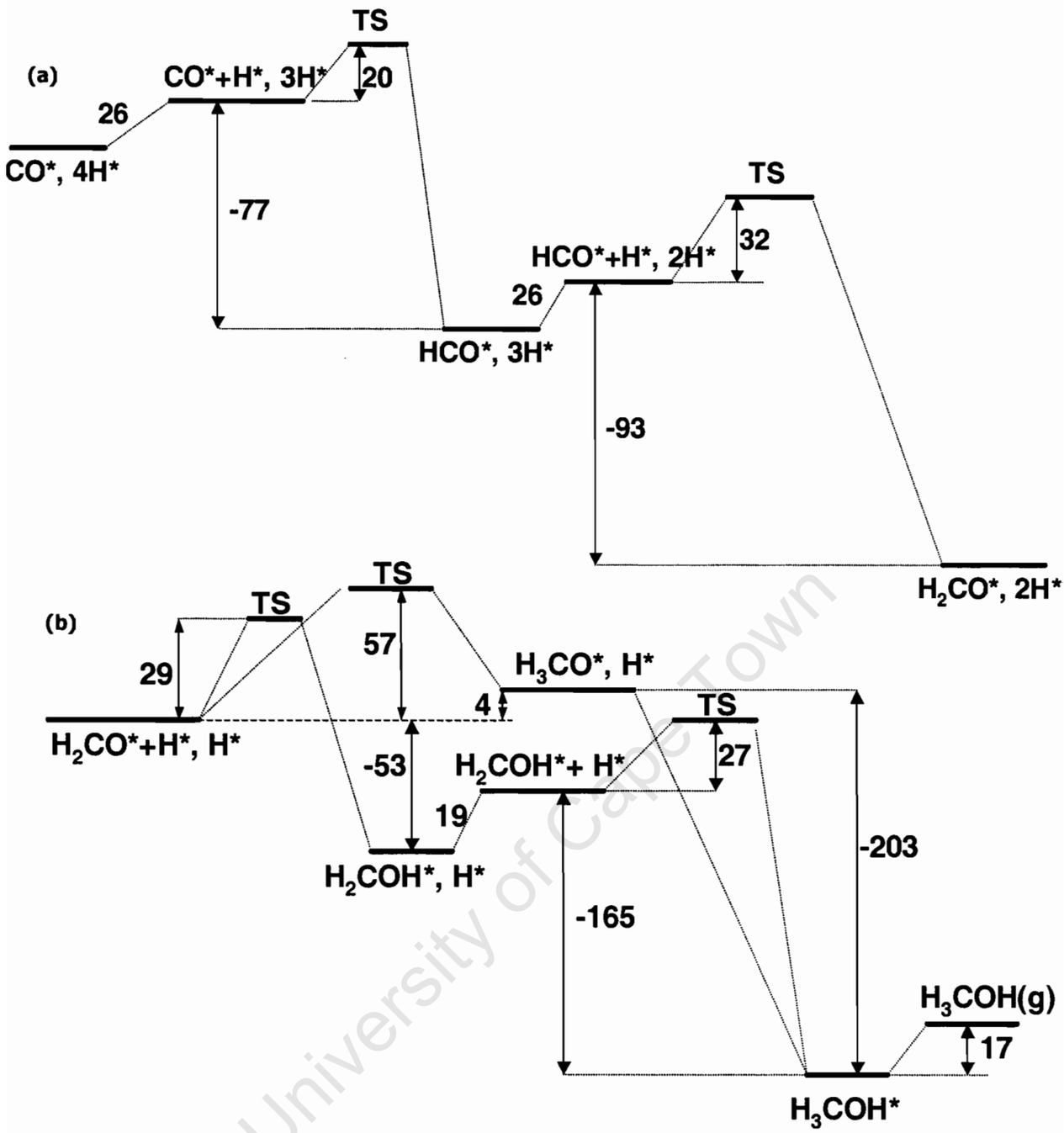

Figure 4.5: Energetics of CO hydrogenation to methanol on Au(111). (a) CO hydrogenation to formaldehyde. (b) Hydrogenation of formaldehyde to methanol. All energies are in kJ/mol. An asterisk denotes an adsorbed species. A*, B* indicates the energy of A and B at a large separation, while A* + B* indicates the energy of coadsorbed A and B.

The hydrogenation of formaldehyde to methoxy (CH_3O) is almost thermoneutral, but the step has an activation energy of 57 kJ/mol. The subsequent conversion of methoxy to methanol will only be diffusion-controlled because methoxy and hydrogen are unstable with respect to the formation of adsorbed methanol. This implies that this step is not activated. Adsorbed methanol has a conveniently small desorption energy of 17 kJ/mol. Greely and Mavrikakis [2002b] and Desai et al. [2002] report methanol desorption energies of 32 and 43 kJ/mol, respectively, on Pt(111), while the desorption energy on Cu(111) is calculated to be 15 kJ/mol. Again, Au and Cu appear to be better suited as methanol synthesis catalysts than Pt.

Alternatively, formaldehyde and hydrogen can couple to form a carbon bonded hydroxymethyl species (H_2COH) by way of addition of a hydrogen atom to the more electronegative O-atom, as opposed to a C-atom addition required for the formation of a methoxy species. The overall reaction is exothermic by 53 kJ/mol, with an activation energy of only 29 kJ/mol. This implies that over the Au(111) surface, formation of hydroxymethyl is both thermodynamically and kinetically more favourable than formation of a methoxy species. Therefore, a methoxy species, commonly assumed to be the key intermediate in Cu catalysed methanol synthesis [Kakumoto and Watanabe, 1997], may not necessarily be the main precursor of methanol over gold catalysts. Previous work [Phala et al., 2003] on single Au atoms using Hartree-Fock (HF) geometries had shown that a gold-hydroxymethyl complex was 50 kJ/mol more stable than a gold-methoxy complex, although hydroxymethyl was oxygen-bonded in that case. On Pt(111) and Pd(111) surfaces, hydrogenation of formaldehyde to hydroxymethyl is exothermic, while hydrogenation to methoxy is endothermic [Desai et al., 2002]. Therefore, on Au, Pt and Pd surfaces hydroxymethyl is a favourable precursor to methanol. Finally, subsequent conversion of hydroxymethyl to methanol has an activation energy of 27 kJ/mol, and the coadsorbed state ($H_2COH + H$) is 19 kJ/mol higher in energy than the separated reactant species.

It is concluded that the conversion of formaldehyde to methanol involves reactions with low barriers and is hence very facile on Au(111). The energetics of initial syngas adsorption should, therefore, be the focus of any attempts to increase the reactivity of a gold surface towards syngas conversion. Furthermore, comparison with literature results shows that Au may be a better CO hydrogenation catalyst that Pt and Pd.

4.4.3. CO_2 Hydrogenation to Methanol on Au(111)

Figure 4.6 shows the energetics of CO_2 hydrogenation to formaldehyde on Au(111). Formate (HCOO) is formed by insertion of CO_2 into the Au – H bond. CO_2 insertion into metal-hydride bonds is known in organometallic chemistry [Gibson, 1999], although surface science analogues have not yet been reported. The activation energy for this step is 257 kJ/mol, while the overall reaction is endothermic by only 23 kJ/mol. A barrier of this magnitude will make the reaction difficult even at 250°C. On a Cu_{22} model of Cu(111), the CO_2 to formate step has a reaction energy of +15 kJ/mol [Gomes and Gomes, 2001]. An apparent source of the large activation barrier might be the bending of the CO_2 molecule. In the transition state, the O-C-O angle was found to be 157°. When a free CO_2 molecule in an 8 $Å^3$ cell was bend to this angle, its single point energy increased by only 38 kJ/mol. This result suggests that mere bending of the CO_2 molecule, without electron transfer, is not the main source of the large activation energy for formate formation. Electron transfer may be the main source of the high activation energy.

Subsequent hydrogenation of formate to dioxomethylene (H_2COO) is the most thermodynamically unfavoured step, being endothermic by 139 kJ/mol. This result is similar to the one obtained on a Cu_{22} cluster, where the dioxomethylene to formate decomposition conversion step was the most exothermic of the dehydrogenation steps, at a reaction energy of -302 kJ/mol [Gomes and Gomes, 2001]. The calculated activation energy on Au(111) is 148 kJ/mol. If formate does form from CO_2, the activation barrier for the reverse reaction to CO_2 and H will be 234 kJ/mol, while the barrier to dioxomethylene formation will be 148 kJ/mol. This scenario implies that formate (if formed) might lie as a spectator on the surface due to huge barriers to its decomposition or transformation, in the absence of an alternative pathway. Cluster calculations at the MP2 level using $Cu_8(6,2)$ yielded an activation energy of 96 kJ/mol for the conversion of formate to dioxomethylene [Hu and Nakatsuji, 1999]. However, as with the formaldehyde conversion, addition of hydrogen to an oxygen atom (forming formic acid), was more favoured than addition onto a carbon atom. This reaction step (formation of HCOOH) has an activation energy of only 21 kJ/mol and has a reaction energy of –126 kJ/mol. However, an activation energy as high as 106 kJ/mol and a reaction energy of +54 kJ/mol characterise the hydrogenation via H-

addition to a C-atom of formic acid to oxycarbinol. Alternatively, the oxycarbinol species can be formed in a non-activated hydrogenation of a dioxomethylene species formed from formate, with a reaction energy of –200 kJ/mol. Direct decomposition of dioxomethylene to formaldehyde and atomic oxygen has a reaction energy of 65 kJ/mol.

The reaction between H_2COOH and H is spontaneous and results in the formation of formaldehyde and adsorbed water. The formation of water, whose desorption activation energy is 17 kJ/mol, is the main cause of the reaction exothermicity. The final steps to methanol from formaldehyde will be the same as discussed under CO hydrogenation.

Since the addition of hydrogen to an oxygen atom appears to be more favoured than addition of hydrogen to a carbon atom, we consider here the two possible formate-hydrogenation pathways to investigate the electronic factors that are responsible for this selectivity.

Figure 4.7 gives an indication of the shape of those crystal orbitals that straddle the Fermi level for the H+HCOO coadsorbed state. These are the orbitals that can be expected to play the main role in bonding interactions between the two fragments (a role similar to that of HOMO and LUMO in molecules). It is evident that both of these frontier orbitals are mostly formed by oxygen p-orbitals and/or hydrogen s-orbitals. Hence, in the frontier-orbital picture of bonding, coupling between the H and HCOO fragments will only lead to resonant level coupling and concomitant energy gain if the hydrogen atom attacks one of the oxygen atoms. The absence of electron density at the carbon atom implies that the energy levels of orbitals involving that atom are outside the energy ranges considered. This might be the reason why hydrogen attack on the carbon atom is energetically more challenging than attack on one of the oxygen atoms. Clearly, the position of the Fermi level is important to both the initial adsorption of reactants and their subsequent coupling [Zheng et al., 1988].

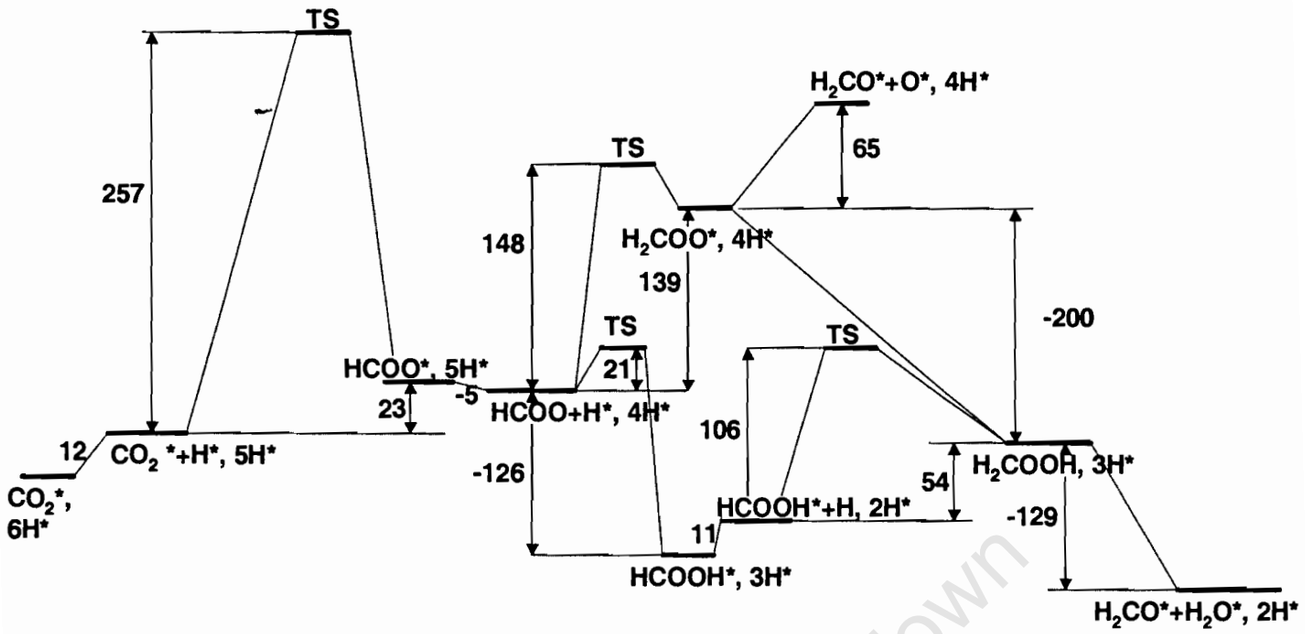

Figure 4.6: Energetics of CO_2 hydrogenation to formaldehyde on Au(111); all energies in kJ/mol. An asterisk denotes an adsorbed species. A*, B* indicates the energy of A and B at a large separation, while A* + B* indicates the energy of coadsorbed A and B.

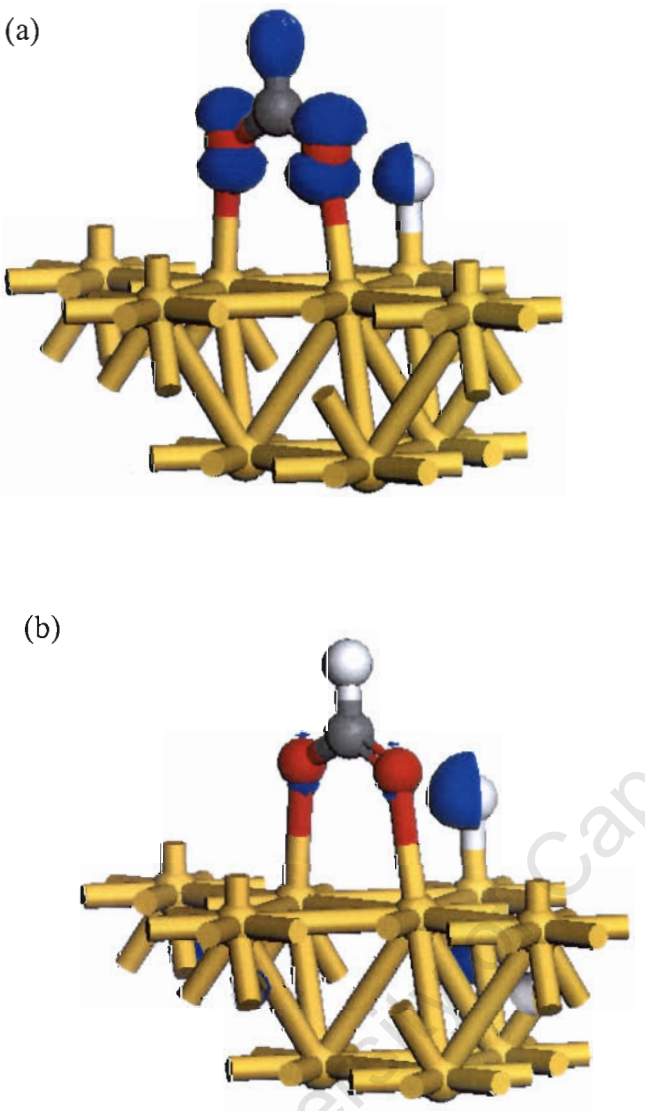

Figure 4.7: Electron density plots for the two bands straddling the Fermi level for H and HCOO coadsorbed on Au(111). (a) Band 42, with an energy range –1.34 to +0.34 eV; (b) Band 43, with an energy range –1.14 to +3.74 eV. The Fermi level is normalized to 0.0 eV. An isosurface value of 0.03 was used.

Gomes and Gomes [2001] present a thermodynamically favourable route for methanol oxidation to CO_2 on a Cu_{22} cluster, while Greely and Mavrikakis [2002a] show that decomposition of methanol to CO is thermodynamically unfavoured on Cu(111). In this section, it was demonstrated that CO hydrogenation is easier than CO_2 hydrogenation on Au(111). Hence the chemistry of synthesis gas conversion on Au and Cu catalysts is likely to be similar, except for the issue of the immediate precursor to methanol.

4.5. Cluster Studies of Key Steps in Syngas Conversion

Experimental studies already show that using small gold particles results in very high turnover frequencies for methanol synthesis [Sakurai and Haruta, 1995 and 1996]. The energetically demanding steps of syngas conversion on gold using an Au_{13} cluster were, therefore, studied. The results are shown in Table 4.1. Only the total reaction energies were computed for the Au_{13} cluster. CO and H_2, which are thought to bond via a donation/backdonation mechanism, are more strongly bound on the Au_{13} cluster than the Au(111) surface. The CO adsorption energy on Au_{13} is the same as the value obtained on stepped Au surfaces [Mavrikakis et al., 2000; Ruggiero et al., 1996; McElhiney and Pritchard, 1976]. A cluster and a stepped Au surface are similar in that low coordination atoms are exposed. H_2 dissociation turns from being endothermic on Au(111) to exothermic on an Au_{13} cluster. According to the Brønsted-Polanyi relation, when reaction mechanism remains unchanged the change in activation energy is proportional to the change in reaction energy [van Santen and Neurock, 1995]. Since the Au_{13} cluster was frozen during the calculations, the energetics will reflect the general coordination and discrete-electron state effects displayed by small crystallites, rather than the precise chemistry of an Au_{13} cluster. The adsorption structural features for the adsorbates considered here were similar to those calculated for the Au(111) surface.

Table 4.1: Energy changes for selected elementary steps on Au(111) and Au_{13} surfaces.

Elementary Step	Energy of Reaction [kJ/mol]	
	Au(111)	Au_{13}
$H_{2,g} \Leftrightarrow H_{ads} + H_{ads}$	+60	-31
$CO_g \Leftrightarrow CO_{ads}$	-13	-62
$CO_{2,g} \Leftrightarrow CO_{2,ads}$	-4	-4
$CO_{2,ads} + H_{ads} \Leftrightarrow HCOO_{ads}$	+23	+17
$HCOO_{ads} + H_{ads} \Leftrightarrow H_2COO_{ads}$	+139	+135

The reactivity differences between stepped and smooth surfaces can be rationalised as follows: when a filled orbital of an adsorbate couples with the d-band of a metal surface, the resultant Pauli repulsion can be lowered once the resulting antibonding orbital rises above the Fermi level [Zheng et al., 1988]. This situation is very likely to occur for stepped surfaces, for which the d-band is much closer to the Fermi level [Liu et al., 2002]. Analogous considerations apply for small clusters, for which the filled antibonding orbital has to rise above the LUMO level in order for chemisoption to occur.

However, the CO_2 molecule is not chemisorbed on Au_{13}. It does not even adsorb on a Pt(111) surface unless an alkali atom is added to facilitate electron transfer to the CO_2 molecule [Illas et al., 2001], despite the fact that the Fermi level cuts the d-band in Pt. The subsequent CO_2 to dioxomethylene steps also do not change energetics significantly on moving from Au(111) to Au_{13}. These results demonstrate that CO_2 hydrogenation will not necessarily be enhanced on a gold nanoparticle. However, high catalytic activity of small supported Au particles is seen experimentally for both CO and CO_2 hydrogenation [Sakurai and Haruta, 1995]. The sensitivity of the reaction to the kind of support used could imply that some of the elementary steps are

facilitated by the support (or perhaps by the gold-support interface). Kakumoto and Watanabe [1997] have shown that a formate species becomes more stable on a Cu dimer as the total charge of the cluster is increased from 0 to +1. Other theoretical studies suggest that the formate to dioxomethylene step is more facile on a Cu-Zn alloy surface than a bare Cu surface [Hu and Nakatsuji, 1999; Morikawa et al., 2001]. All these studies suggest that the support may play a crucial role in methanol synthesis. The CO_2 to methanol pathway occurring on an oxygen vacancy of ZnO was studied by a hybrid QM/MM embedding method [French et al., 2001], and it was found that CO_2 hydrogenation is feasible when an electron trapped in the vacancy activates CO_2. Since Au/ZnO catalysts are the most active for methanol synthesis, studies focussing on the interaction between gold and zinc oxide are required to establish the role of the support. By gaining further insight and understanding of the electronic origins of various reaction barriers, prediction of catalyst formulations with specific syngas activation properties (most importantly, CO_2 activation) will become possible.

During the cluster studies reported here, a symmetrical carbonate-type species was obtained on Au_{13} when CO_2 was allowed to relax over an $Au_{13}O$ cluster. The energy of the carbonate relative to the separated $Au_{13}O$ and CO_2 system was still high at –4 kJ/mol. Addition of a hydrogen atom resulted in formation of a stable $Au_{13}OOCOH$ species, which is structurally similar to formate, except that carbon is bonded to OH instead of H. The role of this species in methanol synthesis has not yet been investigated, but it could provide a route to dioxomethylene that does not involve the energetically demanding direct CO_2/H coupling to formate. Spencer [1995] proposed that two types of carbonate are formed on a Cu surface in $Cu/ZnO/Al_2O_3$ catalyst, and one form may be a formate precursor. On the other hand, exposing $Au_{13}O$ to CO gives Au_{13} and weakly adsorbed CO_2. Thermodynamically, the CO_2/CO ratio will control the gas-phase O chemical potential and hence the stability of $Au_{13}O$ under reaction conditions.

4.6. Conclusions

On an unpromoted Au(111) surface of bulk gold, the activation of syngas molecules (CO, CO_2 and H_2) is a difficult process that will require high reactant temperatures and partial pressures. CO and H_2 have been found to react more easily with a gold cluster than with the bulk Au(111) surface, which is consistent with the observed high CO oxidation activity of gold nanoparticles at sub-zero temperatures. However, the CO_2 molecule remains difficult to adsorb even onto a small cluster.

With regard to the methanol synthesis steps, CO hydrogenation (once CO and H_2 are activated) occurs with low activation energies on Au(111), while CO_2 hydrogenation is energetically very demanding. The use of small particles alone does not seem to improve the energetics of CO_2 hydrogenation. Since CO_2 hydrogenation on oxide-supported gold catalysts is feasible experimentally and exhibits a strong support dependency, it is suggested that some elementary steps in CO_2 hydrogenation might be occurring on the support material, or possibly at the gold-support interface. Studies on the effect of metal-support interactions on the oxidation state of gold may give some light on this issue.

By comparison with literature results on other metal, it appears that Au and Cu surfaces may be superior to Pt and Pd surfaces for methanol synthesis.

Chapter 5

STRUCTURE OF SMALL GOLD CLUSTERS AND THEIR INTERACTION WITH HYDROGEN AND CARBON MONOXIDE

Self-consistent DFT calculations have been performed to study the structure of small gold clusters, Au_1 to Au_{13}, and their interaction with H and CO. Full geometry optimisation was performed for both the naked and molecule-bonded clusters. An odd-even oscillation in the H binding energy onto Au_n clusters was observed, with H adsorption onto odd-numbered clusters being more favourable. Energy matching between the hydrogen 1s electron and the LUMO of the Au_n clusters can explain the trend. For CO chemisorption, the overlap between the CO orbitals and the frontier orbitals of Au_n clusters is important for chemical bonding. As a result, there is no simple relationship between CO chemisorption energy and the frontier orbital energies of Au_n clusters.

5.1. Introduction

Gold nanoparticles have been found to be surprisingly active catalysts for many reactions of industrial and environmental interest [Bond and Thompson, 1999; Haruta, 1997]. It does not seem likely that their high activity can be explained by dispersion alone. While small metal clusters were previously regarded as suitable models for larger supported particles in catalysis studies [González et al., 2003; Illas et al., 2001], evidence has now emerged which suggests that the active sites of gold catalysts may consist of particles of only a few atoms in size [Cunningham et al., 1998; Guzman and Gates, 2001; Heiz and Schneider, 2000; Heiz et al., 2000]. For example, gold clusters consisting of ca. 13 atoms have been detected in an active CO oxidation catalyst under reaction conditions [Cunningham et al., 1998]. Guzman and Gates [2001] have published a method of preparing Au particles on MgO as small as Au_6 using an organogold complex as a precursor. Au_1 through Au_{20} clusters supported on defect-rich and defect-free MgO have been prepared by Heiz and Schneider [2000] and tested for CO oxidation activity. An atom-by-atom tuning of the catalytic reactivity was found, with activity commencing at Au_8. This was attributed to the better contact of Au_8 clusters with the support, facilitating charge transfer and effectively resulting in 'anionic' Au_8. Fluctuations in catalytic activity of these metal-oxide supported nanoclusters could be established, for example Au_{20} and Au_8 were found to be more active than Au_{13} [Heiz et al., 2000]. However, it is of paramount importance to first examine the *intrinsic* ability of unsupported gold clusters to interact with various gas-phase molecules in order to arrive at deeper understanding of their catalytic activity.

A number of experimental and theoretical studies on the interaction of molecules with small Au_n clusters have been performed [Stolcic et al., 2003; Franceschetti et al., 2003; Yoon et al., 2003; Wallace and Whetten, 2002; Lopez and Nørskov, 2002b; Liang and Andrews, 2000; Wu et al., 2002]. Au_n anions produced with a pulsed arc cluster source have been shown to interact with O_2 [Stolcic et al., 2003]. Au_n^- clusters with even numbers of gold atoms (or, alternatively, odd numbers of valence electrons) can react with O_2 up to n=20, above which all clusters are inert. An odd-even oscillation of O_2

chemisorption energies of Au_n^- clusters has been observed in first-principles quantum chemical calculations [Franceschetti et al., 2003; Yoon et al., 2003]. The higher binding energies of O_2 on even-numbered Au_n^- clusters correlate with their lower vertical electron detachment energies [Yoon et al., 2003], emphasising the role of O_2 as a net electron acceptor. Experimentally, co-adsorption of CO and O_2 onto Au_n^- clusters (up to n=20) indeed results in CO_2 production [Wallace and Whetten, 2002]. Calculations show that neutral Au_n clusters bind O_2 with chemisorption energies of 50 to 115 kJ/mol, although in general a given neutral cluster is less reactive than the corresponding anion [Franceschetti et al., 2003; Yoon et al., 2003]. DFT calculations by Lopez and Nørskov [2002b] have shown that the d-states of an Au_{10} nanoparticle are 0.75 eV higher in energy than the d-states of an Au(111) surface, making the gold nanoparticle more efficient in CO oxidation. AuCO has been detected in laser-ablated matrix isolation studies by Liang and Andrews [2000]. They calculated the Au – CO binding energy using DFT to be 56 – 68 kJ/mol (BPW91 functional) and 26 – 34 kJ/mol (B3LYP). MP2, MP4 and CCSD(T) calculations [Mendizabal, 2001] give Au – CO binding energies of 52, 51 and 37 kJ/mol, respectively. BSSE corrections reduce these values by nearly a half. Au_n cations bind CO better than neutral clusters [Wu et al., 2002]. Anionic clusters bind CO the weakest.

Gold anions up to Au_8^- have been shown by Buckart et al. [2003] to adsorb atomic hydrogen. The vertical detachment energies for Au_n^- clusters are similar to those for $Au_{n-1}H^-$ clusters. The structure of the gold core in Au_nH^- clusters is calculated to be similar to that calculated for Au_n^- clusters [Fischer et al., 2002]. H seems to prefer mostly the on-top site for these Au_n^- clusters. Structures of neutral isomers are not provided.

In this chapter, the interaction of neutral Au_n clusters (n=1-10, 13) with atomic H and CO is reported. The objective was to establish whether H and CO chemisorption onto the surface of small gold clusters can be described in terms of properties of isolated clusters and adsorbate molecules, despite the fact that cluster rearrangement is expected upon adsorption of CO and H. This work is motivated by the ongoing interest in both Au-catalysed CO hydrogenation to methanol [Sakurai and Haruta, 1995] and water-gas shift reaction [Andreeva, 2002].

5.2. Computational Method

The results contained in this work have been obtained by gradient-corrected spin-unrestricted DFT as implemented in the commercial software package DMol^3 from Accelrys Inc. [Delley, 1990 and 2000] using the PW91 functional [Perdew and Wang, 1992]. A 19-electron effective core potential (ECP) has been used for the gold atoms, while for the main group elements all electrons were explicitly included in the calculations. A double numerical basis set with polarisation on all atoms and a basis set cut-off radius of 5.5 Å was employed. Convergence of the SCF procedure was facilitated in difficult cases (e.g. for most larger clusters) via the smearing technique implemented in DMol^3, with a thermal occupation (kT) of 0.005 Hartree. Starting geometries for the gold clusters have been excised from the bulk gold fcc lattice and subsequently optimised; CO and H were then separately adsorbed onto the clusters and the entire structures re-optimised. Both the on-top and bridge sites were used in the starting geometries for the optimisation. The Broyden-Fletcher-Goldfarb-Shanno (BFGS) algorithm was used in DMol^3 for geometry optimisations. The energy and gradient convergence tolerances were set at $2x10^{-5}$ a.u and $4x10^{-3}$ Ha/Å respectively. An isosurface value of 0.03 was used for all orbital and electron density plots. When plotting the orbitals, yellow indicates that the wavefunction has a positive sign, while blue indicates a negative sign.

Using the above-mentioned methodology, electron affinity and ionisation potential for a single Au atom have been calculated as 2.06 and 9.60 eV, respectively, comparing reasonably with experimental values [Lide, 1992] of 2.31 and 9.23 eV respectively. Employing a scalar-relativistic all-electron calculation instead of the ECP lead to no improvement; values of similar quality (2.15 and 9.73 eV) were obtained. The computed dissociation energies for AuH and Au_2 are 3.00 and 1.92 eV, respectively, which approximates the quoted experimental values [Lide, 1992] of 2.99 and 2.31 eV. The C–O stretch frequencies in a free CO molecule and AuCO were found to be 2121 and 2003 cm^{-1}, well within 3% of the experimental values at 2143 and 2053 cm^{-1}, respectively [Liang and Andrews, 2000]. For Au_6, the calculated electron affinity is 2.11 eV, which agrees well with the ultraviolet photoelectron spectroscopy value (UPS) value of 2.0 eV

[Taylor et al., 1990]. It is concluded that these calculated parameters are in fair agreement with experimental values, and the methodology employed is considered sound and reliable for the study to be undertaken. All potential energy surface (PES) minima were confirmed as such by verifying the absence of negative eigenvalues in the mass-weighted Hessian matrices. Subsequently, the vibrational data was used to correct all chemisorption energies for zero-point energy (ZPE). Corrections were in the range 0 – 35 kJ/mol.

5.3. Results and Discussion

5.3.1. Bare Gold Clusters

Figure 5.1 shows the optimised Au_n (n=1-10,13) clusters, for which the starting structures were cut from a bulk fcc structure. The dimer interatomic distance at 2.62 Å considerably exceeds the experimental bond distance of 2.47 Å [Huber et al., 1979]. This mismatch can be attributed to relativistic effects because all-electron scalar-relativistic calculations using the same basis set and functional generally gave shorter Au – Au distances, including a dimer bond length of 2.48 Å. The chosen valence-space may also have contributed to the short bond length. The minimal energy conformation of Au_3 is a non-equilateral triangle, however once equilateral symmetry was imposed, the resultant optimised structure (a true minimum) was only 4 kJ/mol higher in energy than the obtuse triangle, rendering the three atoms equivalent at room temperature. It is, thus, not surprising that some calculations may give near-equilateral triangles as the minimum geometries [Grönbeck and Andreoni, 2000]. The HOMO of an equilateral Au_3 was doubly degenerate with an energy of –4.65 eV, while the obtuse trimer had a non-degenerate HOMO with an energy of –5.99 eV. A planar Au_4 was found to be lower in energy than a tetrahedral cluster, which in fact is not a PES minimum and will convert to a planar geometry when optimised. The Au_4 tetrahedron, 100 kJ/mol higher in energy than the planar structure, has its two highest-energy electrons distributed over two triply-degenerate sets of spin orbitals (alpha and beta sets), with energies of –4.74 and –4.50 eV respectively. Planar Au_4, on the other hand, is a cluster with closed-shell electronic

configuration and a non-degenerate HOMO. These results reconfirm the well-known fact that highly symmetrical structures are characterised by orbital degeneracies and will undergo Jahn-Teller distortion. An Au_5 square pyramidal structure was found to be 79 kJ/mol higher in energy than the planar structure. Preference for planar structures up to Au_6 has been predicted in other theoretical studies [Wang et al., 2002; Bravo-Pérez et al., 1999; Häkkinen and Landman, 2000; Wu et al., 2002], and the clusters reported here are in reasonable agreement with those reported in those studies. In the current calculations, the planar form of Au_6 was 77 kJ/mol more stable than its isomer with an atom above a plane formed by the remaining 5 atoms. In fact, transition from 2D to 3D clusters is thought to occur at 7 – 8 atoms [Häkkinen and Landman, 2000; Wang et al., 2002]. Classical molecular dynamics simulations predict 3D structures from Au_5 onwards [Rogan et al., 2004]. The phase-space is extremely large (even for a given cluster dimensionality) for clusters above 6 or 7 atoms. In this study, 3D structures from the bulk-lattice were selected and optimised (bare and molecule-bonded) for clusters larger than Au_6. As Figure 5.1 shows, the local minima of these clusters generally do not deviate much from the original starting geometries. Using a combination of photoelectron spectroscopy and relativistic DFT calculations, Li et al. [2003] has found that an Au_{20} cluster has a structure similar (but different electronic properties) to that of a fragment from bulk gold, with a slight relaxation.

Figure 5.2a shows the variation of the HOMO, LUMO and HOMO-LUMO gap energies of the Au_n clusters. It is evident that, up to Au_9, an odd-even oscillation in both the LUMO- and the HOMO-LUMO gap energies occur. This oscillation is also seen for the HOMO energies, with an anomaly at Au_4. Odd-even oscillations in HOMO-LUMO gaps as well as vertical detachment energies for gold clusters have been observed previously [Wang et al., 2002; Häkkinen and Lundman, 2000; Wu et al., 2002]. Au_6 has the highest HOMO-LUMO gap of 2.14 eV, followed by Au_2 (1.99 eV) and Au_8 (1.43 eV). These results are in reasonable agreement with DFT calculations by Häkkinen and Landman [2000], and calculations by Wang et al. [2002], who obtained Au_6 band gaps of 2.05 and 2.06 eV, respectively. The experimental HOMO→LUMO transition of a neutral Au_6 has been reported as ca. 2.5 eV [Taylor et al., 1990]. The lower gaps for odd-numbered

clusters is due to the fact that the HOMOs in these clusters are singly occupied, and the LUMOs are spin orbitals that would accommodate the corresponding opposite-spin electron, which can be expected to be very close in energy. Above Au_9, the HOMOs and LUMOs are almost degenerate. Li et al. [2003] has, however, reported that an Au_{20} cluster has a large HOMO-LUMO gap.

In Figure 5.2b, the binding energies as well as the cluster fragmentation energies are shown. The per-atom binding energy of a n-atomic cluster is expressed as:

$$E_B(n) = [E(Au_n) - nE(Au)]/n \quad (5.1)$$

while the $Au_n \rightarrow Au_x$ fragmentation energy is defined as:

$$E(Au_n \rightarrow Au_x)(n,x) = E(Au_n) - E(Au_x) - E(Au_{n-x}) \quad (5.2)$$

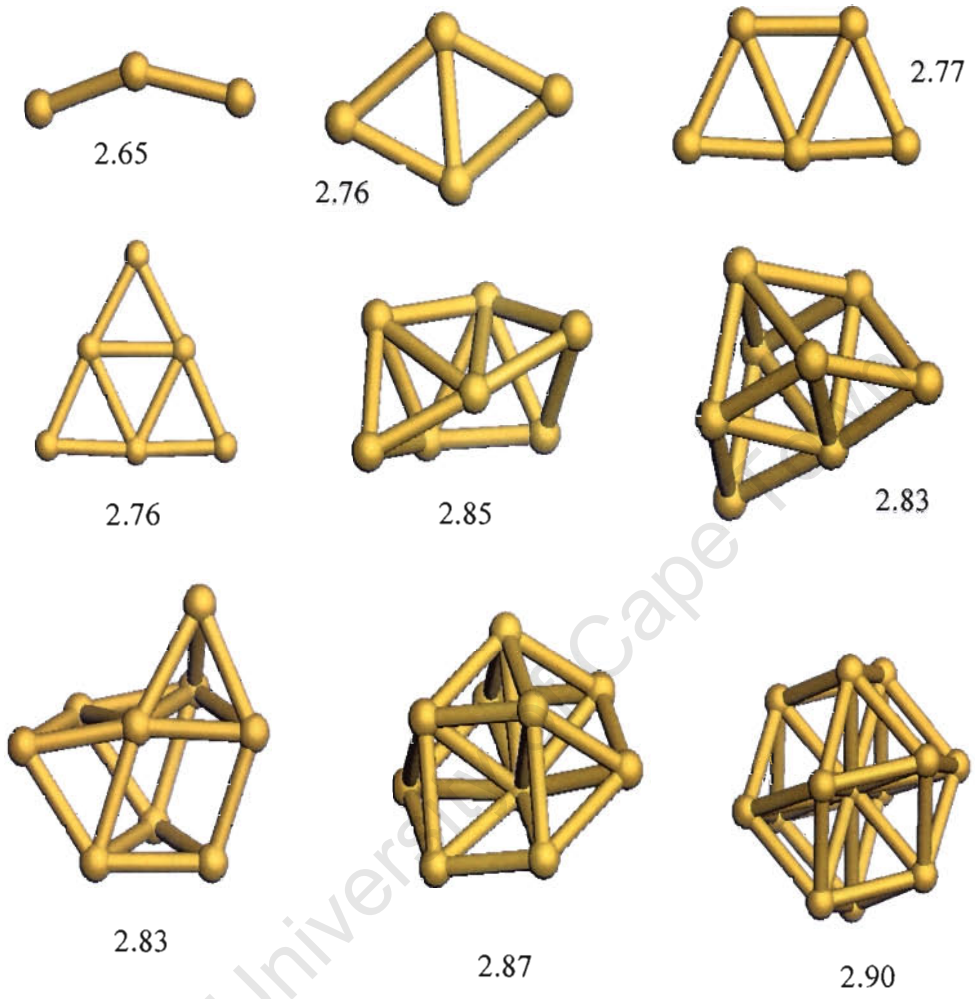

Figure 5.1: Optimised geometries for Au_3-Au_{10}, Au_{13} clusters. The average Au-Au distances, in Å, are shown next to each cluster. The calculated dimer bond length was 2.62 Å.

(a)

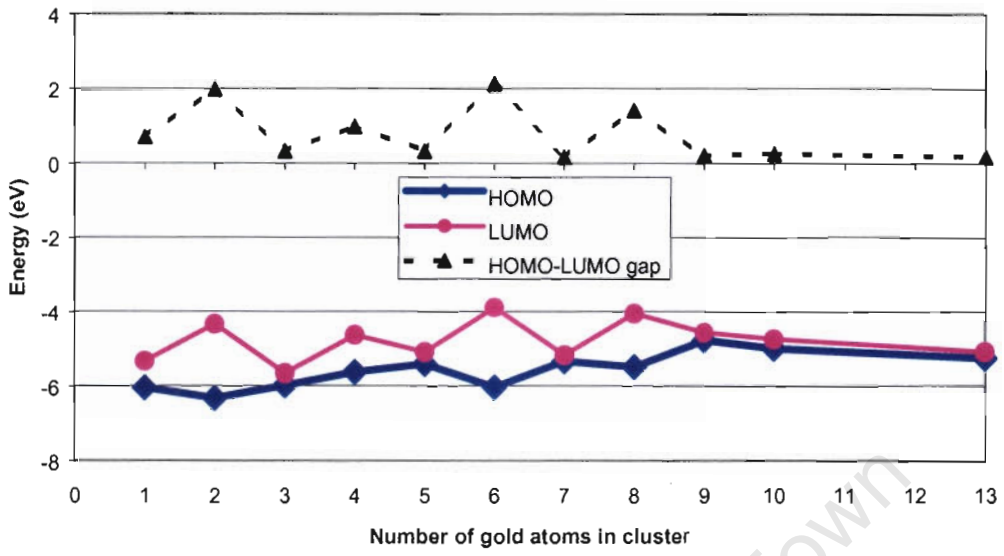

(b)

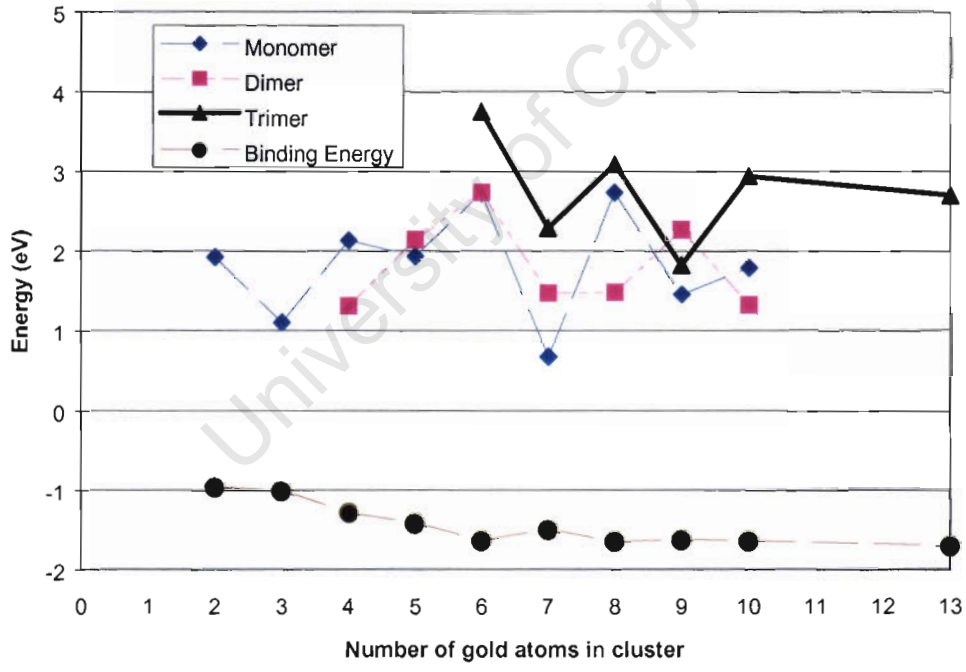

Figure 5.2: (a) Variation of the HOMO, LUMO and HOMO-LUMO gap energies for small Au clusters. The zero of the energy corresponds to vacuum. (b) Per-atom binding energies and monomer/dimer/trimer fragmentation energies.

The per-atom binding energy decreases almost monotonically with cluster size, showing that aggregation of isolated gold clusters is indeed a thermodynamically feasible process. Theoretical fragmentation energies are important for an interpretation of collision-induced or photo-dissociation experiments [Vogel et al., 2003; Schweikhard et al., 2002]. These studies may also help in understanding abundances of metal clusters of certain sizes on oxide supports. Vogel et al. [2003] studied the laser photodissociation of coinage group metal cluster cations consisting of 3 to 21 atoms, establishing that even-numbered cations predominantly exhibit monomer evaporation, while for odd-numbered cations dimer evaporation is a competitive channel of fragmentation. As Figure 5.2b shows, the opposite trend is obtained for the neutral clusters under investigation here. The monomer fragmentation channel is favoured for odd-numbered clusters, while dimer fragmentation is favoured for even numbered clusters. For Au_6, however, both fragmentation channels are competitive. The odd-even fluctuation in the monomer dissociation energies parallels that of the HOMO-LUMO gaps in Figure 5.2a. If one considers removal of a gold atom from a cluster as electronically equivalent to the removal of a single electron from the valence-electron ensemble of the cluster, then trends in monomer dissociation energy are expected to be similar to trends in electron detachment energy. Obviously, removal of an electron (via removal of a monomer) will be unfavoured for even-numbered clusters with large HOMO-LUMO gaps when compared to removal of an electron from odd-numbered low band gap (high HOMO energy) clusters. For cationic or anionic clusters, with their extra electron present or absent, the reverse oscillation pattern is expected (and indeed obtained experimentally for cationic Au_n [Vogel et al., 2003]). For all clusters, trimer fragmentation is the most unfavoured channel, except for Au_9, where trimer fragmentation is easier than dimer fragmentation.

5.3.2. H and CO Chemisorption onto Gold Clusters

Having studied the electronic properties of isolated gold clusters, the aim was now to understand the nature of their interaction with species of catalytic relevance. Figures 5.3a-c illustrate the optimal geometries for H binding onto Au_n clusters, while Figures 5.5a-e show structures for CO binding. The binding energies, corrected for ZPE, are also shown near the clusters. These binding energies are defined as:

$$E_{bind}(M\text{-}Au_n) = E(M\text{-}Au_n) - E(M) - E(Au_n), \quad (5.3)$$

where $E(M) = 0.5E(H_2)$ for H binding and E(CO) for CO binding.

The highest Au-H and C-O stretch frequencies are also shown next to each Au_nH and Au_nCO cluster respectively. The on-top, bridge and 3-fold hollow sites were considered for all clusters greater than Au_3 (and terminating at Au_7 for H binding). It was found that in most cases optimisations that started from the hollow-site configurations led to migration onto either the on-top or bridge configurations. Adsorbates were generally introduced into low coordination atoms. For Au surfaces, low coordinatiuon Au atoms are generally more reactive than atoms of high coordination [Mavrikakis et al., 2000].

H Chemisorption onto Au_n Clusters

For H binding onto Au_1 to Au_7 clusters, where different adsorption sites were considered, the bridge site is the most favourable adsorption site (see Figures 5.3a-b). The on-top configuration is nearly equal in energy to the bridge site for Au_4. On Au_5, the initial starting geometry with H on-top optimized to a bridge configuration. As binding onto Au_5, Au_6 and Au_7 clearly shows (see Figure 5.3b), the hollow site is the least favourable adsorption site. Surprisingly for Au_nH^- clusters (n=2-6), the on-top sites are generally of lower energy than the bridge sites, except for the Au_6H^- clusters [Fischer et al., 2002].

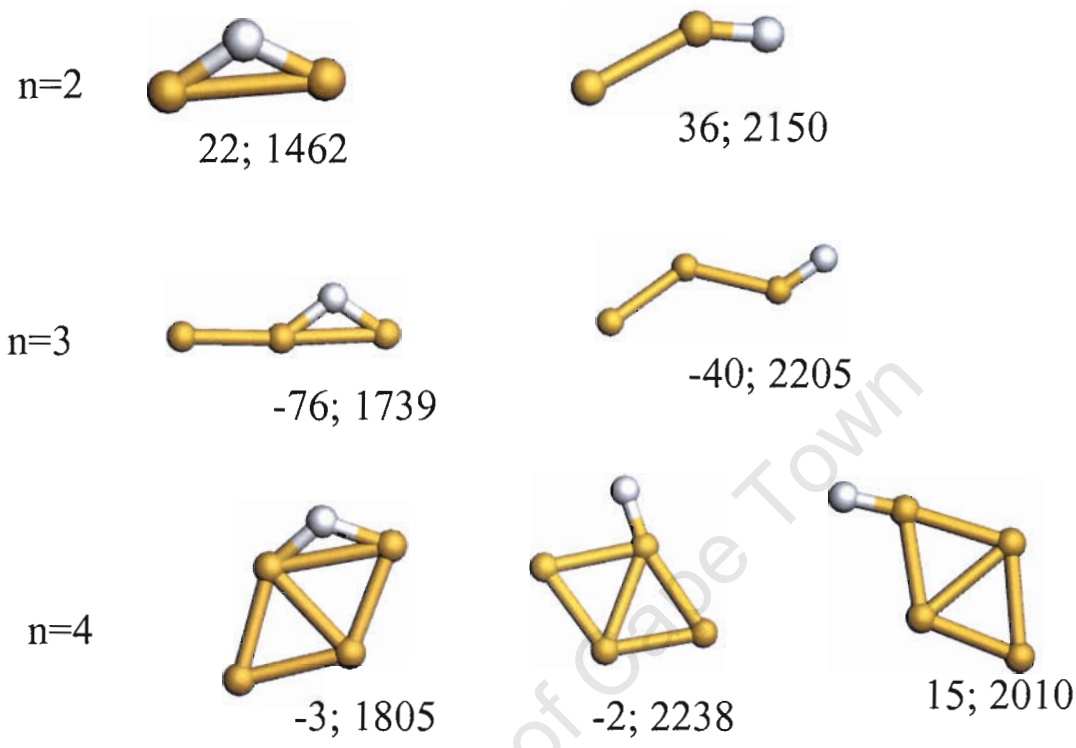

Figure 5.3a: Optimised geometries for H binding onto Au_n clusters (n=2-4). The binding energies, in kJ/mol, are given relative to the isolated Au_n cluster and $0.5H_2$. The Au-H stretch frequencies, in cm^{-1}, are also given. For AuH, the H binding energy is -70 kJ/mol, and the Au-H stretch frequency is 2075 cm^{-1}.

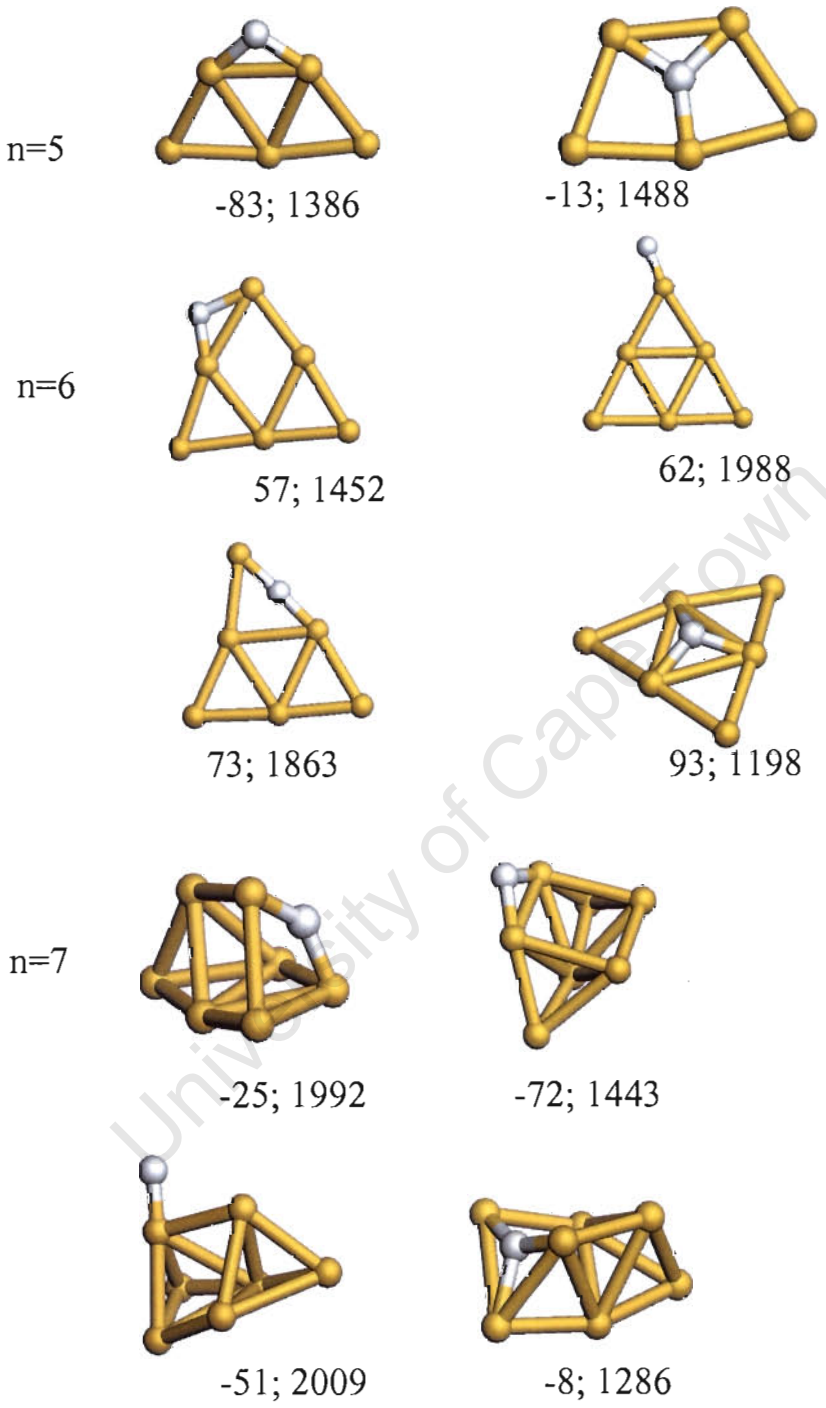

Figure 5.3b: Optimised geometries for H binding onto Au_n clusters (n=5-7). The binding energies, in kJ/mol, are given relative to the isolated Au_n cluster and $0.5H_2$. The Au-H stretch frequencies, in cm^{-1}, are also given.

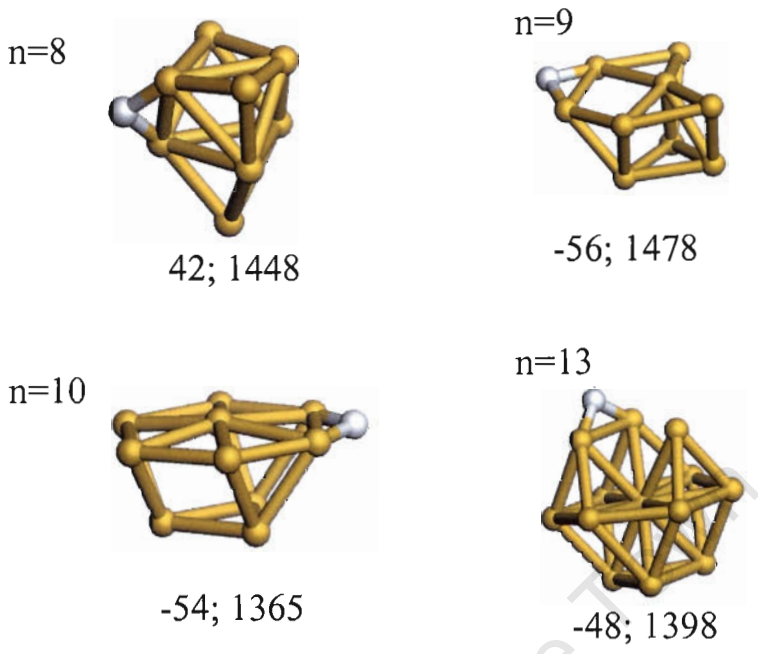

Figure 5.3c: Optimised geometries for H binding onto Au_n clusters (n=8-13). The binding energies, in kJ/mol, are given relative to the isolated Au_n cluster and $0.5H_2$. The Au-H stretch frequencies, in cm^{-1}, are also given.

Triguero et al. [1995] studied H chemisorption onto Cu_n clusters (n=3-9), and found that the bridge site was the most preferred adsorption site for n=3-6 (where complete optimization was performed). On Rh_n clusters (n=1-6), there is no definite preferred binding site between the on-top and bridge site. [Mainardi and Balbuena, 2003]. On the {111} surfaces of Ni and Pd, calculations show that the hollow site is the most preferred adsorption site, while on Pt(111) all binding sites show similar H adsorption energies [Watson et al., 2001]. In general, bonding onto surfaces may not be similar to bonding onto small clusters.

Putting H on the the bridge sites as starting geometries for clusters beyond Au_7, H remained in the bridge site after optimisation (see Figure 5.3c).

The Au-H stretch frequency is above 2000 cm^{-1} for the on-top site, and below for other binding sites.

Figure 5.4 shows the variation of the H binding energy with the size of the number of atoms in the Au_n clusters. The low-energy isomers are used for the binding energies.

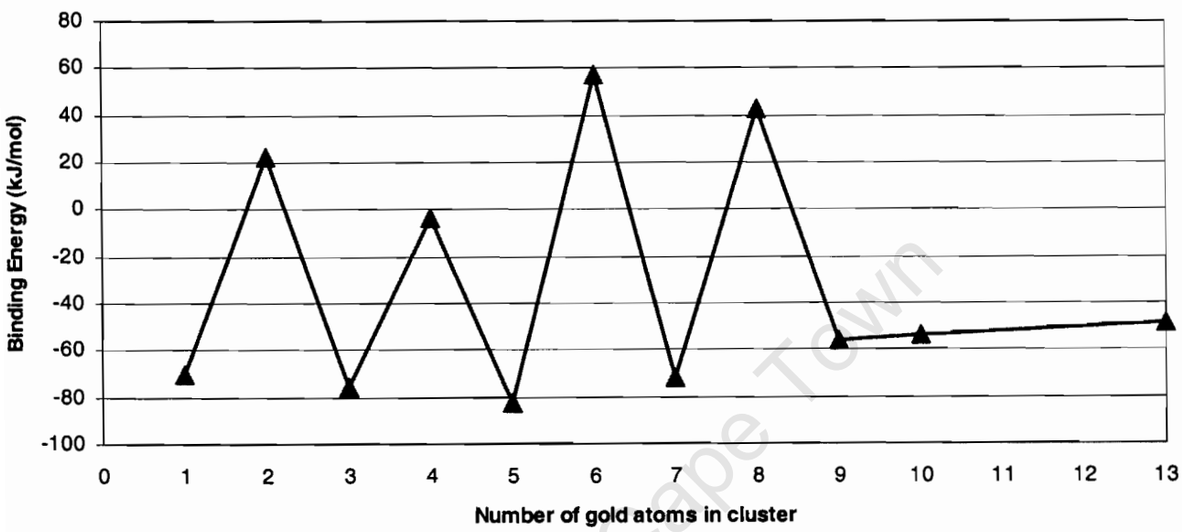

Figure 5.4: ZPE-corrected binding energies for H adsorption onto Au_n clusters. The energies are referenced to Au_n and $0.5H_2$ at infinite separation. H_2 lies 414 kJ/mol (including a 26 kJ/mol correction) below the sum of the energies of two isolated H atoms (experimental value [Lide, 1992] is 432 kJ/mol).

The binding energies for hydrogen adsorption show a marked odd-even oscillation. In general, adsorption of H onto odd-numbered clusters is more favoured than adsorption onto even-numbered clusters. This odd-even oscillation pattern has been observed for H binding onto small copper clusters as well [Triguero et al., 1995]. This may suggest that during adsorption, transfer of an electron into the LUMO of Au is an important process. Therefore, a close energy match of the Au_n-LUMO and H-1s levels is required for optimal adsorption, which would explain why Au_2, Au_6 and Au_8, which have already been identified as having the highest LUMO energies, bind H the weakest. In Figure 5.2a the order of the LUMO energies is $Au_6 > Au_8 > Au_2$, which is exactly the order in which H binding becomes more and more favourable on these clusters, as shown in Figure 5.5. For Au_9 and above, the H adsorption energy is almost constant at around -50 kJ/mol, as the LUMO energy does not change much among these clusters (see Figure 5.2a). H binding is strongest (-83 kJ/mol) and weakest (+57 kJ/mol) on Au_5 and Au_6 respectively, while the differences in binding energies on Au, Au_3, Au_5 and Au_7 are relatively minor (-70, -76, –83 and -72 kJ/mol respectively). To elucidate the electronic reasons for this, the frontier spin orbitals of both Au_5 and Au_6 is shown in Figure 5.5a. Their appearance suggests varying degrees of mixing between the 5d orbitals and the 6s orbitals of Au in these clusters. In particular, the LUMO and especially the HOMO of Au_6 appear to have significantly less contribution from gold 6s-orbitals than those of Au_5. The appearance in symmetry and composition of the LUMO of Au_5 is similar to that of its HOMO because it represents the *virtual* beta-spin partner of the alpha-spin HOMO. Conversely, the Au_6 LUMO displays a somewhat more pronounced s-contribution than the HOMO. Considering the fact that the HOMO of hydrogen is of s-character (spherically symmetrical), it may be deduced that adsorption of H to these clusters should be influenced by energy matching as well as orbital overlap. Hence, H bonding to Au_5 should be more favourable than to Au_6 for two reasons – firstly, the better energy match of Au_5-LUMO and H-1s level, and secondly their better overlap. The Mulliken atomic charges calculated for H in HAu_5 and HAu_6 are +0.33 e and +0.38 e respectively, suggesting a net shift in electron density from H to the gold clusters. Since Mulliken analysis is a charge partitioning scheme that is somewhat arbitrary, spin density (i.e. charge density difference between alpha- and beta-spin electrons) was calculated for the

Au_6H cluster in order to establish the presence of a net shift in electron density from H to Au_6. This is shown in Figure 5.5b. Bare Au_6 has zero net spin density in its electronic ground state - but an incoming H-atom brings in an extra alpha-spin electron, which does not remain fully localised on the H-atom but spreads into spin orbitals of nearby gold atoms. The H atom can, therefore, indeed be expected to be positively polarised. The spatial symmetry of the edge Au atoms in Au_6 looks to be optimal for interaction with an s-orbital of a hydrogen atom. Surprisingly, the bridge site is still the most favourable adsorption site, by about 5 kJ/mol (see Figure 5.3b). Since the HOMO of Au_6 is also localised on the Au atoms, it may be hypothesized that HOMO-HOMO interactions between H and Au are minimised when H is at a bridge site. This can explain why the bridge site is generally more preferred than the on-top site.

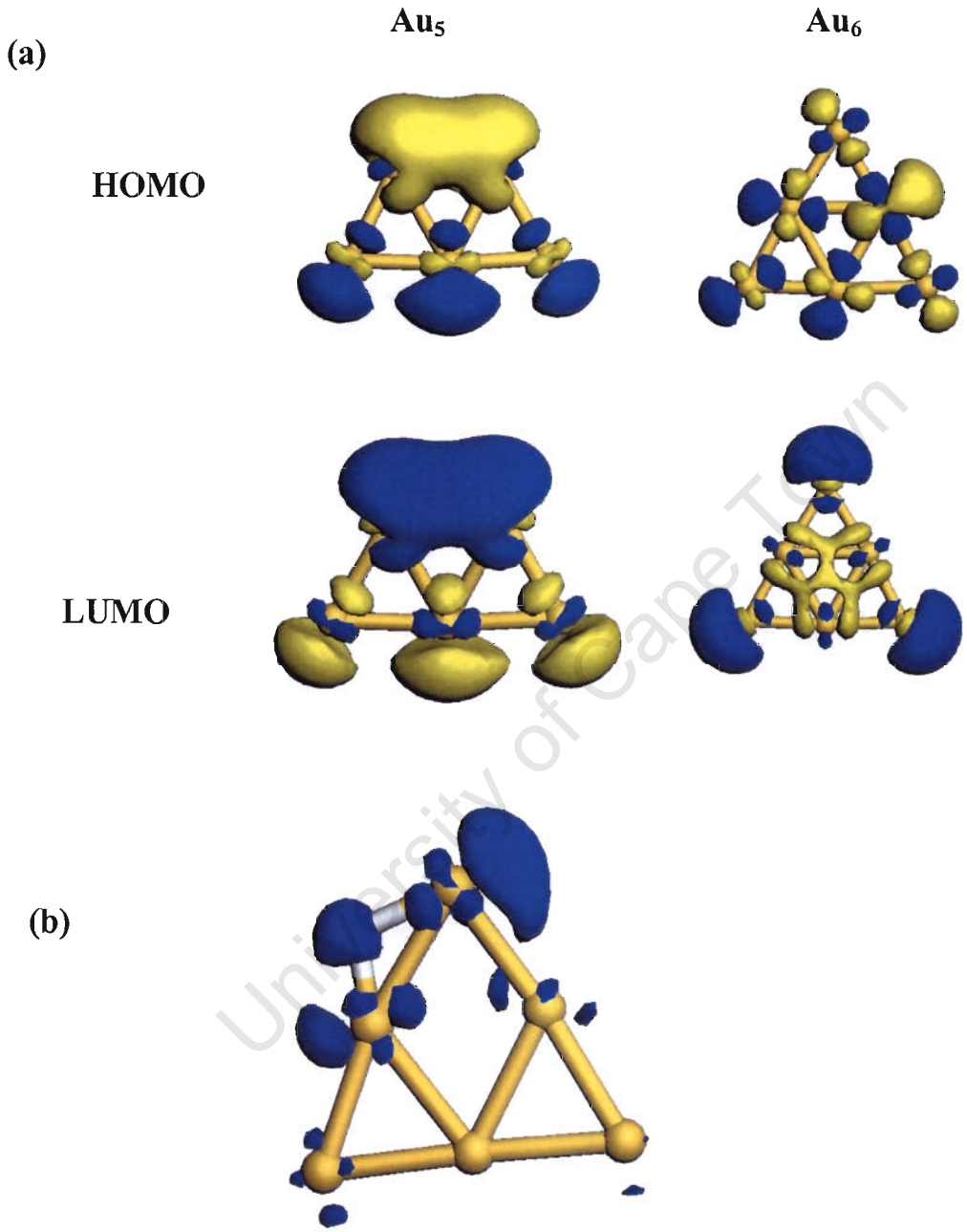

Figure 5.5: (a) Frontier spin orbitals of Au_5 and Au_6 clusters. (b) Spin density for the Au_6H cluster.

CO Chemisorption onto Au_n Clusters

Figure 5.6a-d shows the optimised geometries for CO adsorbed onto Au_n clusters. The binding energies, in kJ/mol, as well as the C-O stretch frequencies, in cm^{-1}, are also indicated. During the calculations, it was found CO adsorbed on the hollow site was unstable, and becomes bonded to either the bridge site or on-top site upon optimisations. Only for Au_5 was it possible to obtain a stable hollow site configuration, and it was 106 kJ/mol higher in energy than the bridge and on-top cordinations.

In agreement with previous findings [Wu et al., 2002], Au_1CO adopts a bent conformation (see Figure 5.6a). This can be understood as a consequence of the repulsion between the filled Au-d_z^2 orbital and the filled 5σ-orbital of CO. Also, the overlap between the $2\pi^*$ orbital of CO with the Au-6s orbital is maximised when the CO molecule bends, because the former is two lobed (+ and – signs). In support of this argument, a calculation shows that an $AuCO^+$ complex is linear. For all the gold clusters except Au_{13}, CO binding onto the on-top site is the most favourable configuration bonding mode. However, for binding onto Au_5, the on-top and bridge configurations are degenerate. The CO binding energies and the structures of the lowest energy isomers for the Au_2CO, Au_3CO, Au_4CO, Au_5CO and Au_6CO clusters reported here are similar to the low energy clusters reported by Wu et al. [2002], where on-top coordination was also found to be of lower energy. Wu et al. [2002] also used the PW91-GGA functional. In the work reported here, the on-top configuration is still shown to be dominant for clusters larger than Au_6 (see Figures 5.6b-c). For Au_8, the most bridge starting configurations led to the on-top configuration upon optimisation. The C-O stretch frequency is below 2000 cm^{-1} for the bridge bonded species, and above 2000 cm^{-1} for the on-top bonded-species. Calculations for CO bonding onto Cu clusters also predict the on-top site as the most favourable adsorption site [Cao et al., 2002]. For CO adsorption onto Nb clusters, on the other hand, the hollow site is the most favourable adsorption site [Grönbeck and Rosén, 1996].

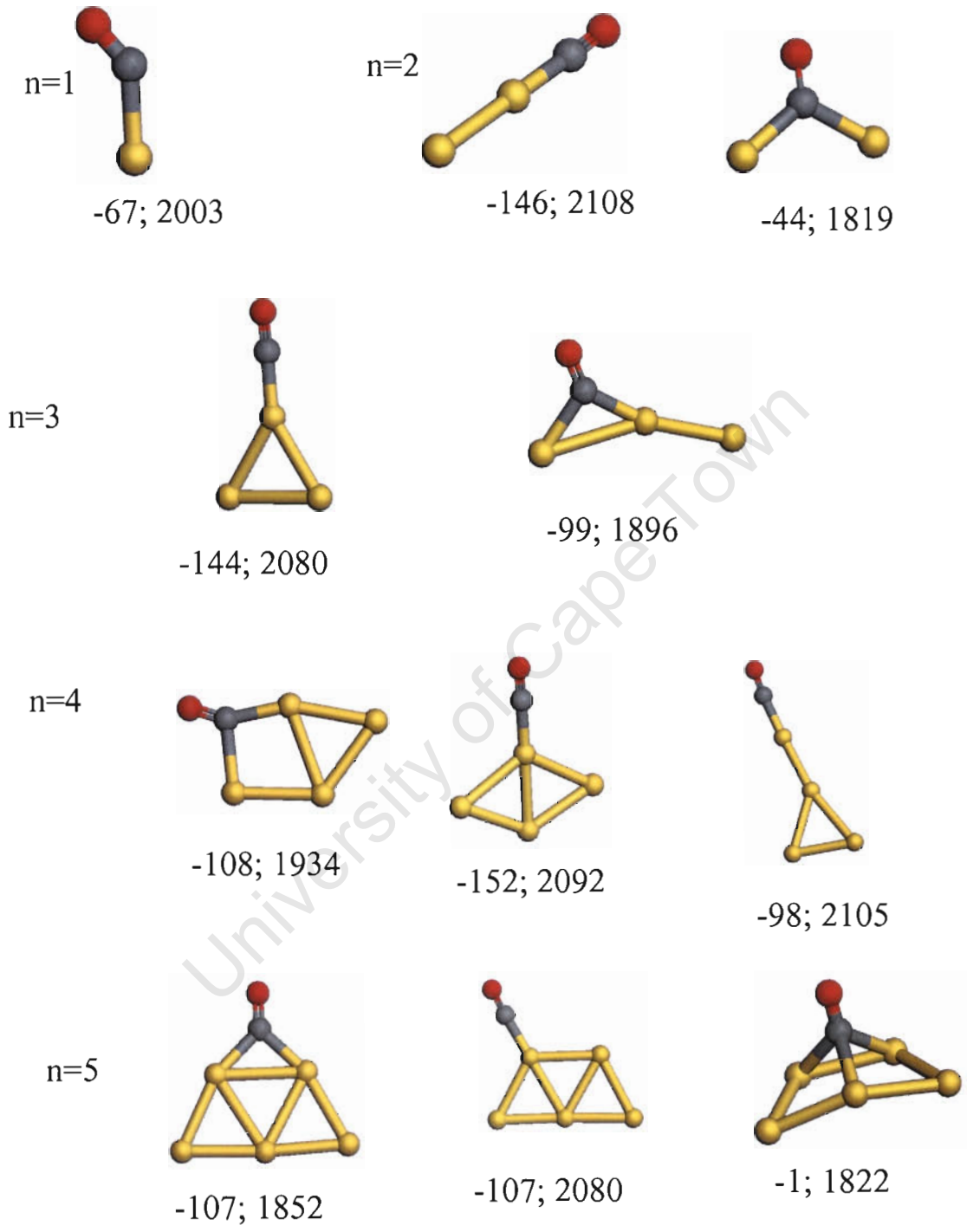

Figure 5.6a: Optimised geometries for CO binding onto Au_n clusters (n=1-5). The binding energies, in kJ/mol, are given relative to the isolated Au_n cluster and CO. The C-O stretch frequencies, in cm^{-1}, are also given.

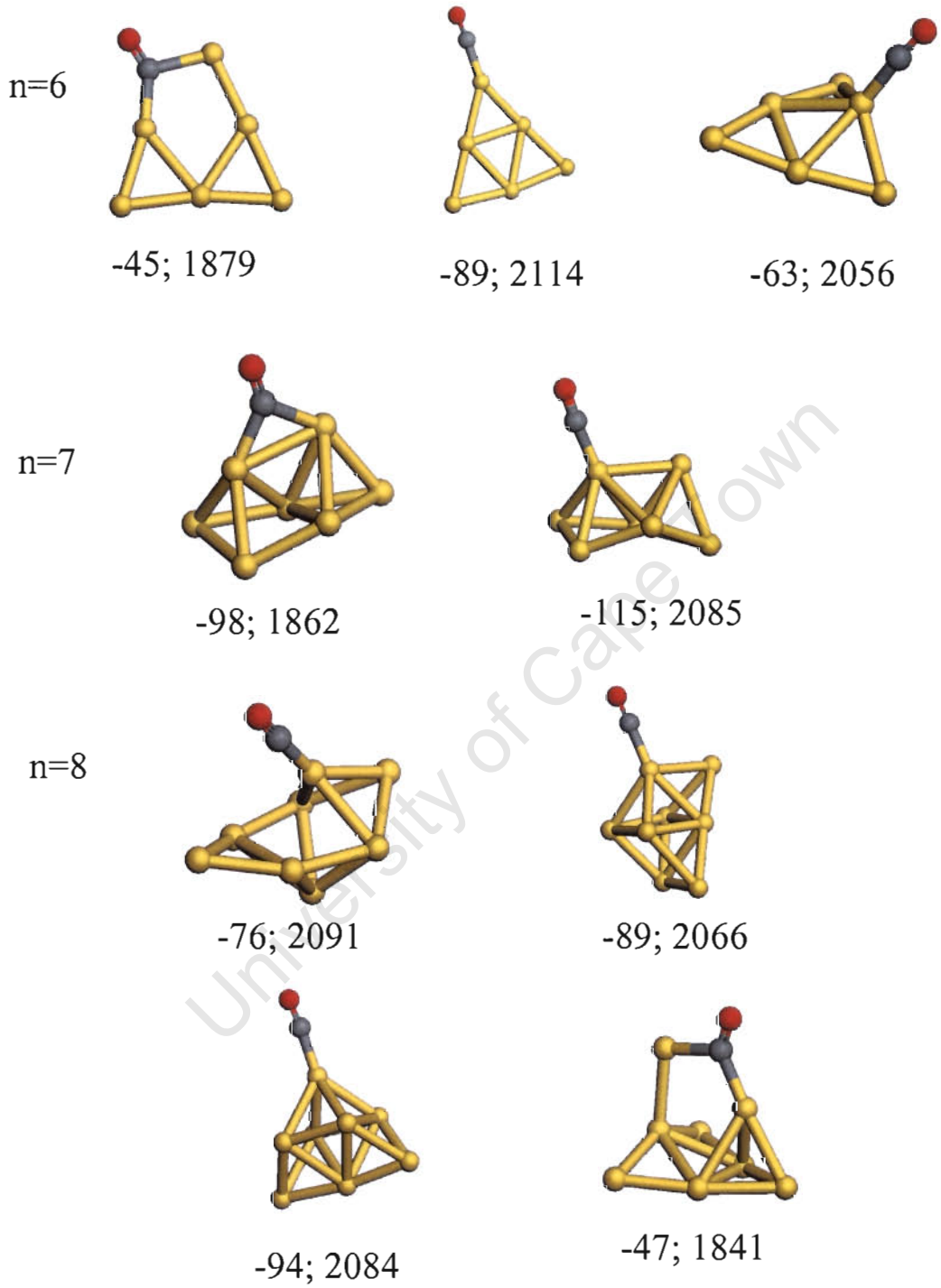

Figure 5.6b: Optimised geometries for CO binding onto Au_n clusters (n=6-8). The binding energies, in kJ/mol, are given relative to the isolated Au_n cluster and CO. The C-O stretch frequencies, in cm^{-1}, are also given.

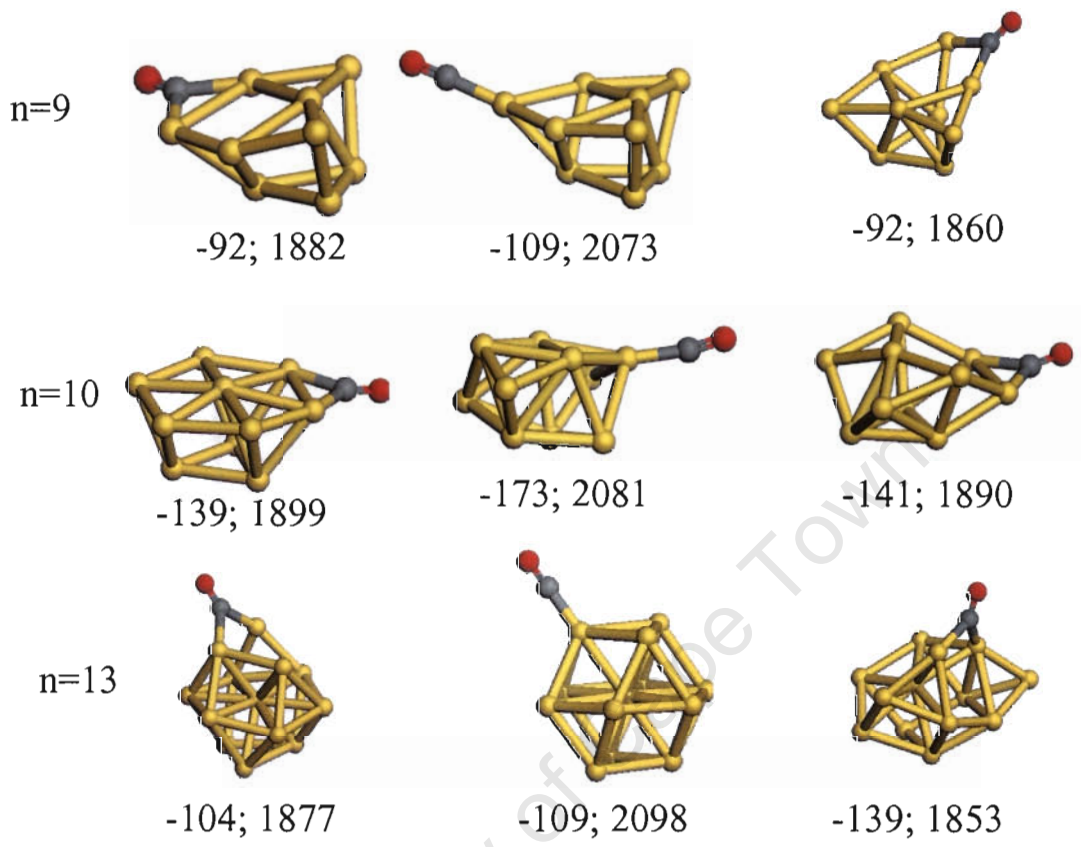

Figure 5.6c: Optimised geometries for CO binding onto Au_n clusters (n=6-8). The binding energies, in kJ/mol, are given relative to the isolated Au_n cluster and CO. The C-O stretch frequencies, in cm^{-1}, are also given.

The anomaly at Au_{13}, i.e. the bridge site being more favoured than the on-top site, was obtained after introduction of CO onto a hollow site. Upon relaxation, the cluster rearranged substantially (as has been seen for Au_8 and Au_{10}). The final geometry of the Au atoms in the cluster is therefore most likely of another isomer of Au_{13} that has a lower energy than the original cluster excised from bulk and relaxed. This point also illustrates the general computational difficulty in covering the complete phase space of clusters. For the rearrangements that were obtained for Au_8 and Au_{10}, the final geometries (with CO on the bridge site) were higher in energy than the clusters with CO at the on-top site.

Amongst the Au_{13} clusters where the cluster largely retains the shape of the original cluster upon CO adsorption, the on-top configuration is 5 kJ/mol lower in energy than the bridge site. It may well be that for large clusters, the on-top and bridge sites are energetically not very different.

Au clusters with average sizes between 1.8 and 3.1 nm supported on TiO_2 adsorb CO with experimentally determined binding energies of -76 to -52 kJ/mol [Meier and Goodman, 2004]. The small clusters considered here, therefore, bind CO much more strongly. The inertness of bulk gold surfaces towards CO chemisorption has been attributed to the large separation between the d-band centre and the Fermi level, leading to large Pauli repulsions [Ruban et al., 1997 and Mavrikakis et al., 2000]. For small gold clusters, however, substantial mixing of the d-orbitals into the HOMO occurs, as has been shown for Au_5 and Au_6. Hence coupling of the d-orbitals with CO orbitals can occur even within the frontier-orbital picture. A single gold atom still has deep lying d-orbitals, and CO adsorption there is not as favourable as onto the on-top sites of Au clusters. The preference for on-top site may be a consequence of the fact that, as has been seen for Au_6 (see Figure 5.5a), the molecular orbitals of the gold clusters are localised on the Au atoms, rather than on the spaces between the atoms. Therefore, maximum overlap between the CO orbitals and the Au orbitals (especially the $5\sigma \rightarrow$ Au forward donation) is established there. For some clusters, e.g. Au_5 (see Figure 5.5a), the frontier orbitals of the Au clusters may have contributions in the interatomic region, making the bridge site equally favourable. This situation is expected for large clusters of the metallic surface, where electrons are generally delocalised throughout the solid and not localised on atomic nuclei.

Figure 5.7 shows the variation of the CO binding energy with the Au cluster size for the CO adsorbed at the low energy on-top. Wu et al. [2002] found, for CO binding onto Au_1 to Au_6 clusters, that the CO adsorption energy increases (i.e. adsorption of CO becomes more and more favourable) with the number of Au atoms and reaches a maximum at Au_4.

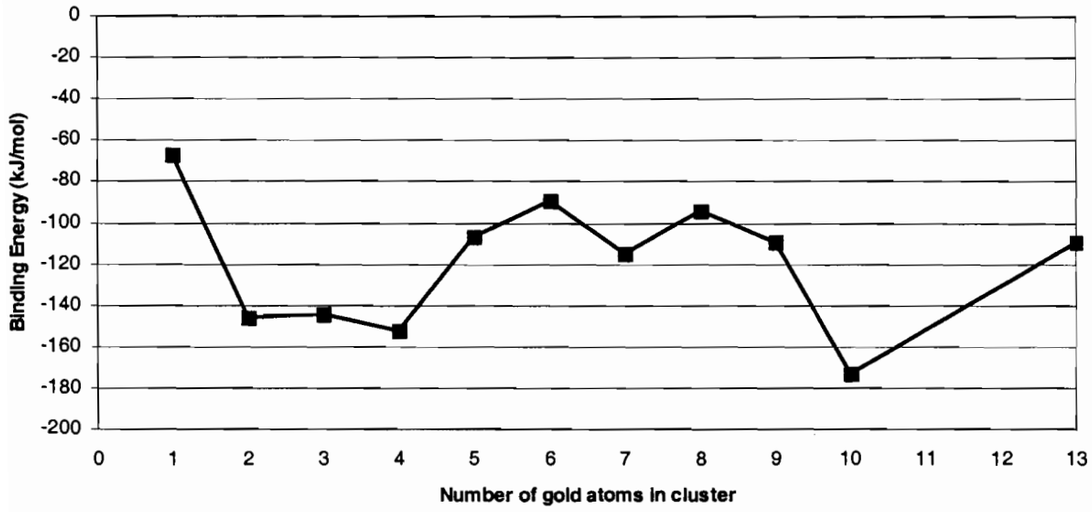

Figure 5.7: ZPE-corrected binding energies for CO adsorption onto the on-top sites of Au_n clusters. The energies are referenced to Au_n and CO at infinite separation.

The trend is reproduced in the current calculations. However, it is shown that CO binding becomes strong at Au_7 and after Au_8. More generally, there is no pronounced correlation between the frontier orbital energies of the bare Au clusters and the CO binding energies on to the Au clusters. For example, the Au_2 and Au_6 clusters have similar HOMO-LUMO gaps (1.99 eV for Au_2 and 2.14 eV for Au_6) but bind CO with different binding energies (CO binding energies are –146 and –45 kJ/mol for Au_2 and Au_6 respectively). It appears that energetic matching between orbitals is not the main factor accounting for the difference in binding energies, in contrast to what was found for H chemisorption. Rather, orbital overlap considerations may be more important. The abrupt changes in cluster morphology within this quantum-size regime means that the spatial symmetry of the frontier orbitals vary abruptly from cluster to cluster. Consequently, for very large clusters and extended surfaces, energetic considerations can be expected to gain importance again as their common general morphology will fix the overall symmetry of

the surface orbitals. The importance of symmetry in CO bonding to Cu clusters has been emphasised in the light of spherical-jellium calculations [Holmgren et al., 1996]. Overlap issues also determine the differences in adsorption energies between different cluster sites, as has already been pointed out.

5.3.3. Coadsorption of CO and H onto Au_6

Adsorption of one reactant will in general affect the subsequent adsorption of a second reactant [Wallace and Whetten, 2002]. For CO adsorption, pre-dosing with hydrogen (for example during catalyst reduction) will affect the CO adsorption if the spatial symmetry of the CO adsorption site is modified relative to the clean surface. Similarly, H adsorption onto a cluster pre-dosed with CO will be different to adsorption onto a bare cluster. Adsorbate-adsorbate interactions will also affect the system energetics. Coadsorption effects on CO/H binding onto Au_6 were investigated. Figure 5.8 shows the energetics of CO and H coadsorption onto Au_6 cluster. In the coadsorbed state, CO and H were adsorbed on the on-top and bridge sites of the Au_6 cluster respectively. The zero of the energy is taken as the bare Au_6 cluster with CO and $0.5H_2$ at infinite separation. Also, the reaction energy to a formyl species is included for completeness. The positive reaction energy for hydrogen adsorption is the main negative factor in the whole pathway from the Au cluster to the formyl species. The thermodynamically preferred route is the path that starts with preadsorption of the cluster with CO. Preadsorption of any one the adsorbates favours the subsequent adsorption of the second adsorbate species. For example, adsorption of H onto Au_6CO is -61 + 89 = +28 kJ/mol, which is lower than the +57 kJ/mol calculated for adsorption onto a bare Au_6. In general, the thermodynamic profile will differ with cluster size, due to the variation of adsorption energies of the individual species with the number of atoms in the cluster. However, the picture presented here illustrates the dangers of making conclusions regarding the chemical reactivity of a given cluster/surface on the basis of the strength of adsorption of only one of the species involved. In general, the symmetry of the orbitals at sites far from where one adsorbate has coordinated will not be similar to those of the bare cluster. This is illustrated in

Figure 5.9, which shows the frontier orbitals of Au6CO and Au6H clusters. The cluster orbitals bear no resemblance at all to those of bare Au_6.

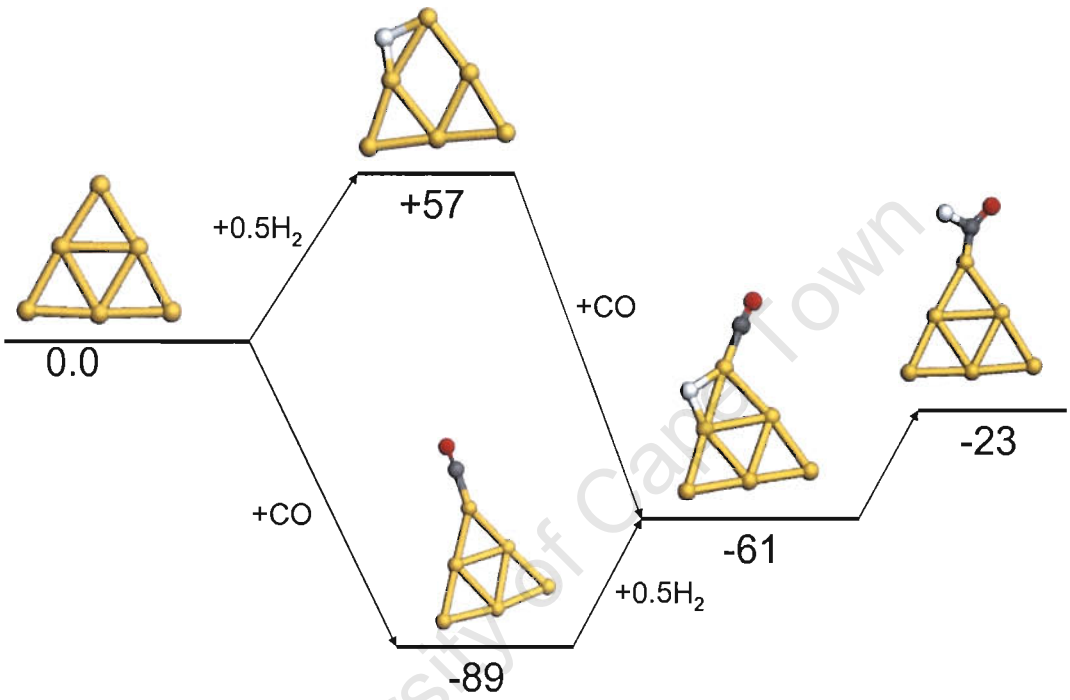

Figure 5.8: A thermodynamic profile of CO and H coadsorption onto Au_6 and their subsequent reaction to a formly species. The zero of the energy is the sum of the energies of bare Au_6, CO and $0.5H_2$ at infinite separation. The relative energies are given in kJ/mol.

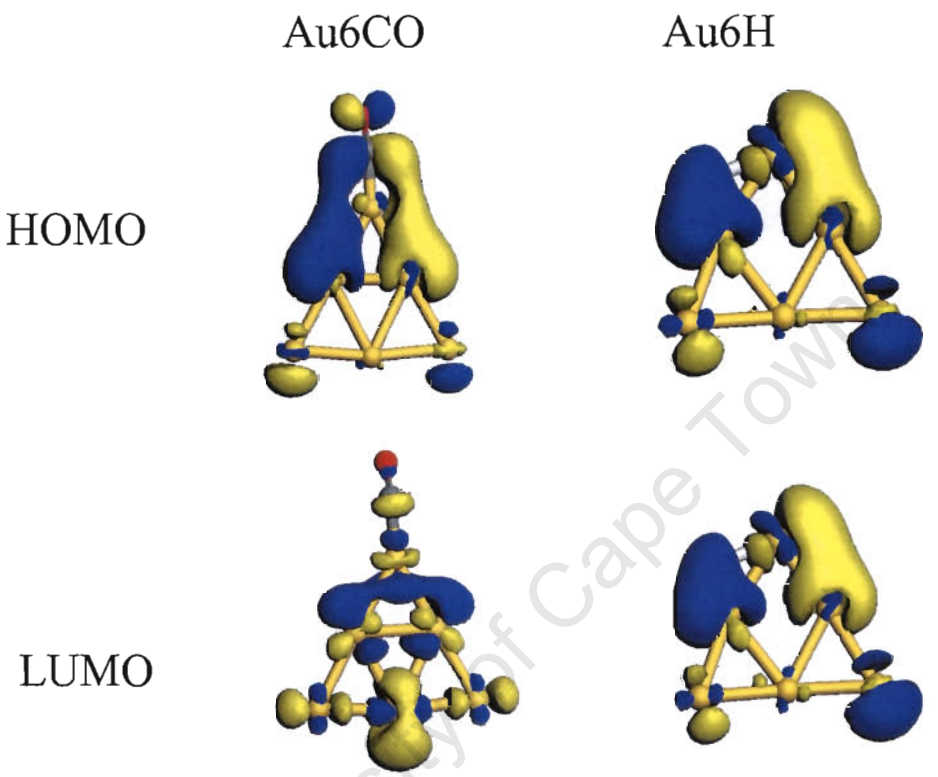

Figure 5.9: Plots of the frontier orbitals for Au_6CO and Au_6H clusters, to be compared with those of bare Au_6 in Figure 5.5a. The adsorbate-cluster interactions induce changes in the overall symmetry of the frontier orbitals, which affects the subsequent interaction with a second adsorbate.

5.4. Conclusions

The variations in frontier orbital energies and HOMO-LUMO gaps of small clusters have been shown to result in special cluster fragmentation patterns, which in turn provide useful information for the analysis of collision-induced dissociation experiments. The H chemisorption energies onto Au_n clusters show a marked odd-even oscillation. This can be attributed to the fact that the key interaction for this process is electron transfer from the hydrogen atom to the LUMO of Au_n. Consequently, clusters with a lower LUMO energy bind H more easily. For CO adsorption, it is important to consider symmetry matching between the frontier orbitals of the adsorbent and those of the gold clusters. Consequently, a direct correlation between frontier orbital energies of Au_n and CO chemisorption energies is not expected (at least when the cluster orbital energies are not very different).

Chapter 6

THE NATURE OF THE OXIDATION STATES OF Au ON ZnO

The interaction between gold in the 0, +1, +2and +3 oxidation states and the zinc-terminated ZnO(0001) surface is studied via the QM/MM electronic embedding method using density functional theory and interatomic potentials. The surface sites considered are the vacant zinc interstitial surface site (VZISS) and the bulk-terminated island site (BTIS). It is found that on the VZISS, only Au^0 and Au^+ are stable oxidation states of gold. However, all of +1 to +3 oxidation states are stable as substitution for Zn^{2+} in the bulk terminated island site. $Au(OH)_x$ complexes (x=1-3) can adsorb exothermically onto the VZISS, indicating that higher oxidation states of gold can be stabilised there in the presence of stabilizing hydroxyl groups. CO was used as a probe molecule to study the reactivity of Au in different oxidation states in VZISS and BTIS. In all cases, it was found that surface Au^+ binds the CO molecule the strongest. Furthermore, CO binding onto Au^0 is stronger when the gold atom is adsorbed onto VZISS compared to CO binding onto a gas phase neutral gold atom. These results indicate that the nature of the oxidation states of Au on ZnO(0001) will depend on the type of adsorption site. Therefore, the role of ZnO in Au/ZnO catalysts is not merely to disperse gold atoms/particles, but to also modify their electronic properties.

6.1. Introduction

Despite the nobility of Au in its bulk state, small gold particles, on oxide supports, show appreciable activity for a wide range of technologically important reactions [Haruta, 1997]. It remains an issue of contention as to how the catalytic action is related to the structure and electronic properties of the gold particles. ^{197}Au Mössbauer effect spectroscopy studies on Au/TiO_2 catalysts have suggested that only Au^0, and not ionic gold, is present on a working catalyst for CO oxidation [Goosens et al., 2002]. Hodge et al. [2002] prepared Au/Fe_2O_3 catalysts by coprecipitation of the gold and iron salts, and found that catalysts calcined at 400°C consisted of exclusively metallic gold particles and had very low CO oxidation activity, while catalysts that were not calcined (only dried at 120°C) consisted of a dispersed mixture of $Au^{\delta+}$ (as AuOOH.xH_2O) and Au^0 and had very high CO oxidation activity. Thsee catalysts were characterised by XRD, HREM and ^{197}Au Mössbauer spectroscopy. With the simultaneous presence of Au^0, an increase in the fraction of Au^+ in Au/MgO catalysts has been found to increase the rate of CO oxidation [Guzman and Gates, 2004]. For the Au/CeO_2 catalyst in the water-gas shift reaction ($CO + H_2O \rightarrow CO_2 + H_2$), catalysts leached with a cyanide solution to remove all metallic gold particles (X-ray photoelectron spectroscopy (XPS) suggested presence of only Au^+ and Au^{3+} in leached samples) were just as active as unleached samples (activity expressed per total surface area of the catalyst), suggesting that Au^0 species might be spectators and only cationic gold is active in this reaction [Fu et al., 2003]. It needs to be pointed out that all assignments of oxidation states of Au, based on irradiation techniques in vacuum, can carry significant margins of error. The radiation source can alter the oxidation state of sub-nanometer gold particles. Furthermore, the orbital energies of small metal particles are different from those of the bulk material, making assignments of electron binding energies on the basis of reference values from bulk material erroneous. This can be complicated by the fact that the electrostatic potential at the metal adsorption site on the support will generally shift the metal orbitals relative to the unsupported metal. Theoretical calculations have shown that both TiO_2-supported [Vittadini and Selloni, 2002] and bare [[Wu et al., 2002] Au clusters bind CO strongest when they carry a positive charge.

Amongst the active catalyst formulations, Au/ZnO catalysts are active for oxidation of carbon monoxide to carbon dioxide [Zhang et al., 2003; Wang et al.,2003] and

conversion of synthesis gas to methanol [Sakurai and Haruta, 1995 and 1996]. The methanol yields for the Au/ZnO catalysts in methanol synthesis are comparable to those obtained with the commercial Cu/ZnO-based catalysts. Extended X-ray absorption fine structure (EXAFS) and XPS measurements on Cu/ZnO catalysts have suggested the existence of both Cu^0 and Cu^+ species [Kulkarni and Rao, 2003]. The rate of methanol formation per surface area of gold particles increases with a decreasing average diameter of gold particles, clearly showing that the high activity of gold nanoparticles is not a simple surface area effect. Infrared studies have suggested the existence of both metallic and oxidised gold clusters in Au/ZnO catalysts [Boccuzzi et al., 1995]. In this study, it is shown that Au^0 and Au^+ may be stabilised on the vacant-zinc interstitial surface sites (VZISS) of the ZnO surface, while Au^+, Au^{2+} and Au^{3+} are stable as Zn substitution sites. Adsorption of $Au(OH)_x$ species on the ZnO surface is shown to be a feasible process. The interaction between CO and adsorbed gold atoms in different oxidation states was investigated to understand the chemical nature of the interfacial gold atoms.

6.2. Computational Details

6.2.1. The ZnO(0001) Surface Model

The polar zinc-terminated ZnO(0001) surface on itself can adsorb CO, CO_2 and other C_1 oxygenates [Akhter et al., 1985]. An *ideal* polar surface of ZnO would have two inequivalent alternating layers of opposite charge along the surface normal, i.e. alternating Zn and O layers. Since each repeat unit bears a dipole moment, the electrostatic potential increases monotonously with thickness, making the polar surfaces unstable [Noguera, 2000]. While the *ideal* polar surfaces are unstable on electrostatic grounds, modification of the electronic charge on the outermost layers can stabilize the polar surfaces [Noguera, 2000]. Such charge modification can be achieved by (i) charge transfer between the O- and Zn- terminated surfaces, (ii) adsorption of an impurity, e.g. H^+ on the O- terminated surface or OH^- on the Zn-terminated surface [Wander and Harrison, 2001], or (iii) creation of vacancies on the surface. Scanning transmission microscopy (STM) experiments on the polar surfaces of ZnO have suggested that mechanism (iii) may be a natural way of stabilising the polar surfaces [Dulub et al., 2002]. The ZnO(0001) zinc-terminated surface with Zn-vacancies was, therefore,

considered in detail as a realistic model of the ZnO(0001) surface. 6 out of every 25 surface zinc atoms were removed to create the vacancies. This reduces the Zn surface charge density from 100% to 76%. Classically, the condition for stabilization of the polar ZnO orientation requires a surface charge density of approximately 76.5% [Noguera, 2000]. The geometry of a surface vacancy makes it a natural location for adsorption of metal atoms during cluster growth. This surface model has been used successfully to model the Cu-ZnO interaction [Bromley et al., 2003].

A quantum mechanical/molecular mechanics (QM/MM) electronic embedding technique was employed to model the ZnO(0001) surface of zincite [Sherwood et al., 2003]. A schematic of the embedding methodology is shown in Figure 6.1. The QM region of the surface consisted of a total of 13 zinc and oxygen atoms for the vacant zinc interstitial surface site (VZISS), and 14 atoms for the bulk-terminated island site (BTIS). All the QM regions included an oxygen atom in the second layer. In the MM active region, the Zn cations were represented by classical charges, while the oxygen atoms were treated via the shell model [Dick and Overhauser, 1958] to account for electronic polarisation of the oxygen atoms in the ZnO surface and bulk by the change in the electron density in the QM region due to adsorbates. The atoms in the MM frozen region (~13 Å radius from the QM region centre) were treated similarly to the atoms in the MM active region, except that the ions in the MM frozen region were frozen at their preliminarily reconstructed and MM relaxed surface positions during geometry optimisations.

Whenever charged species were introduced in the QM region, a correction to the adsorption energies due to polarisation of the MM frozen region was made (see Chapter 3.10). The QM and the MM regions were connected by the interface region, using Zn atoms to link the QM and the MM regions. The Zn ions in the interface were represented by pseudopotentials, without basis sets, to take into account the non-point like nature of the charge distribution on the Zn cations and prevent electrons in the QM region from collapsing onto the Zn cations. The MM region still sees the Zn ions as classical charges. Finally, point charges were added to the hemispherical cluster to reproduce the electrostatic potential at a set of points in the QM region to within 10^{-4} V. The hemispherical ZnO(0001) cluster (~25 Å radius from the central region) is shown in Figure 6.1. The MM relaxed ZnO(0001) surface shows two types of surface sites: the

vacant zinc interstitial surface sites (VZISS) and the bulk-terminated island sites (BTIS) (Figure 6.2).

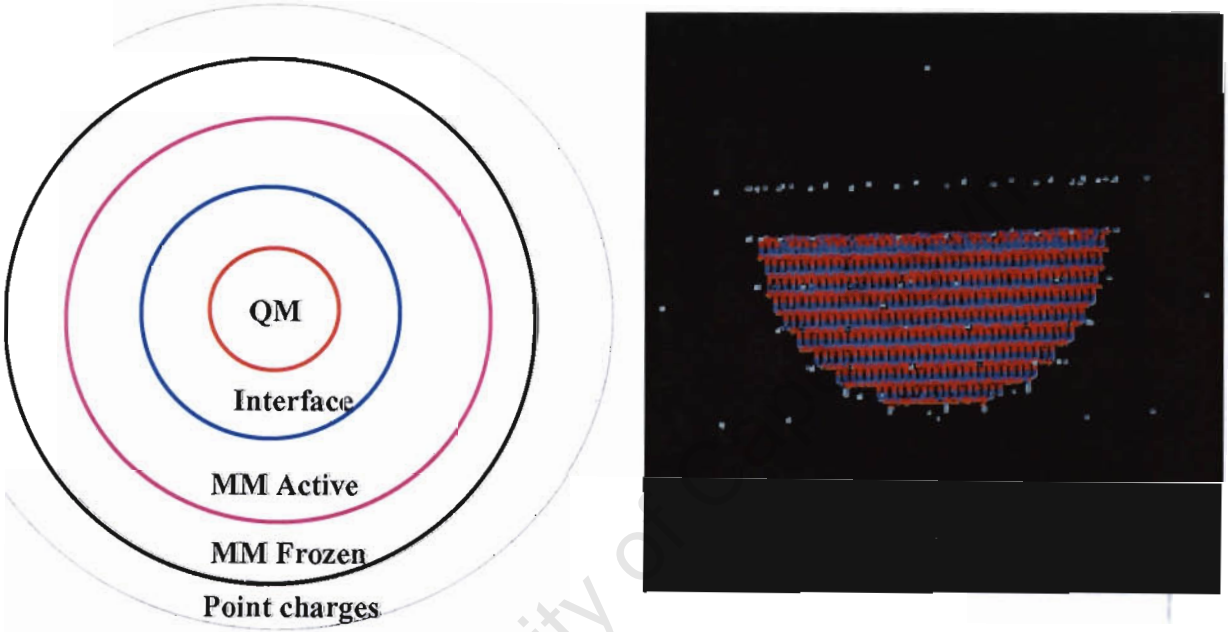

Figure 6.1: The embedded cluster methodology employed in this work.

These two sites (VZISS and BTIS) were separately considered as the QM regions in the calculation of Au interaction with the ZnO(0001) surface. Excluding the adsorbates, the QM/MM cluster consisted of a total of 3114 atoms.

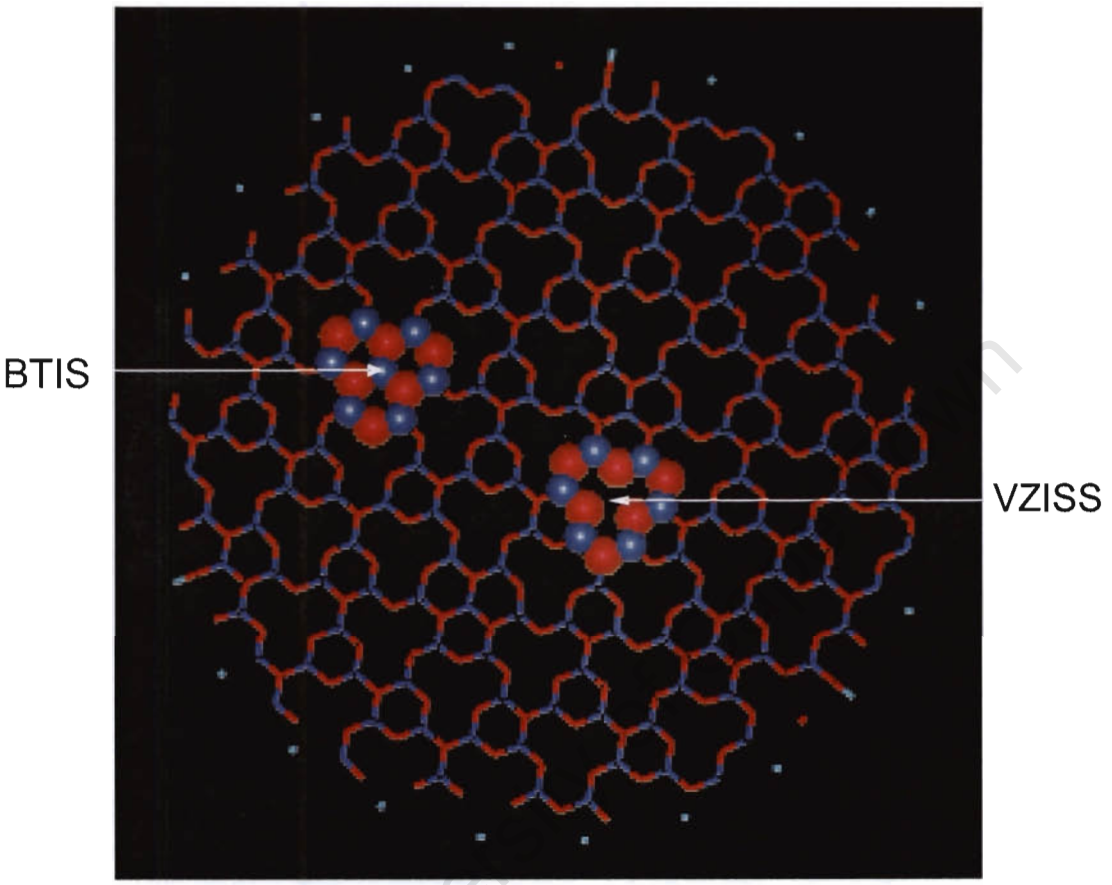

Figure 6.2: The top view of the ZnO(0001) surface indicating the bulk-terminated island site, BTIS (left) and the vacant zinc interstitial site,VZISS (right) used as the QM regions in this work. Only the top, reconstructed surface layer is shown. The full QM regions included an oxygen atom in the second layer.

To mimic deposition of Au atoms onto the ZnO(0001) surface in the 0 to +3 oxidation states, we considered $AuZnO(0001)^0$, $AuZnO(0001)^+$, $AuZnO(0001)^{2+}$, and $AuZnO(0001)^{3+}$ clusters for adsorption onto a VZISS. These will be called $[Au]^0_{VZISS}$, $[Au]^+_{VZISS}$, $[Au]^{2+}_{VZISS}$, $[Au]^{3+}_{VZISS}$ clusters respectively. The superscript indicates the total cluster charge that was used in the calculations.

The central Zn atom in the BTIS was replaced by an Au atom to model substitution of Zn cations by Au cations at that site. For the substitution process, calculations on neutral cluster, $[Au]^0_{BTIS}$, and singly cationic and anionic charged clusters, $[Au]^+_{BTIS}$ and $[Au]^-_{BTIS}$, were considered to model cases where the Zn^{2+} cation is replaced by an Au^{2+}, Au^{3+} and Au^+ cations respectively. Thermodynamic cycles for formation of these substitutions from hydroxyls, chlorides or via surface diffusion, were considered. CO adsorption onto these sites was subsequently investigated to analyse the chemical nature of these species. The adsorption of $Au(OH)_x$ species (x=1-3) onto the VZISS was also considered as $Au(OH)_x$ species are expected to exist in solution during liquid phase preparation of Au/oxide catalysts [Haruta, 1997]. These calculations, therefore, address a realistic number of possibilities during the initial steps in the deposition of gold onto zinc oxide.

6.2.2. Total Energy Calculations

The total energy of the QM/MM cluster is a sum of the QM and MM contributions. The QM energy was calculated using DFT using GAMESS-UK [Guest et al., 1980] and employing the B97-1 hybrid functional [Hamprecht et al., 1998]. The Au atoms were treated using a 60-electron effective core potential (ECP) and a modified and reoptimised TZVP basis set (with an extra diffuse p function) from Stuttgart [Andrae et al., 1990]. An ionization potential calculated for Au with this basis set is 9.13 eV, which agrees well with the experimental value of 9.23 eV [Lide, 1992]. The calculated Au_2 binding energy and bond distance were 1.97 eV (experiment: 2.30 eV [Lide, 1992]) and 2.56 Å (experiment: 2.47 Å [Huber et al., 1979]) respectively. The higher Au_2 bond distance is a consequence of a non-relativistic treatment. The basis sets on Zn and O atoms of the surface were of TZVP quality and have been optimised for ZnO. A large core ECP (28-electron) was used on the Zn atom. Basis sets on C, O, H and Cl adsorbate atoms were {11s6p3d/5s3p2d}, {12s7p2d/6s4p1d}, {5s2p/3s2p} and

{15s10p4d/6s5p2d} respectively. The GULP code [Gale, 1997] was used for all MM terms using interatomic potential parameters that have been optimised for ZnO [Whitmore et al., 2002]. The QM/MM embedding method is implemented in the code Chemshell [Sherwood et al., 2003], which serves as an interface between the QM and MM codes and allows the QM and MM energies to be calculated self-consistently. The Broyden-Fletcher-Goldfarb-Shanno (BFGS) algorithm was used in Chemshell, with a force tolerance of 0.001 a.u. The electronic energy in GAMESS-UK was converged to 1 x 10^{-7} a.u.

6.3. Results and Discussion

6.3.1. Au Atoms on the ZnO(0001) Surface Sites

The calculated electronic and structural properties of the single atoms interacting with the VZISS and the BTIS are shown in Table 6.1. For the $[Au]^0_{VZISS}$ cluster the optimised location of a neutral gold atom is 2.50-2.65Å from the surface oxygen atoms. The Au-O distance decreased with increasing total positive charge on the cluster. This situation is analogous to what was obtained for Cu adsorption onto the same site [Bromley et al., 2003]. For the $[Au]^{3+}_{VZISS}$ cluster, the Au atom was lying practically at the level of the surface oxygen atoms (see Figure 6.3).

Figure 6.3: QM region of the optimised structures of the $[Au]^0_{VZISS}$ (left) and $[Au]^{3+}_{VZISS}$ (right) clusters.

Table 6.1: Frontier orbital energies and the Mulliken charge on Au atoms in AuZnO(0001) clusters. The total energies are also included. VZISS is the vacant zinc interstitial surface site, while BTIS is the bulk-terminated island site (see text and Figures 6.3 and 6.4).

	E[Ha][a]	HOMO[eV][b]	LUMO[eV][c]	$D_{Au\text{-}Osurf}$ [Å][d]	$Q_{Au}[e^-]$[e]
Gas phase single atoms					
Au^0	-135.8685	-6.36	-4.39	-	+0
Au^+	-135.5334	-16.64	-11.98	-	+1
Au^{2+}	-134.7692	-28.09	-25.10	-	+2
Au^{3+}	-133.4818	-51.32	-39.92	-	+3
Supported atoms					
Bare VZISS	-845.5696	-5.49	+1.21	-	-
Bare BTIS	-855.9866	-5.46	+0.49	-	-
Bare BTIS[f]	-781.2704	-5.46	+0.45	-	-
$[Au]^0_{VZISS}$	-981.4755	-3.40	-1.84	2.50-2.65	-0.30
$[Au]^+_{VZISS}$	-981.3543	-6.81	-2.26	2.06-2.52	+0.40
$[Au]^{2+}_{VZISS}$	-981.1016	-9.70	-6.96	2.03-2.18	+0.85
$[Au]^{3+}_{VZISS}$	-980.7469	-11.89	-9.49	1.95-2.05	+1.22
$[Au]^0_{BTIS}$	-990.7890	-5.38	-2.80	2.05-2.36	+0.77
$[Au]^-_{BTIS}$	-990.9009	-3.17	+0.61	2.22-2.29	+0.31
$[Au]^+_{BTIS}$(singlet)	-990.6127	-7.04	-4.07	2.01-2.13	+1.20
$[Au]^+_{BTIS}$(triplet)	-990.5755	-7.12	-6.26	2.03-2.48	+0.09
$[Au]^0_{BTIS}$[f]	-916.0831	-5.26	-2.52	2.05-2.33	+0.84
$[Au]^-_{BTIS}$[f]	-916.1880	-3.03	+0.81	2.24-2.25	+0.37

[a]Total energy of the cluster

[b]Energy of the highest occupied molecular orbital

[c]Energy of the lowest unoccupied molecular orbital

[d]The range of distances between the Au atom and the surface oxygens

[e]The Mulliken charge on the gold atom in the clusters

[f]Values that were obtained during initial calculations where the surface model for BTIS did not include a second layer oxygen atom in the QM region.

The HOMO-LUMO gap of VZISS is overestimated as a consequence of the finite cluster approach (a much larger number of atoms in the QM region is needed to fully reproduce the band gap). The error is expected to be in the LUMO description, because it is made up of delocalised orbitals that are fictitiously constrained in the QM region by the embedding potential [Bromley et al., 2003]. Using an experimental band gap of 3.37 eV for bulk ZnO, the correct LUMO energy is estimated to be –2.12 eV. The HOMO of the $[Au]^0_{VZISS}$ cluster, which is mainly the Au 6s orbital, lies higher in energy compared to the HOMO of a free Au atom. The orbitals of the metal are, therefore, shifted upwards by the electrostatic potential in the Zn vacancy. This upshift is also seen when all Zn and O ions are treated by MM and only the Au atoms are treated by QM. More importantly, the HOMO of Au in VZISS does not rise above the bottom of the conduction band of bare VZISS, implying that a neutral atom will not be ionised simply by loss of an electron into the conduction band of ZnO. This would be expected from the high ideal Schottky barrier of 4.24 eV (-2.12 + 6.36 eV) between a free Au atom and VZISS. For $[Au]^+_{VZISS}$, the HOMO is below the 6s level of a free Au atom, implying that the gold atom has indeed been ionised (considering that the Au orbitals are additionally shifted upwards by about 3 eV at the Zn vacancy) and this configuration can correctly be thought to be Au^+ZnO. Mulliken charges are generally unreliable in absolute terms, but the trends can give helpful insights. The $+0.7e^-$ increase in the Mulliken positive charge (removal of electron density from the Au atom) on Au relative to the value on the neutral cluster supports this picture. Additional support is from the fact that the Mulliken charges on all surface oxygen atoms were very similar for the neutral and singly charged clusters, suggesting that electron density was removed only from the Au atom when the cluster positive charge was increased.

For $[Au]^{2+}_{VZISS}$, the HOMO energy is above that of a free Au^+ atom, suggesting that an electron density from HOMO of Au^+ has not been removed completely. The $[Au]^{2+}_{VZISS}$ cluster is, therefore unlikely to be a pure $Au^{2+}ZnO(0001)$ state but more likely a superposition of $Au^+ZnO(0001)^+$ and $Au^{2+}ZnO(0001)$ states. A Mulliken charge analysis shows an $0.45e^-$ increase in positive charge on Au relative to the singly charged cluster case, not as dramatic as the charge change on Au between the neutral and the singly charged clusters. On similar grounds, it can be estimated that in the $[Au]^{3+}_{VZISS}$ cluster, gold is highly unlikely to be in the full +3 oxidation state. Mulliken charge analysis, however, does indicate that the positive charge on Au increases relative to the

doubly ionised cluster. The average Mulliken charge on the three surface oxygens nearest to the gold atom was found to be $-1.40e^-$ and $-1.28e^-$ for the doubly charged (+2) and triply charged (+3) clusters respectively, compared to $-1.50e^-$ and $-1.51e^-$ for the neutral and singly charged clusters respectively. This is a strong indication that an electron hole for the +2 and +3 charge states is localised on the oxygen atoms, and the Au atoms remains in a charge state close to +1 even when the total cluster positive charge is increased. There was no clear trend in the Mulliken charges for the different surface Zn atoms, except that the average charge on the Zn atoms were $+1.65e^-$, $+1.69e^-$, $+1.72e^-$ and $+1.73e^-$ for the $[Au]^0_{VZISS}$, $[Au]^+_{VZISS}$, $[Au]^{2+}_{VZISS}$, and $[Au]^{3+}_{VZISS}$ clusters respectively. Both LUMOs for $[Au]^{2+}_{VZISS}$ and $[Au]^{3+}_{VZISS}$ clusters lie below the HOMO of bare VZISS, implying that these species are unstable with respect to reduction via electron transfer from adjacent VZISS clusters.

Reaction energies for formation of the gold-loaded surface, from neutral and ionised gas-phase atoms are shown below. Electrons from the neutral Au atoms are assumed to be localised in nearby Zn-vacant sites. Adsorption energy of an electron into a bare VZISS cluster was found to be -0.74 eV. Energies of charged species have been corrected for long-range polarisation effects beyond the cutoff radius of the MM Active region (see Chapter 3.10: R = 13 Å and $\varepsilon = 9.78$, giving $W_p = -0.45q^2$ eV).

$Au^0_g + VZISS \rightarrow [Au]^0_{VZISS}$	E = -1.02 eV	(6.1)
$Au^0_g + VZISS \rightarrow [Au]^{+1}_{VZISS} + e^-_s$	E = +1.09 eV	(6.2)
$Au^+_g + VZISS \rightarrow [Au]^{+1}_{VZISS}$	E = -7.29 eV	(6.3)
$Au^0_g + VZISS \rightarrow [Au]^{+2}_{VZISS} + 2e^-_s$	E = +5.88 eV	(6.4)
$Au^{2+}_g + VZISS \rightarrow [Au]^{+2}_{VZISS}$	E = -22.56 eV	(6.5)
$Au^0_g + VZISS \rightarrow [Au]^{+3}_{VZISS} + 3e^-_s$	E = +12.54 eV	(6.6)
$Au^{3+}_g + VZISS \rightarrow [Au]^{+3}_{VZISS}$	E = -50.19 eV	(6.7)

Adsorption of a neutral atom onto the VZISS, without any subsequent ionisation, is a feasible step. However, formation of charged species from a neutral gas-phase atom becomes increasingly difficult as the oxidation state of the final cluster increases, owing to Au's high first to third ionisation potentials. The highly favourable adsorption energy of the gold cations is not enough to make up for the high ionisation potentials of Au.

It is noted that the adsorption energy of an electron onto a the VZISS, calculated to be –0.74 eV, is only an upper bound to the true value as the current calculations do not give the correct value for the LUMO energy of ZnO. The error can easily be in the order of ~1-2 eV because the 'true' LUMO energy is just over 2 eV below the zero level. With this in mind, the formation of $[Au]^{+}_{VZISS}$ can be considered feasible. On the other hand, Au^{2+} and Au^{3+} cannot form from simple ionization of Au^{0}.

Figure 6.4 shows the QM region of Zn-substituted BTIS clusters. The neutral $[Au]^{0}_{BTIS}$ cluster can be formed when Zn cations are substituted by Au cations of the same oxidation state, i.e. Au^{2+} substituting Zn^{2+}. The anionic and cationic clusters can be formed from $Zn^{2+} \rightarrow Au^{+}$ and $Zn^{2+} \rightarrow Au^{3+}$ substitutions respectively. Substitution by higher oxidation states leads to structures where Au is nearly at the same level as the Zn atoms. It was this structural feature of the higher oxidation states that necessitated the inclusion of a second layer oxygen atom in the QM region of these clusters. However, as seen in Table 6.1, the electronic properties properties for $[Au]^{-}_{BTIS}$ and $[Au]^{0}_{BTIS}$ clusters were reasonably reproduced by the surface model that did not include a second layer surface oxygen.

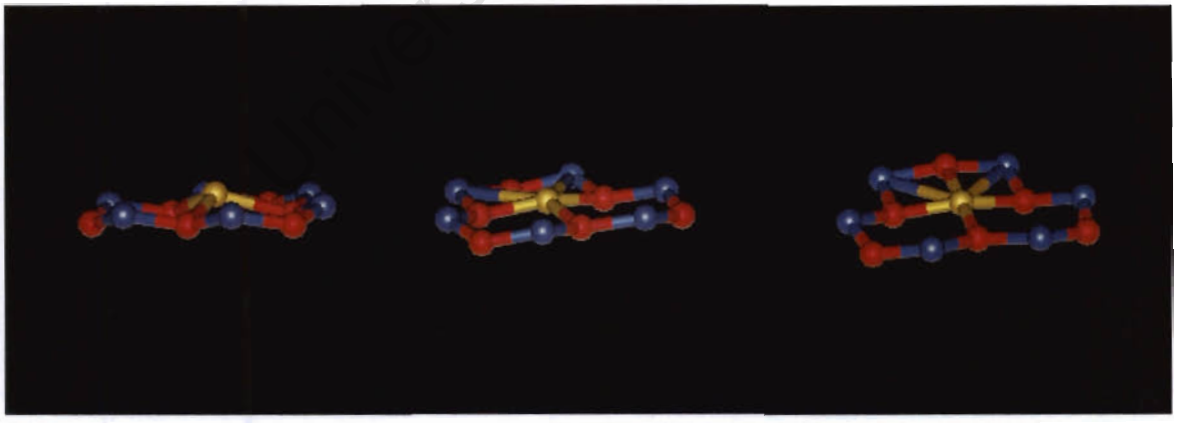

Figure 6.4: The QM region of the optimised $[Au]^{-}_{BTIS}$ (left), $[Au]^{0}_{BTIS}$ (middle) and $[Au]^{+}_{BTIS}$ (right) clusters.

Au is coordinated to four oxygen atoms for the $Zn^{2+} \rightarrow Au^{3+}$ substitution. The closest Au-O distances in the anionic, neutral and cationic clusters are 2.22 Å, 2.05 Å and 2.01

Å for $[Au]^-_{BTIS}$, $[Au]^0_{BTIS}$ and $[Au]^+_{BTIS}$(singlet) clusters respectively. The LUMOs for all the clusters lie above the HOMO of a bare BTIS. Au^+, Au^{2+} and Au^{3+} are all, therefore, stable as substitutional impurities for Zn^{2+} in the BTIS. A higher spin state (triplet) for $[Au]^+_{BTIS}$ was found to be higher in energy than the singlet state. Furthermore, the LUMO of the triplet state lies below the HOMO of bare BTIS and will thus not be an ideal state for stabilising Au^{3+} in a ZnO matrix. This was also an indication that the ground state of gold in the Au^{3+} exchange is a pure d^8s^0 state. The low Mulliken positive charge on Au in the triplet state suggests promotion of electrons from nearby oxygen atoms to the Au atom. It is noted that an $[Au]^{-2}_{BTIS}$ cluster, thought to represent a $Zn^{2+} \rightarrow Au^0$ substitution, was found during initial calculations with a 13-atom BTIS cluster to be an unstable species with respect to loss of electrons to vacuum (i.e. it had a positive HOMO energy) and would thus spontaneously collapse to one of the clusters considered.

Mechanisms by which substitution of Zn cations by Au cations occurs during catalyst preparation may involve exchange of hydroxyl or chloride complexes (depending on solution pH) when ZnO is mixed with the gold-precursor solution. The energetics of some of the possibilities were considered in the thermodynamic cycles that follow.

Charge neutral substitutions will naturally result in formation of $[Au]^0_{BTIS}$. It is proposed that in practice once such neutral species forms, it can donate an electron to a nearby $[Au]^0_{BTIS}$ cluster to reduce them to $[Au]^-_{BTIS}$ (where Au now exists as Au^+), with the original donor remaining as $[Au]^+_{BTIS}$. These considerations formed the basis for the thermodynamic cycles considered below (for charged clusters, long-range polarisation effects have been included, and the free electron is assumed to be trapped in a zinc-vacant site).

$AuOH + BTIS \rightarrow [Au]^0_{BTIS} + ZnOH$	E = +3.66 eV	(6.8)
$AuCl + BTIS \rightarrow [Au]^0_{BTIS} + ZnCl$	E = +3.85 eV	(6.9)
$Au(OH)_2 + BTIS \rightarrow [Au]^0_{BTIS} + Zn(OH)_2$	E = +1.86 eV	(6.10)
$AuCl_2 + BTIS \rightarrow [Au]^0_{BTIS} + ZnCl_2$	E = +1.56 eV	(6.11)
$Au + BTIS \rightarrow [Au]^0_{BTIS} + Zn$	E = +3.61 eV	(6.12)
$[Au]^0_{BTIS} \rightarrow [Au]^+_{BTIS} + e^-_s$	E = +6.65 eV	(6.13)
$[Au]^0_{BTIS} + e^-_s \rightarrow [Au]^-_{BTIS}$	E = -2.75 eV	(6.14)

It appears that substitution reactions for formation of $[Au]^0_{BTIS}$ from hydroxides or chlorides are not favoured. However, the reaction energies for exchanges involving the Au(II) complexes are significantly lower than for exchanges involving Au(I) complexes. Also, $[Au]^0_{BTIS}$ appears to be quite stable with respect to electron loss to form the electron deficient cluster, $[Au]^+_{BTIS}$. However, $[Au]^0_{BTIS}$ can readily accept an electron to form an Au^+-based species, $[Au]^-_{BTIS}$. This analysis shows that in general the substitutions in solution will not be easy and will require the presence of many other donor and acceptor impurities. A simple deposition of gold complexes onto an already formed ZnO crystal (bulk-terminated sites) will not result in any gold-zinc exchanges. Coprecipitation of both the Au and ZnO precursor complexes can, on the other hand, introduce gold as an impurity into the ZnO matrix. On the other hand, gold complexes can adsorb favourably on the surface in a non-exchange manner, as will be shown in the coming section.

Another possible mechanism for introduction of $Au^{\delta+}$ into BTIS is via surface diffusion of Au atoms between VZISS and BTIS. The energetics of this pathway were analysed for Zn^{2+} substitution by Au^{2+}, where it was assumed that a neutral gold atom, trapped in VZISS, migrates over the surface and replaces a zinc atom in BTIS, which ends up in VZISS. Although in principle a single large QM cluster containing both BTIS and VZISS is required to accurately analyse this possibility, the simplified consideration sketched in Figure 6.5 still gives valuable insight. The VZISS and the BTIS calculations were performed separately.

As Figure 6.5 shows, initial diffusion of a neutral gold atom from VZISS to BTIS is only mildly endothermic and hence feasible. This results in formation of an Au-Zn dimer over the BTIS. However, the 'flipping' of the dimer to incorporate Au into the BTIS is a highly unfavourable process (reaction energy of +3.66 eV). As a result, the whole pathway is unfavourable, and hence an unlikely mechanism for introduction of gold into the bulk-terminated island site of the ZnO(0001) surface.

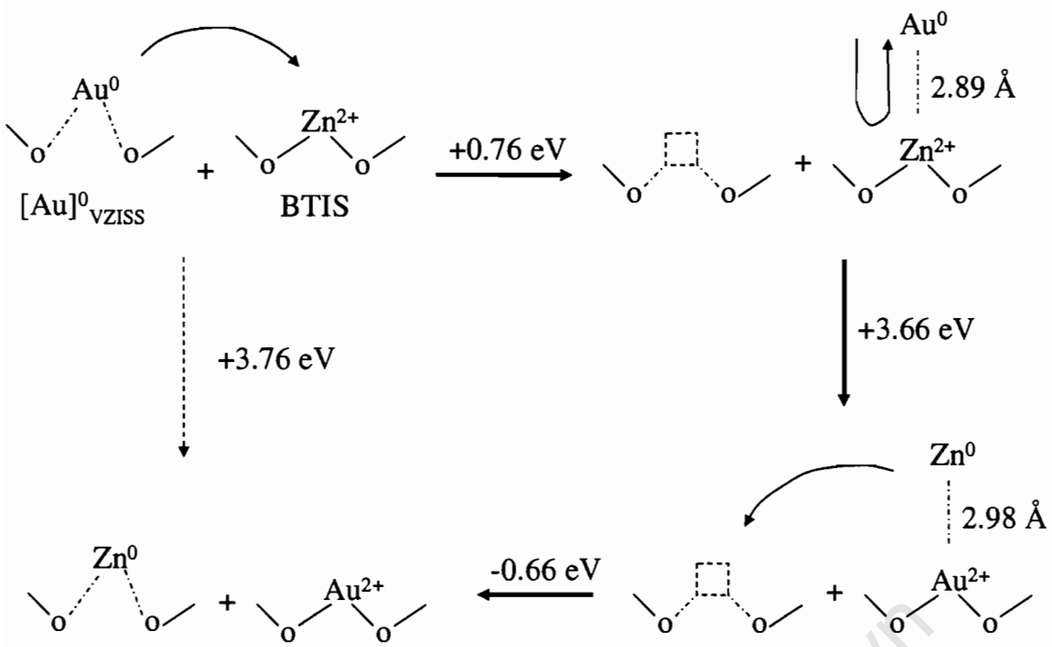

Figure 6.5: Computed energetics for diffusion of a gold atom from the zinc vacancy to the bulk-terminated island site of the ZnO(0001) surface. The calculated Au-Zn distances for the surface AuZn dimers formed in the process are also shown.

6.3.2. Deposition of Gold Hydroxyls on the Zinc Vacant ZnO(0001) Surface Site

Deposition of $Au(OH)_x$ complexes onto the VZISS was considered as a means of stabilising high oxidation states of gold in the VZISS. This consideration is different from the exchange thermodynamic analysis performed for BTIS, where the actual surface does not contain any hydroxyl groups. The geometries of the stable structures are shown in Figure 6.6. As shown below, these model precipitation reactions were found to be favourable:

$AuOH + VZISS \rightarrow [AuOH]_{VZISS}$ E = -2.78 eV (6.12)

$Au(OH)_2 + VZISS \rightarrow [Au(OH)_2]_{VZISS}$ E = -2.66 eV (6.13)

$Au(OH)_3 + VZISS \rightarrow [Au(OH)_3]_{VZISS}$ E = -4.84 eV (6.14)

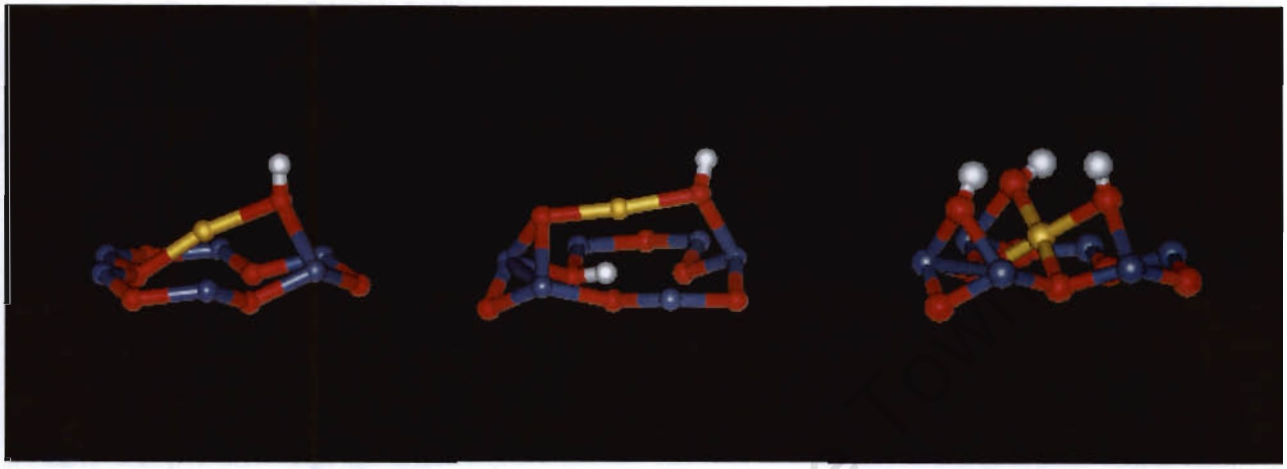

Figure 6.6: A section of the Au(OH), $Au(OH)_2$ and $Au(OH)_3$ complexes adsorbed onto the VZISS of ZnO(0001).

In AuOH adsorption, the Au atom of the hydroxyl complex interacts with a surface O atom and consequently the Au atom will remain oxidised. For $Au(OH)_2$ adsorption, the Au atom remains bonded to the O atoms from the bare complex, and an H-atom from one of the hydroxyls in $Au(OH)_2$ is lost to a surface oxygen, to form a surface hydroxyl. For $Au(OH)_3$ adsorption, a hydroxyl group is lost to the nearby zinc atom, and the gold atom bonds to two surface oxygen atoms to complete a square-planar arrangement of four oxygen atoms around the gold atom, which is typical for d^8 complexes. The closest Au-O distances in adsorbed $Au(OH)_2$ were 1.98-2.03 Å, which are close to the Au-O distances of 1.93 Å and 1.98 Å calculated for gas-phase $Au(OH)_2$ and Au(OH) complexes respectively. The Au-O distances in adsorbed $Au(OH)_3$ were 2.00-2.01 Å and 2.06-2.07 Å for bonding to the surface and the hydroxyl oxygens respectively. The Au-O distance in a gas-phase $Au(OH)_4^-$ complex was found to be 2.01 Å. It is concluded that under non-reducing hydrothermal conditions, gold cations in +1 to +3 oxidation states, stabilised by hydroxyl groups, can be formed on the ZnO surface during liquid phase preparation of Au/ZnO catalysts.

6.3.3. Interaction Between Adsorbed Au Atoms and CO

To understand how the electronic properties of gold can be perturbed by the support material, the interaction of Au atoms adsorbed in VZISS and BTIS with a CO molecule was studied. On passing CO over Au/ZnO catalysts prepared by coprecipitation and calcined in air at 400°C, IR bands at 2106 cm^{-1} and 2133 cm^{-1} were observed [Boccuzzi et al., 1995]. These bands were assigned to CO bonded to metallic and oxidized gold particles respectively. The bonding of CO onto transition metals is generally thought to involve donation of electrons from the 5σ orbital of CO onto the empty metal orbitals of the right symmetry (e.g. d_Z^2), and back-donation of electrons from the metal to the empty 2π* orbital of CO [Sung and Hoffmann, 1985]. All the frontier orbitals of CO are antibonding in origin. Therefore removal of electron density from the 5σ orbital strengthens the C-O bond, while filling of the 2π* orbital weakens the CO bond. These features of CO bonding make this molecule ideal for probing the electronic properties of a given potential active site.

Table 6.2 shows the energetics, structural parameters, and CO vibrational frequencies of CO adsorbed onto gas-phase Au atoms as well as Au atoms adsorbed on the ZnO(0001) surface sites. Figure 6.7 shows a section of the CO molecule adsorbed onto the gold atoms in the VZISS, while Figure 6.8 shows CO adsorbed onto the gold atoms in the BTIS.

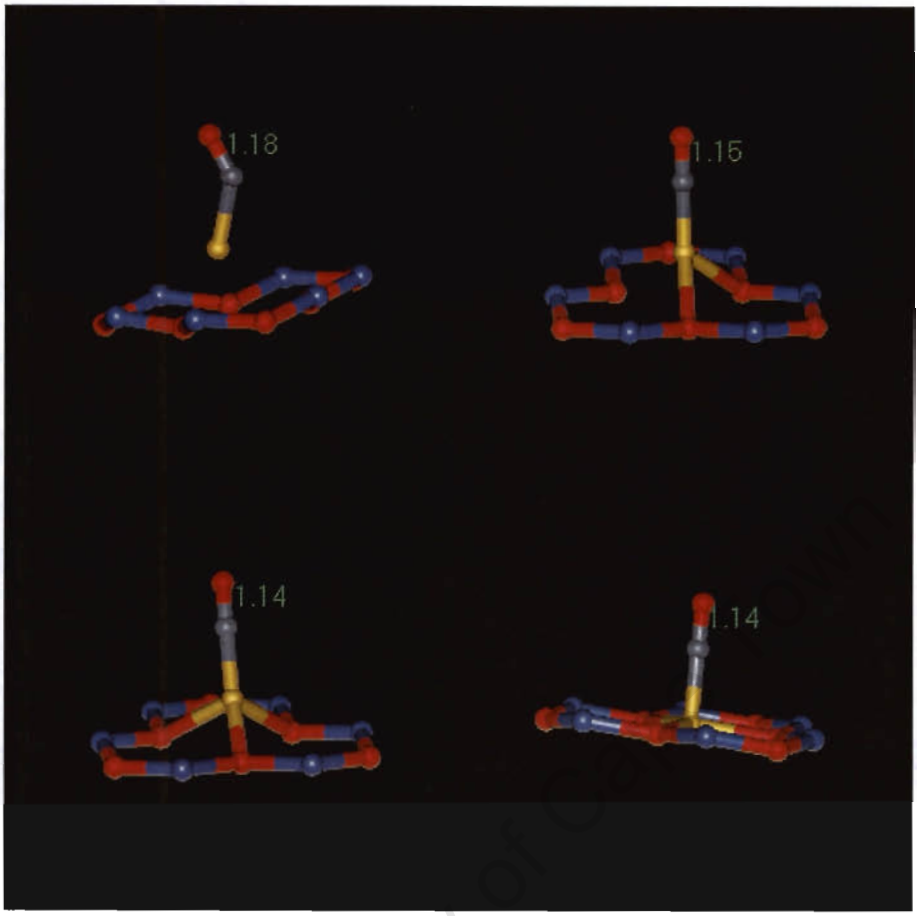

Figure 6.7: QM region of the CO-$[Au]^{0}_{VZISS}$ (top left), CO-$[Au]^{+}_{VZISS}$ (top right), CO-$[Au]^{2+}_{VZISS}$ (bottom left) and CO-$[Au]^{3+}_{VZISS}$ (bottom right) clusters.

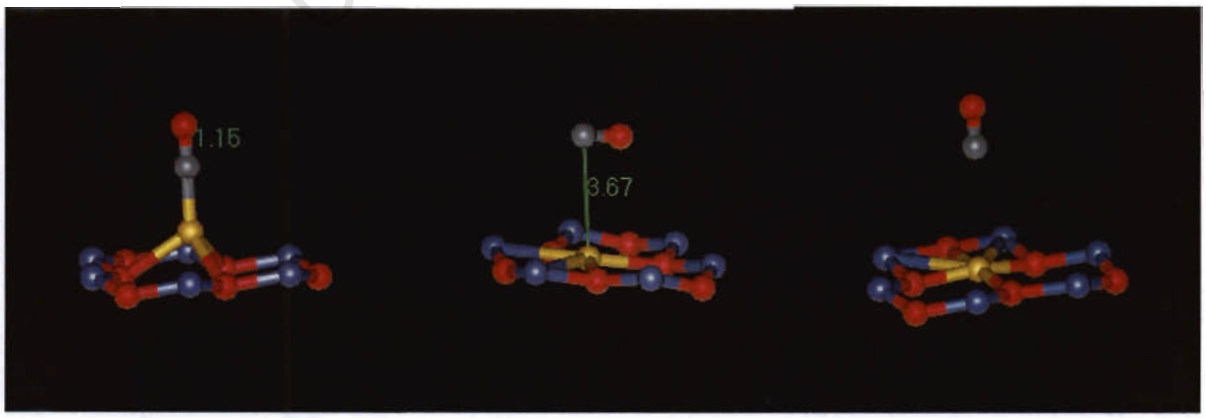

Figure 6.8: Top layer of the QM region of the CO-$[Au]^{-}_{BTIS}$ (left), CO-$[Au]^{0}_{BTISS}$ (middle) and CO-$[Au]^{+}_{BTISS}$ (right) clusters.

Table 6.2: Energetic and structural features of CO adsorbed on free and supported Au atoms in different oxidation states. The CO stretch frequency was calculated with all other atoms of the cluster frozen at their optimized positions.

	d_{Au-C} [Å]	d_{C-O} [Å]	$d_{Au-Osurf}$[a] [Å]	$\angle_{Au-C-O}$ [°]	ω_{CO} [cm^{-1}]	$E_{CO,Ads}$[b] [kJ/mol]
Gas Phase						
CO	-	1.14	-	-	2162	-
$AuCO^0$	2.06	1.15	-	136.1	2009	-43
$AuCO^+$	1.95	1.13	-	179.9	2263	-193
$AuCO^{2+}$	2.01	1.12	-	180.0	2319	-430
$AuCO^{3+}$	2.03	1.13	-	178.8	2245	-1124
Supported						
$CO\text{-}[Au]^0_{VZISS}$	1.99	1.18	2.46	140.1	1849	-78
$CO\text{-}[Au]^+_{VZISS}$	1.87	1.15	2.25	178.7	2089	-143
$CO\text{-}[Au]^{2+}_{VZISS}$	1.92	1.14	2.05	174.0	2149	-49
$CO\text{-}[Au]^{3+}_{VZISS}$	1.93	1.14	1.98[c]	178.0	2181	-56
$CO\text{-}[Au]^0_{BTIS}$[d]	3.67	1.14	2.04	-	2159	-6
$CO\text{-}[Au]^-_{BTIS}$	1.87	1.15	2.34	179.5	2065	-413
$CO\text{-}[Au]^+_{BTIS}$(singlet)	3.71	1.14	2.00	-	2349	0
$CO\text{-}[Au]^-_{BTIS}$[e]	1.87	1.15	2.35	179.9	2061	-122

[a]Shortest distance between the Au atom and the oxygen atoms of the ZnO(0001) surface

[b]Energy of the CO bonded cluster minus the energy of CO and the cluster with Au in VZISS or BTISS at infinite separation, or isolated atoms.

[c]This is the distance to an oxygen atom in the second layer of the ZnO surface. The shortest distance to the topmost surface oxygens was 2.15Å.

[d]There were three negative frequencies in the -52 to -7 cm^{-1} region during calculation of the CO stretch frequency. This is not expected to affect the conclusion that CO does not bind to the Au atom in this cluster. For the singly charged cluster, a single negative frequency was at –32 cm^{-1}. The negative frequencies may be caused by the constrained frequency calculation method, as the surface atoms are still coupled to the CO molecule.

[e]Calculation with the BTIS surface model that did not have an oxygen atom in the second layer.

The experimental vibrational frequency for a gas phase CO molecule is 2143 cm^{-1} and agrees well with the calculated value of 2162 cm^{-1}. The computed bond length is 0.01Å longer than the experimental value.

Adsorption of CO onto a neutral Au atom is stronger when the Au atom is supported on VZISS than on the gas phase. The CO bond is 0.03 Å longer on CO-$[Au]^0_{VZISS}$ than on $AuCO^0$, and in both cases longer than for the gas phase CO molecule, suggesting that backdonation of electrons to the $2\pi^*$ orbitals of CO has occured. The backdonation evidently occurs to a larger degree when the Au atom is supported. On analysis of the Au and CO–derived orbitals in gas-phase AuCO, it was found that there was very little mixing between the d-orbitals of Au and the orbitals from CO. Therefore, backbonding occured via donation of an electron in the 6s orbital of Au. This could explain why the Au-C-O angle is not 180°, since bending will maximize orbital overlap between the 2-lobed $2\pi^*$ orbital of CO and the spherical 6s orbital of Au. The bending also minimizes the repulsion energy between the filled Au d_z^2 orbital and the 5σ orbital of CO. This bending is predicted by other calculations [Liang and Andrews, 2000; Wu et al., 2002; see also Chapter 5]. As for the increased adsorption strength of CO when the Au atom is supported, it was found that the 6s orbital of Au (and other Au orbitals) is raised in energy by the electrostatic potential in the Zn-vacancy by about 2.7 eV, thus getting the energy level closer to that of the empty CO orbitals. The electrostatic potential in the VZISS affects the CO molecule as well, reducing the CO stretch frequency (or increasing the C-O bond length) even further. This is an example of the well known vibrational Stark effect [Brewer and Franzen, 2003].

Bonding of CO to cationic gold in the gas phase results in shortening of the CO bond and a subsequent increase in the CO frequency. The CO bond is shortened by removal of electron density from the 5σ orbital of CO. The CO frequency decreases relative to a free CO molecule when the gold cation is supported on VZISS. The up shifted d-orbitals of Au can now overlap with the CO molecule (i.e. back-bonding occurs). However, the positive charge on Au will be slightly reduced through interaction with the support, and consequently decrease the electrostatic contribution to the CO adsorption energy. This balance between orbital overlap and Coulomb interaction in this case resulted in a slight decrease in the CO adsorption energy relative to the gas-phase complex. The CO frequency is higher than for CO adsorbed on a neutral gold atom

(supported or gas-phase). However, the overall indication is that Au^+ on VZISS binds CO more strongly than Au^0 on VZISS. The higher charge states $[Au]^{2+}_{VZISS}$ adsorb CO with similar energies, which are lower than binding onto Au^{1+}. It has already been stated that as the cluster charge increases, the electron hole is simply localized on nearby oxygen atoms. Consequently, the gold atoms remain in more or less the same electronic state. However, their lower CO binding energies relative to the singly charged cluster might indicate the bonding to be purely electrostatic without any significant orbital interaction. The closeness of the C-O bond lengths and vibrational frequencies to the gas-phase value support this suggestion.

Regarding the gold cations in the BTIS, the structural and vibrational features of CO binding onto the $Zn^{2+} \rightarrow Au^+$ cluster agree with those obtained for CO binding onto Au^+ in VZISS. This confirms the similarity of the electronic state for gold in the two environments. However, CO binds much more strongly to Au^+ in BTIS, and appears to pull the surface Au atom out of the surface. Calculations with a BTIS surface model that had no oxygen in the bottom layer gave similar results, but with a lower adsorption energy (compared to the use of a 14-atom BTIS model). CO binds much less weakly to the BTIS clusters where higher oxidation states of gold have substituted the Zn^{2+} cation. For example in CO-$[Au]^0_{BTIS}$, where Au is in the +2 oxidation state, the CO molecule is about 3.7 Å away from the surface. While this trend is similar to that for Au cations in VZISS, the interactions with Au in BTIS here are much weaker for the higher Au oxidation states, and CO exists almost as a free gas-phase species above the cluster. The computed frequency for CO on $[Au]^+_{BTIS}$ is anomalous in light of the calculated CO bond length, and may indicate some limitations in the partial frequency calculation method.

6.4. Conclusions

It has been shown that Au^0 and Au^+ oxidation states of gold can exist on the zinc vacant site of ZnO(0001). The higher oxidation states of gold are likely to be reduced by electron transfer from the valence band of ZnO due to their deep lying LUMO levels. All the cationic states, Au^+, Au^{2+} and Au^{3+} can be stable as substitutional impurities in the bulk-terminated island site, i.e as replacements for Zn^{2+}. However, their formation mechanism is not certain. It appears that simple exchange from gold chlorides and

hydroxides is not a feasible route. However, the gold complexes can adsorb non-substitutionally onto the VZISS with high adsorption energies. This means that high oxidation states for gold can exist in the zinc-vacancy when stabilised by hydroxyls under mild conditions. Gold atoms at the Au/ZnO interface have different chemical properties compared to their gas-phase counterparts, as shown by CO adsorption studies. A supported neutral Au atom on the zinc vacancy binds CO stronger than a gas-phase neutral atom. Furthermore, Au^{+} stabilized in the zinc-vacancy or bulk-terminated island site is the most effective of all oxidation states in binding the CO molecule. Overall, the results discussed in this chapter show that the role of a support in Au/oxide catalysts is not to merely disperse gold atoms but to also alter the electronic structure of interfacial gold atoms, and hence tune gold's reactivity. It will be interesting to find out how the support influences the nucleation of gold clusters.

Chapter 7

NUCLEATION OF Au_N (N=1-4) CLUSTERS ON ZnO

In this chapter, the nucleation of gold clusters on the vacant zinc interstitial surface site (VZISS) is studied via the QM/MM method. The geometries of adsorbed clusters are generally not similar to the gas-phase geometries. Furthermore, supported charged clusters show smaller Au-Au distances than gas-phase clusters, due to a reduced Coulomb interaction. As with the single atoms, clusters with +2 and +3 charge states are unstable with respect to electron gain from adjacent bare VZISS clusters.

7.1. Introduction

The objective in this chapter is to study the adsorption and nucleation energetics of neutral and charged gold clusters on ZnO. This builds up on the insights into Au/ZnO CO oxidation and methanol synthesis catalysts already gained in Chapter 6. The vacant zinc interstitial surface site (VZISS) is chosen as a nucleation site, due to its morphology that is suited for trapping of metal atoms.

7.2. Computational Method

The polar zinc-terminated ZnO(0001) surface was chosen to represent the ZnO surface. This is one of the two polar surfaces that are exposed when the hexagonal ZnO crystal is cleaved perpendicular to the *c* axis. This polar surface, which is unstable upon idealised bulk-like termination, is naturally stabilised by creation of Zn vacancies on the surface [Dulub et al., 2002]. In the current model, 6 out of every 25 Zn atoms were removed on the surface to create a realistic model of the ZnO surface. The presence of vacant zinc and oxygen interstitial sites on the zinc and oxygen-terminated surfaces respectively has been shown to account to some of the spectroscopic features of the hydrogenated ZnO surface [French et al., 2003]. The top view of the hemispherical reconstructed zinc-terminated ZnO(0001) surface is shown in Figure 7.1, with the QM region indicated by CPK space filling model drawing. The QM region of the surface consisted of six zinc atoms and seven oxygen atoms, plus adsorbates (Au clusters in +0 to +3 charge states). Further details of the surface model, the QM/MM embedding methodology, and the basis sets on the QM atoms, the MM and QM codes, and the DFT functional employed, are as described in Chapter 6. For Au_3 and Au_4 clusters, at least two starting geometries were considered to arrive at the low energy structures reported here. The starting geometries were chosen to simulate adsorption, one at a time, of gold atoms onto the surface. This is different from the common approach were 'pre-formed' gas-phase clusters are adsorbed more or less intact onto the surface and then re-optimized. Mass selected Au_n clusters, starting from the monomer, have been deposited onto oxide supports by laser evaporation techniques [Heiz and Schneider, 2000]. Hence the predictions made in this study are experimentally verifiable.

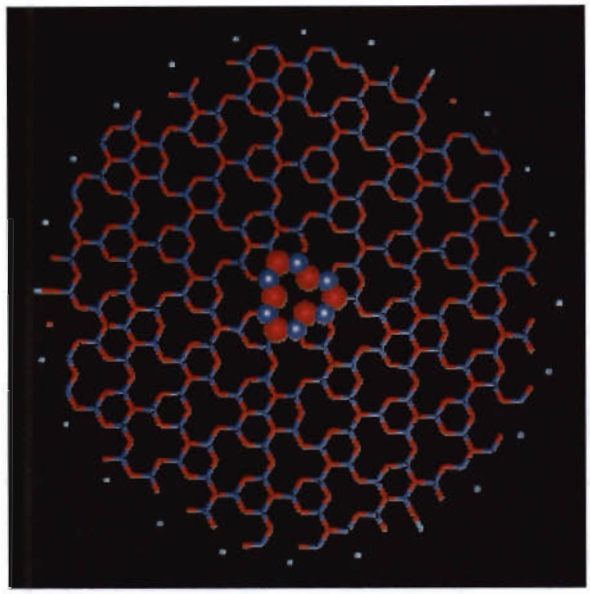

Figure 7.1: The top view of the hemispherical ZnO(0001) cluster. The QM region (VZISS) is indicated.

7.3. Results and Discussion

7.3.1. Geometry of Supported Gold Clusters

Neutral Au_n clusters

Figure 7.2 shows the geometries of neutral Au_n (n=1-4) clusters supported on ZnO(0001) surface. Only the top section of the QM region is shown. In the gas-phase, the calculated average Au-Au distances for neutral clusters, in Å, are 2.57, 2.62 and 2.76 for Au_2, Au_3 and Au_4 clusters respectively. The Au_4 cluster is planar rhombic, while Au_3 is an obtuse triangle. As Figure 7.2 shows, the Au-O distance is shorter for supported Au_3 and Au_4 compared to Au_1 and Au_2. The dimer and trimer Au-Au distances are slightly expanded relative to their gas-phase values. The supported Au_4 cluster, on the other hand, has quite a distribution of bond distances. This may make it difficult to experimentally determine the cluster size from experimental average Au-Au distances only.

Au_n^+ clusters

Supported singly charge gold clusters are shown in Figure 7.3. The gas-phase Au-Au distances, in Å, are 2.69, 2.70 and 2.76 for Au_2^+, Au_3^+ and Au_4^+ clusters respectively. Gas-phase Au_3^+ is an equilateral triangle, while Au_4^+ is planar rhombic. The latter structures agree with those reported in the literature [Wu et al., 2002]. Comparing neutral and charged gas-phase clusters, there is an expansion of the gold clusters with an increase in charge (as expected due to increased Coulomb repulsion between the atoms) which is not present for Au_4^+. For the supported singly charged clusters, the Au-O distances are generally much smaller than for the adsorption of neutral clusters. All of Au_2-Au_4 clusters show some bonding to adjacent zinc atoms. However, there is no striking differences in the Au-Au distances that would allow easy experimental differentiation between supported neutral and charged gold clusters on the basis of bond distances alone. This insensitivity of the Au-Au distances to the cluster oxidation states is seen for the +2 and +3 charged clusters as well. It is most likely due to the fact that the Coulomb repulsion between the supported gold atoms is much smaller than in the gas-phase because the positive charge is distributed throughout the whole cluster (including oxygen and zinc atoms of the support), and not just on the gold atoms (as pointed out in Chapter 6). This allows existence of, for example, a supported Au_2^{2+} cluster, which in the gas-phase only exist as an excited state.

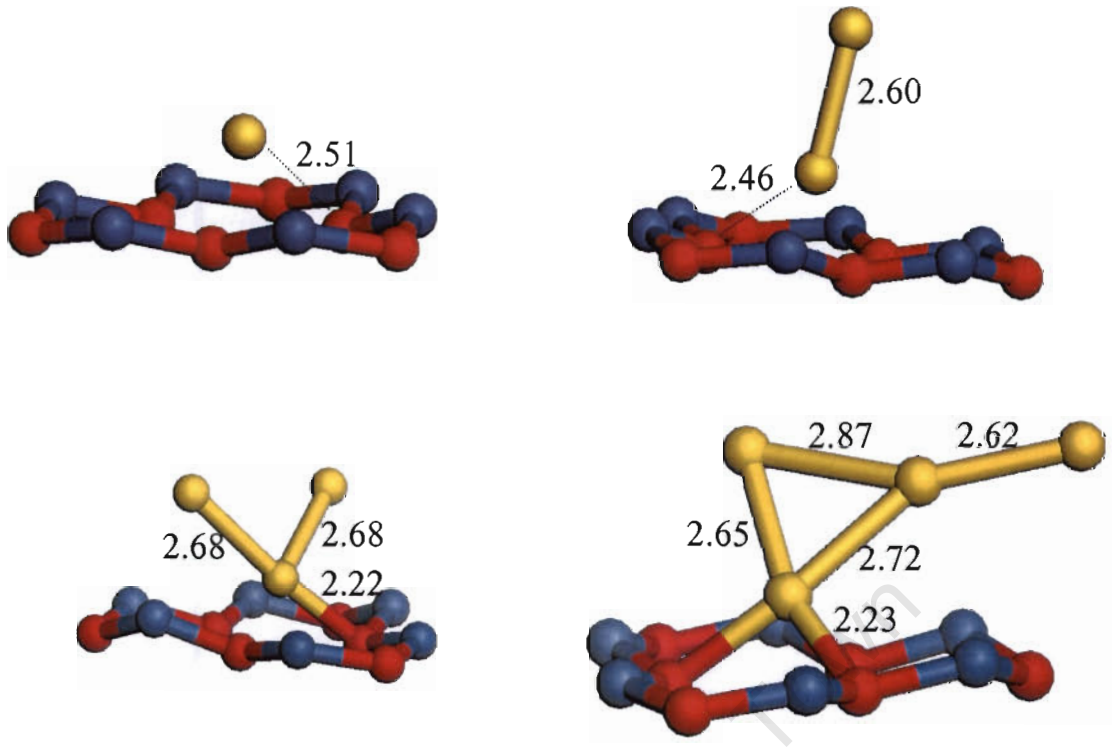

Figure 7.2: Structures of neutral Au_n clusters supported on the vacant-zinc interstitial site (VZISS) of the ZnO(0001) surface. The bond distances are in Å. The nearest cluster-oxygen distances are also shown.

Au_n^{2+} clusters

Figure 7.4 shows the structures of supported Au_n^{2+} clusters. As already mentioned, gas-phase Au_2^{2+} is unbound due to the high Coulomb repulsion between the gold atoms. Only the excited (triplet) state exists (with an Au-Au distance of 2.88 Å). Gas-phase Au_3^{2+}, which can practically be equilateral or obtuse due to the low variation of the total energy (~0.005 eV variation) as the bond angle is changed from 60 to 114°, has an average bond distance of 2.84 Å. The Au_4^{2+} gas-phase cluster is tetrahedral, as found by Pyykkö and Runeberg [1993], with an Au-Au distance of 2.83 Å. It can be seen in Figure 7.4 that the Au-Au distances of supported clusters are smaller than the values stated for gas-phase clusters. Again, this is because the positive charge is hardly localised on the gold cluster in the presence of the support. On average, the seed gold atom is closer to the surface oxygen atom than for the neutral and +1 charged clusters.

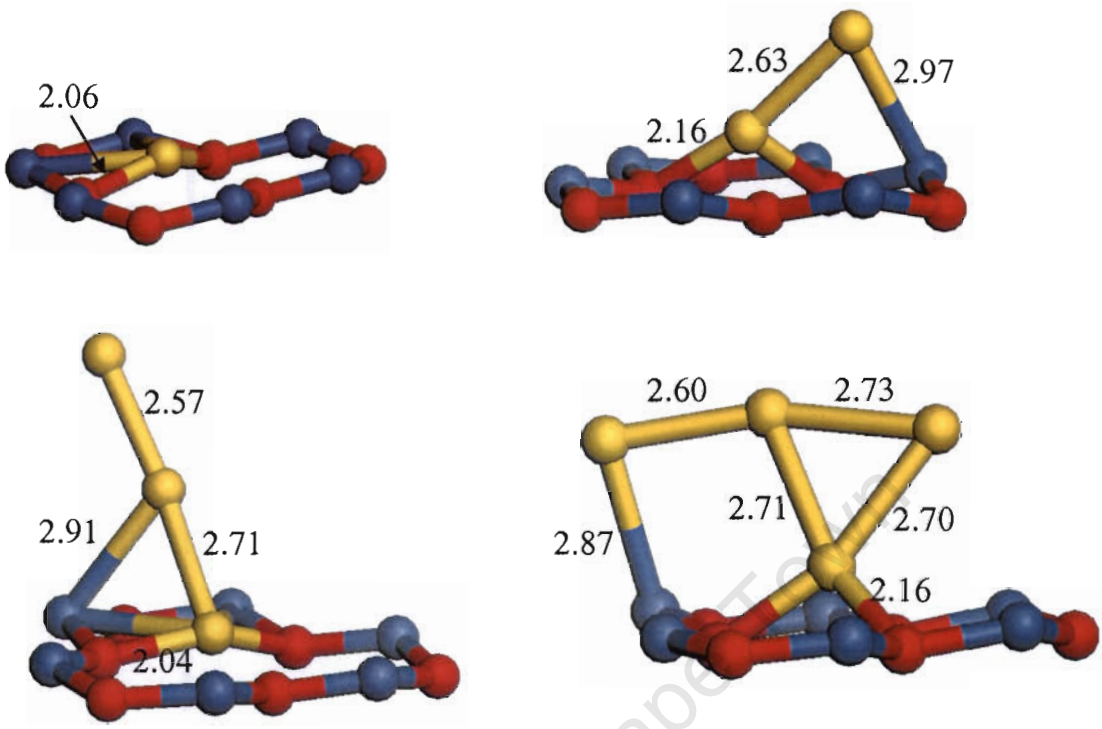

Figure 7.3: Structures of Au_n^+ clusters supported on the vacant-zinc interstitial site (VZISS) of the ZnO(0001) surface. The bond distances are in Å. The nearest cluster-oxygen distances are also shown.

Au_n^{3+} clusters

In the gas-phase, all triply charged clusters up to n=4 are unbound. As seen in Figure 7.5, the interaction with the support allows nucleation to Au_4^{3+} to be possible. With the exception of supported Au_3^{3+}, the seed atom is at or below the level of surface zinc atoms, interacting strongly with the oxygen atom. For Au_3^{3+}, the cluster lifts up one of the surface oxygen atoms. As will be shown below, the highly charged clusters (+2 and +3) are highly unstable with respect to reduction to either neutral or +1 charged clusters.

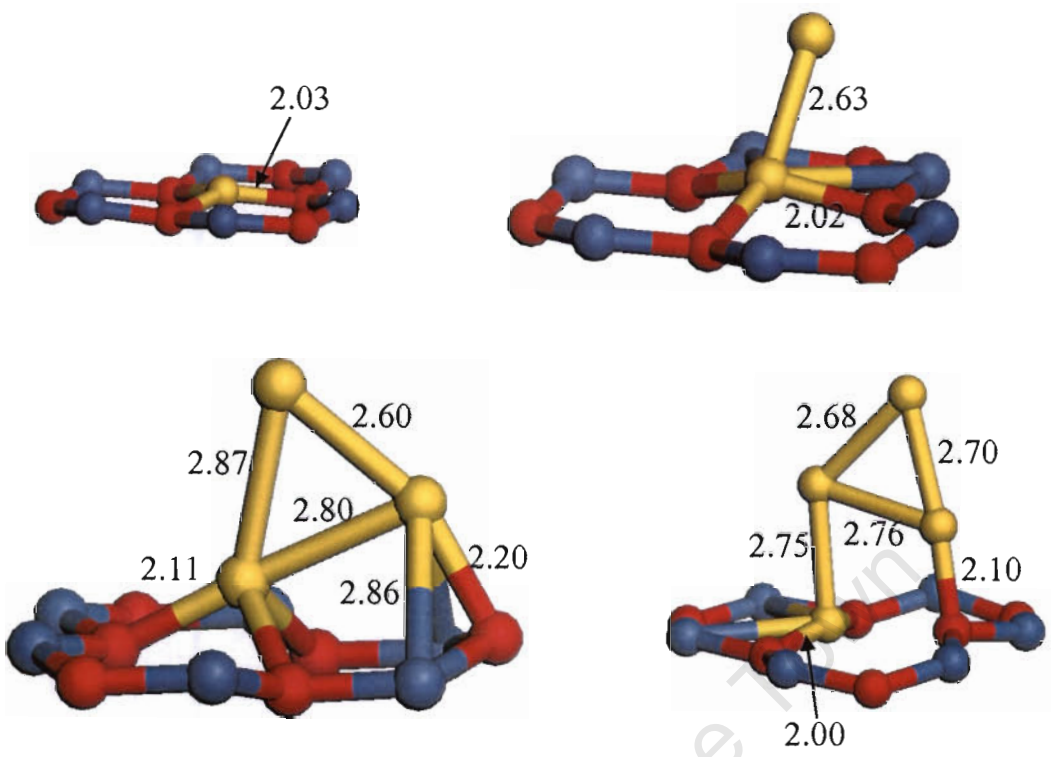

Figure 7.4: Structures of Au_n^{2+} clusters supported on the vacant-zinc interstitial site (VZISS) of the ZnO(0001) surface. The bond distances are in Å. The nearest cluster-oxygen distances are also shown.

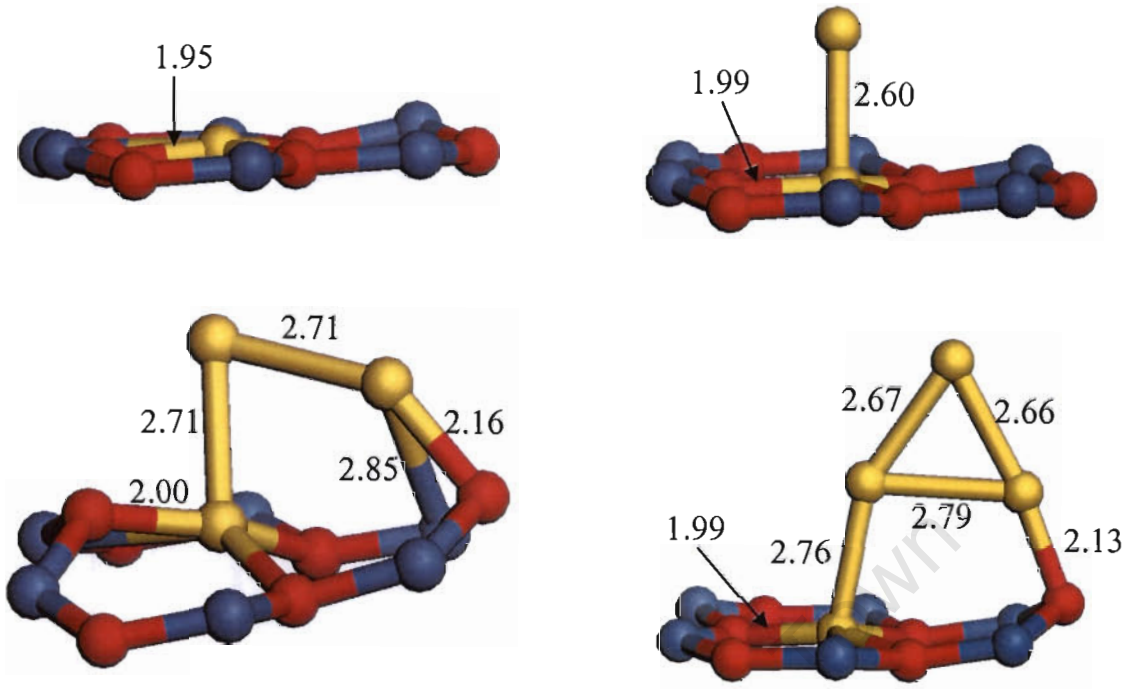

Figure 7.5: Structures of Au_n^{3+} clusters supported on the vacant-zinc interstitial site (VZISS) of the ZnO(0001) surface. The bond distances are in Å. The nearest cluster-oxygen distances are also shown.

7.3.2. Energetics of Cluster Nucleation

Table 7.1 shows the energetics of nucleation of gold clusters in four different charge states onto the vacant zinc interstitial surface site (VZISS). By comparison of the frontier orbital energies (HOMO and LUMO energies) of the supported clusters with those of the bare ZnO surface, it can be deduced that only Au_n^0 and Au_n^+ were stable with respect to reduction by electron gain from the valence band of ZnO.

Table 7.1: Energetics of adsorption and nucleation of Au_n(n=1-4) clusters on the vacant interstitial surface site (VZISS) of the ZnO(0001) surface.

	Total Energy [Ha]	HOMO[eV][a]	LUMO[eV]	Adsorption Energy [eV][b]	Nucleation Energy [eV][c]
n					
	Neutral clusters				
1	-981.4755	-3.40	-1.84	-1.02	-
2	-1117.4442	-4.75	-0.90	-1.70	-2.72
3	-1253.3860	-4.32	-2.68	-2.76	-2.00
4	-1389.3339	-5.04	-2.23	-2.16	-2.91
	Au_n^+ clusters				
1	-981.3543	-6.81	-2.27	-7.29	-
2	-1117.2748	-7.17	-5.10	-6.74	-1.42
3	-1253.2059	-7.04	-4.01	-4.77	-1.71
4	-1389.1416	-7.23	-5.42	-5.79	-1.83
	Au_n^{2+} clusters				
1	-981.1016	-9.70	-6.96	-22.56	-
2	-1117.0108	-9.70	-7.21	DNE[d]	-1.11
3	-1252.9519	-9.16	-7.19	-14.77	-1.98
4	-1388.8898	-9.06	-6.43	-12.35	-1.89
	Au_n^{3+} clusters				
1	-980.7469	-11.89	-9.49	-50.19	-
2	-1116.6610	-11.41	-9.35	DNE[d]	-1.24
3	-1252.6087	-11.37	-9.21	DNE[d]	-2.15
4	-1388.5692	-11.36	-9.00	DNE[d]	-2.51

[a]For bare VZISS, the HOMO was calculated to be -5.49 eV.

[b]Defined, for any charge state δ, as the energy for the reaction Au_n^{δ} + VZISS → $[Au_n]^{\delta}_{VZISS}$.

[c]Defined as the energy for the reaction Au_1^0 + $[Au_{n-1}]^{\delta}_{VZISS}$ → $[Au_n]^{\delta}_{VZISS}$.

[d]Cannot be computed because the gas-phase cluster is not bound.

As seen in Table 7.1, all clusters, neutral or charged, can adsorb from the gas-phase to the VZISS favourably. In principle, any single atom in any given charge state can act as a seed atom for nucleation of gold clusters because of favourable energetics. However, nucleation of Au atoms seems to be most favourable when the seed atoms are neutral, except for nucleation onto $[Au_2]^{3+}_{VZISS}$. For Au_3, adsorption energy onto the VZISS cluster is greater than nucleation to that cluster. This suggests that fragmentation to a dimer and a monomer upon adsorption is a strong possibility. As noted, the LUMO of all clusters with a total charge equal to or greater than +2 have LUMO energies that are lower than HOMO of bare VZISS (-5.49 eV). This means that these clusters are unstable with respect to electron gain from the valence band of bare VZISS. Therefore, only neutral and singly charge clusters are expected to grow on the VZISS of the ZnO(0001) surface. For a given cluster charge state, the HOMO and LUMO energies change with the cluster size. A cluster-size sensitivity to reactivity is, therefore, expected. The question of which cluster will be more reactive than the other will depend on the nature of the adsorbate. The high activity of singly charged gold for CO adsorption has already been pointed out in Chapter 6.

7.4. Conclusions

Au_n (n=1-4) in the 0 to +3 charge states can grow on the zinc-vacant surface site of ZnO(0001) with geometries that are different from those expected from the gas-phase. Supported charged clusters show smaller Au-Au distances than gas-phase clusters. This is because on the supported clusters, the positive charge is distributed throughout the surface-Au_n entity. As a result, the Coulomb repulsion that existed between the gas-phase gold atoms is decreased by interaction with the support. All Au single atoms, irrespective of the charge state, can act as seed atoms for nucleation of the gold clusters. However, nucleation onto a neutral gold atom is the most favourable. Clusters with +2 and +3 charge states are not expected to have high lifetimes experimentally due to their instability with respect to reduction to either neutral or +1 charged clusters. This is because their LUMO energies are far below the HOMO of a bare VZISS cluster.

Chapter 8

GENERAL CONCLUSIONS

8.1. From Bulk to Clusters

Using activation of syngas molecules (CO, CO_2 and H_2) as a test case, periodic and cluster density functional calculations were performed to investigate the change in nobility of gold from the extended surface to small clusters. The most closed packed surface of gold, the (111) surface, is capable of facilitating the reaction between adsorbed species derived from CO_x and H_2, leading to methanol. The activation energies for one pathway over another one can be related to the position of the adsorbate energy levels relative to the Fermi level. For a reaction to commence, the neutral starting molecules have to adsorb on the surface. It was found that this crucial initial step is not a feasible step on the Au(111) surface of bulk gold, which is ascribed to the nobility of bulk gold. It is important to stress that the nobility is due to the inability of gold to bind CO, CO_2 and H_2 efficiently, not because the radical intermediates cannot react with each other.

While CO and H_2 adsorption energetics are improved on a frozen Au_{13} cluster, CO_2 adsorption remains unfeasible. This suggests that for CO_2 activation non-neutral gold particles or the support may be beneficial. Of course, this inertness of gold towards CO_2 makes it a good CO_2 production catalyst (e.g. from CO oxidation). In agreement with the experimental finding that small gold particles seem to be beneficial for catalytic activity for both CO oxidation and CO_x hydrogenation, it was found that small gold clusters (1 to 13 atoms in size) can bind both CO and H strongly. Due to the abrupt changes in the orbital symmetries and the energies of the HOMO and LUMO in this small cluster size range, the adsorption energies depend very strongly on the number of gold atoms present, i.e. each atom makes a difference as it changes the energy and symmetry of the frontier orbitals. For H adsorption, there is a very marked odd-even oscillation in adsorption

energies, with the odd-numbered clusters being generally more reactive than the even clusters, up to about 10 atoms when the HOMO-LUMO gap ceases to fluctuate strongly. These results clearly shed some useful insights into the chemical reactivity of small gold particles. Before they can be fully related to experimental runs where the metal particles are supported, a study of the metal-support interactions is necessary. The high chemical reactivity of naked clusters also imply that they will bind strongly to the support, which can alter their electronic properties.

8.2. Metal-Support Interactions: The Au-ZnO(0001) Case

Using the polar zinc-terminated ZnO(0001) surface as a model support, the role of the metal-support interactions in gold catalysis was investigated using a hybrid QM/MM Embedding method. Gold atoms can exist on the zinc-vacant site of the support surface as either Au^0 or Au^+. The electrostatic potential in the zinc vacancy shifts up the orbital energies of the gold atoms relative to their gas-phase values. Gold atoms of higher oxidation states in this site are likely to be reduced to these 0 and +1 oxidation states, as the higher oxidation states have the LUMO energies that are below the HOMO energies of bulk ZnO(0001). However, it is possible for the higher oxidation states to exist when gold is stabilized by hydroxyl groups, e.g. $Au(OH)_2$ and $Au(OH)_3$. This is an important finding as practical gold catalysts are generally prepared by mixing the support material with aqueous solutions of $HAuCl_4.xH_2O$, where the solution pH determines the nature of the gold complexes in solution. Another possible site on the support where gold can be stabilized in high oxidation states is the bulk-terminated island site. This is essentially the perfect Zn-terminated site with Zn^{2+} substituted by Au atoms. It was found that both Au^+, Au^{2+}, and Au^{3+} can substitute Zn^{2+} at this site and remain stable with respect to electron gain from the top of the valence band of bare ZnO(0001). For Au^{3+}, the electronic state for Au appears to be a pure d^8s^0.

CO was used as a test molecule to probe the chemical reactivity of the gold atoms in different sites and oxidation states. It was generally found that Au^+ was the most reactive towards CO. The higher oxidation states in the bulk-terminated island site do not bind the

CO molecule at all (weak physisorption). Furthermore, a neutral gold atom can bind CO more strongly when it is supported (in the vacancy site) than on the gas-phase. This implies that the support can change the reactivity of supported clusters even in cases where there is no change in the oxidation state of the metal.

Finally, the gold clusters prefer to nucleate on the support when a neutral atom is a seed atom, as opposed to a charged atom. There is no marked difference in the Au-Au bond lengths for supported clusters with different total charges.

8.3. Suggested Future Direction

The marked changes in the reactivity of gold clusters with the surface structure and the precise number of atoms may partly explain the discrepancy in experimental literature on gold catalysis. Furthermore, the support can stabilize different oxidation states of the metal on different sites. Therefore, the mode of catalyst preparation, which may influence the type of surface imperfections and impurities present, will affect the chemical reactivity. This, again, will lead to differences in experimental reaction-characterization of catalysts. However, there are new good methods of preparing and characterizing catalysts with a high degree of control of the surface structure. The challenge, for theory, is to provide a detailed understanding of the catalyst preparation methods, in particular to answer the following general questions:

- How does gold-complexing ligands interact with the support?
- What is the support-dependency of the nature of the metal-support interactions?
- What is the structure of metal clusters on the surface, and the support-surface structure, under typical catalytic conditions?

While the first two questions can, in principle, be tackled using methodologies that are already available, it will probably be a while before the third question can be fully tackled. This is because for small clusters the phase space is already large without introducing the support. However, this may be more of a time issue and not due to

complete lack of methodologies. The problem of 'vacuum' to 'real' conditions can be tackled using statistical thermodynamic techniques. By beginning to address the above questions, high-level theoretical calculations can go beyond electronic structure prediction and expand their involvement by addressing questions related to catalyst selection and synthesis.

Chapter 9

REFERENCES AND BIBLIOGRAPHY

Aida, T., Higuchi, R. and Niiyama, H.,
Decomposition of Freon-12 and Methyl Chloride over Supported Gold Catalysts
Chemistry Letters (1990) 2247 – 2250.

Akhter, S., Lui, K. and Kung, H.H.,
Comparison of the Chemical Properties of the Zinc-Polar, the Oxygen-Polar, and the Nonpolar Surfaces of ZnO
Journal of Physical Chemistry **89** (1985) 1958 – 1964.

Ali Omar, M.,
Elementary Solid State Physics: Principles and Applications
Addison-Wesley Publishing Company, Phillipines, 1975.

Andrae, D., Häussermann, U., Dolg, M., Stoll, H. and Preuss, H.,
Energy-Adjusted Ab Initio Pseudopotentials for the Second and Third Row Transition Elements
Theoretica Chimica Acta **77** (1990) 123 – 141.

Andreeva, D.,
Low Temperature Water Gas Shift over Gold Catalysts
Gold Bulletin **35:3** (2002) 82 – 88.

Andreeva, D., Tabakova, T., Idakiev, V. and Naydenov, A.,
Complete Oxidation of Benzene over Au-V_2O_5/TiO_2 and Au-V_2O_5/ZrO_2 Catalysts
Gold Bulletin **31:3** (1998) 105 – 106.

Andreeva, D., Idakiev, V., Tabakova, T. and Andreev, A.,
Low-Temperature Water-Gas Shift Reaction over Au/α-Fe_2O_3
Journal of Catalysis **158** (1996) 354 – 355.

Badlani, M. and Wachs, E.,
Methanol: a "Smart" Chemical Probe Molecule
Catalysis Letters **75:3-4** (2001) 137 – 149.

Baiker, A., Koeppel, R.A., Schild, C. and Wokaun, A.
Carbon Dioxide Hydrogenation over Au/ZrO_2 Catalysts from Amorphous Precusors: Catalytic Reaction Mechanism
Journal of the Chemical Society: Faraday Transactions **87:17** (1991) 2821 – 2828.

Baiker, A., Kilo, M., Maciejewski, M., Menzi, S. and Wokaun, A.
Hydrogenation of CO_2 over Copper, Silver and Gold/Zirconia Catalysts: Comparative Study of Catalyst Properties and Reaction Pathways
Guczi, L., Solymosi, F. and Tétényi, P. (Editors)
Proceedings of the 10th International Congress on Catalysis
Budapest, 1992.
Studies in Surface Science and Catalysis **75B** (1993) 1257 – 1272.

Bamwenda, G.R., Tsubota, S., Nakamura, T. and Haruta, M.,
The Influence of the Preparation Methods on the Catalytic Activity of Platinum and Gold Supported on TiO_2 for CO Oxidation
Catalysis Letters **44** (1997) 83 – 87.

Blick, K., Mitrelias, T.D., Hargreaves, J.S.J., Hutchings, G.J., Joyner, R.W., Kiely, C.J. and Wagner, F.E.,
Methane Oxidation using Au/MgO Catalysts
Catalysis Letters **50** (1998) 211 – 218.

Boccuzzi, F., Chiorino, A. and Manzoli, M.,
Au/TiO_2 Nanostructured Catalyst: Pressure and Temperature Effects on the FTIR Spectra of CO Adsorbed at 90 K
Surface Science **502-503** (2002) 513 – 518.

Boccuzzi, F., Chiorino, A., Manzoli, M., Andreeva, D. and Tabakova, T.,
FTIR Study of the Low-Temperature Water-Gas Shift Reaction on Au/Fe_2O_3 and Au/TiO_2 Catalysts
Journal of Catalysis **188** (1999) 176 – 185.

Boccuzzi, F., Cerrato, G., Pinna, F. and Strukul, G.,
FTIR-UV-Vis, and HRTEM Study of Au/ZrO_2 Catalyst: Reduced Reactivity in the $CO-O_2$ Reaction of Electron-Deficient Gold Sites Present on the Used Samples
The Journal of Physical Chemistry B **102:30** (1998) 5733 – 5736.

Boccuzzi, F., Chiorino, A., Tsubota, S. and Haruta, M.,
FTIR Study of Carbon Monoxide Oxidation and Scrambling at Room Temperature over Gold Supported on ZnO and TiO_2
Journal of Physical Chemistry **100** (1996) 3625 – 3631.

Boccuzzi, F., Chiorino, A., Tsubota, S. and Haruta, M.,
An IR Study of CO-Sensing Mechanism on Au/ZnO
Sensors and Actuators B **24-25** (1995) 540 – 543.

Bond, G.C. and Thompson, D.T.,
Gold-Catalysed Oxidation of Carbon Monoxide
Gold Bulletin **33:2** (2000) 41 – 51.

Bond, G.C. and Thompson, D.T.,
Catalysis by Gold
Catalysis Reviews - Science and Engineering **41**(3 & 4) (1999) 319 – 388.

Bond, G.C. and Sermon, P.A.,
Gold Catalysts for Olefin Hydrogenation,
Gold Bulletin (1973) 102 – 105.

Bond, G.C.,
The Catalytic Properties of Gold
Gold Bulletin (1972) 11 – 12.

Bravo-Pérez, G., Garzón, I.L. and Novaro, O.,
Ab Initio Study of Small Gold Clusters
Journal of Molecular Structure (Theochem) **493** (1999) 225 – 231.

Brewer, S.H. and Franzen, S.,
A Quantitative Theory and Computational Approach for the Vibrational Stark Effect
Journal of Chemical Physics **119** (2003) 851 – 858.

Bromley, S.T., French, S.A., Sokol, A.A., Catlow, C.R.A. and Sherwood, P.,
Metal Cluster Support Interactions in the Cu/ZnO System: A QM/MM Study
Journal of Physical Chemistry B **107** (2003) 7045 – 7057.

Buckart, S., Ganteför, G., Kim, Y.D. and Jena, P.,
Anomalous Behaviour of Atomic Hydrogen Interacting with Gold Clusters
Journal of the American Chemical Society **125** (2003) 14205 – 14209.

Buffat, Ph. and Borel, J.-P.,
Size Effect on the Melting Temperature of Gold Particles
Physical Review A **13** (1976) 2287 - 2298.

Cao, Z., Wang, Y., Zhu, J., Wu, W. and Zhang, Q.,
Static Polarizabilities of Copper Cluster Monocarbonyls Cu_nCO (n = 2 -13) and Selectivity of CO Adsorption on Copper Clusters
Journal of Physical Chemistry B **106** (2002) 9649 – 9654.

Carrey, J., Maurice, J.-L., Petroff, F. and Vaurès, A.,
Growth of Clusters on Amorphous Al_2O_3: Are Small Clusters More Mobile than Atoms?
Surface Science **504** (2002) 75 – 82.

Catlow, C.R.A., Bulatov, V.L. and Grimes, R.W.,
Computational Studies of the Structures, Energetics and Dynamics of Clusters
Nuclear Instruments and Methods in Physics Research B **122** (1997) 301 – 310.

Cha, D.Y. and Parravano, G.,
Surface Reactivity of Supported Gold I. Oxygen Transfer Between CO and CO_2
Journal of Catalysis **18** (1970) 200 – 211.

Chang, C.-K., Chen, Y.-J. and Yeh, C.-T.,
Characterizations of Alumina-Supported Gold with Temperature-Programmed Reduction
Applied Catalysis A: General **174** (1998) 13 – 23.

Centeno, M.A., Paulis, M., Montes, M. and Odriozola, J.A.,
Catalytic Combustion of Volatile Organic Compounds on $Au/CeO_2/Al_2O_3$ and Au/Al_2O_3 Catalysts
Applied Catalysis A: General **234** (2002) 65 – 78.

Costello, C.K., Kung, M.C., Oh, H.-S., Wang, Y. and Kung, H.H.,
Nature of the Active Site for CO Oxidation on Highly Active Au/γ-Al_2O_3
Applied Catalysis A: General **232** (2002) 159 – 168.

Costello, C.K., Yang, J.H., Law, H.Y., Wang, Y., Lin, J.-N., Marks, L.D., Kung, M.C. and Kung, H.H.,
On the Potential Role of Hydroxyl Groups in CO Oxidation over Au/Al_2O_3
Applied Catalysis A: General **243** (2003) 15 – 24.

Cunningham, D.A.H., Vogel, W., Kageyama, H., Tsubota, S. and Haruta, M.,
The Relationship Between the Structure and Activity of Nanometer Size Gold When Supported on $Mg(OH)_2$
Journal of Catalysis **177** (1998) 1 – 10.

Delley, B.,
From Molecules to Solids with the $DMol^3$ Approach
Journal of Chemical Physics **113** (2000) 7756 – 7764.

Delley, B.,
An All-Electron Numerical Method for Solving the Local Density Functional for Polyatomic Molecules
Journal of Chemical Physics **92** (1990) 508 – 517.
$DMol^3$ is available as part of Materials Studio™ version 2.2 from Accelrys, Inc.
Copyright 2001 – 2003. The form of the ECPs in $DMol^3$ is that due to:
Dolg, M., Wedig, U., Stoll, H. and Preuss, H.,
Energy-Adjusted Ab Initio Pseudopotentials for the First Row Transition Elements
Journal of Chemical Physics **86** (1987) 866 – 872.

Desai, S.K., Neurock, M. and Kourtakis, K.,
A Periodic Density Functional Study of the Dehydrogenation of Methanol over Pt(111)
Journal of Physical Chemistry B **106** (2002) 2559 – 2568.

Dick, B.G. and Overhauser, A.W.,
Theory of the Dielectric Constants of Alkali Halide Crystals
Physical Review **112** (1958) 90 – 103.

Ding, X., Li, Z., Yang, J., Hou, J.G., Zhu, Q.,
Adsorption Energies of Molecular Oxygen on Au Clusters
Journal of Chemical Physics **120** (2004) 9594 - 9600

Dulub, O., Boatner, L.A. and Diebold, U.,
STM Study of the Geometric and Electronic Structure of ZnO(0001)-Zn, $(000\bar{1})$-O, $(10\bar{1}0)$, and $(11\bar{2}0)$ Surfaces
Surface Science **519** (2002) 201 – 217.

Efremenko, I. and Sheintuch, M.,
Quantum Chemical Study of Small Palladium Clusters
Surface Science **414** (1998) 148 – 158.

Ercolessi, F., Andreoni, W. and Tosatti, E.,
Melting of Small Gold Particles: Mechanism and Size Effects
Physical Review Letters **66:7** (1991) 911 – 914.

Fischer, D., Andreoni, W., Curioni, A., Grönbeck, H., Buckart, S. and Ganteför, G.,
Chemisorption on Small Clusters: Can Vertical Detachment Energy Measurements Provide Chemical Information? H on Au as a Case Study
Chemical Physics Letters **361** (2002) 389 – 396.

Franceschetti, A., Pennycook, S.J. and Pantelides, S.T.,
Oxygen Chemisorption on Au Nanoparticles
Chemical Physics Letters **374** (2003) 471 – 475.

French, S.A., Sokol, A.A., Bromley, S.T., Catlow, C.R.A., Rogers, S.C. and Sherwood, P.,
Assignment of the Complex Vibrational Spectra of the Hydrogenated ZnO Polar Surfaces using QM/MM Embedding
Journal of Chemical Physics **118** (2003) 317 – 320.

French, S.A., Sokol, A.A., Bromley, S.T., Catlow, C.R.A., Rogers, S.C., King, F., and Sherwood, P.,
From CO_2 to Methanol by Hybrid QM/MM Embedding
Angewante Chemie International Edition **40** (2001) 4437 – 4440.

Frisch, M.J., Trucks, G.W., Schlegel, H.B., Gill, P.M.W., Johnson, B.G., Robb, M.A., Cheeseman, J.R., Keith, T., Petersson, G.A., Montgomery, J.A., Raghavachari, K., Al-Laham, M.A., Zakrzewski, V.G., Ortiz, J.V., Foresman, J.B., Cioslowski, J., Stefanov, B.B., Nanayakkara, A., Challacombe, M., Peng, C.Y., Ayala, P.Y., Chen, W., Wong, M.W., Andres, J.L., Replogle, E.S., Gomperts, R., Martin, R.L., Fox, D.J., Binkley, J.S., Defrees, D.J., Baker, J., Stewart, J.P., Head-Gordon, M., Gonzalez, C., and Pople, J.A., Gaussian 94, Revision E.2, Gaussian, Inc., Pittsburgh PA,. 1995.

Frost, J.C.
Junction Effect Interactions in Methanol Synthesis Catalysts
Nature, **334** (1988) 577 – 580.

Froyen, S.,
Brillouin-zone Integration by Fourier Quadrature: Special Points for Superlattice and Supercell Calculations
Physical Review B **39** (1989) 3168 – 3172.

Fu, Q., Saltsburg, H. and M. Flytzani-Stephanopoulos, M.,
Active Nonmetallic Au and Pt Species on Ceria-Based Water-Gas Shift Catalysts
Science **301** (2003) 935 – 938.

Gale, J.D.,
GULP - a Computer Program for the Symmetry Adapted Simulation of Solids
Journal of Chemical Society Faraday Transaction **93** (1997) 629 – 637.

Gay, D.H. and Rohl, A.L.,
MARVIN - A New Computer Code for Studying Surfaces and Interfaces and Its Application to Calculating the Crystal Morphologies of Corundum and Zircon
Journal of Chemical Society Faraday Transaction **91** (1995) 925 – 936.

Gibson, D.H.,
Carbon Dioxide Coordination Chemistry: Metal Complexes and Surface-bound Species. What Relationships?
Coordination Chemistry Reviews **185-186** (1999) 335 – 355.

Gil, A., Clotet, A., Ricart, J.M., Kresse, G., García-Hernández, M., Rösch, N. and Sautet, P.,
Site Preference of CO Chemisorbed on Pt(1 1 1) from Density Functional Calculations
Surface Science **530** (2003) 71 – 87.

Giordano, L., Pacchioni, G., Bredow, T. and Sanz, J.F.,
Cu, Ag, and Au Atoms Adsorbed on TiO_2(110): Cluster and Periodic Calculations
Surface Science **471** (2001) 21 – 31.

Gomes, J.R.B. and Gomes, J.A.N.F.,
A DFT Study of the Methanol Oxidation Catalyzed by a Copper Surface
Surface Science **471** (2001) 59 – 70.

Gomes, J.R.B., Gomes, J.A.N.F. and Illas, F.,
First-Principles Study of the Adsorption of Formaldehyde on the Clean and Atomic Oxygen Covered Cu(1 1 1) Surface
Journal of Molecular Catalysis A: Chemical **170** (2001) 187 – 193.

Gomes, J.R.B. and Gomes, J.A.N.F.,
Comparative Study of Geometry and Bonding Characterfor Methoxy Radical Adsorption on Noble Metals
Journal of Molecular Structure: Theochem **503** (2000a) 189 – 200.

Gomes, J.R.B. and Gomes, J.A.N.F.,
Adsorption of Formyl Species on Transition Metal Surfaces
Journal of Electrochemical Chemistry **483** (2000b) 180 – 187.

Goossens, A., Crajé, M.W.J., van der Kraan, A.M., Zwijnenburg, A., Makkee, M., Moulijn, J.A. and de Jongh, L.J.,
Supported Gold Catalysts Studied with ^{197}Au Mössbauer Effect Spectroscopy
Catalysis Today **72** (2002) 95 – 100.

González, S., Sousa, C. and Illas, F.,
Theoretical Study of the Chemisorption of CO on Bimetallic RhCu Surfaces and Nanoparticles
Surface Science **531** (2003) 39 – 52.

Gottfried, J.M., Schmidt, K.J., Schroeder, S.L.M. and Christmann, K.,
Oxygen Chemisorption on Au(110)-(1 x 2) I. Thermal Desorption Measurements
Surface Science **525** (2003a) 184 – 196.

Gottfried, J.M., Schmidt, K.J., Schroeder, S.L.M. and Christmann, K.,
Oxygen Chemisorption on Au(110)-(1 x 2) II. Spectroscopic and Reactive Thermal Desorption Measurements
Surface Science **525** (2003b) 197 – 206.

Govind, N., Petersen, M., Fitzgerald, G., King-Smith, D. and Andzelm, J.,
A Generalized Synchronous Transit Method for Transition State Location
Computational Materials Science **28** (2003) 250 – 258.

Graoui, H., Giorgio, S. and Henry, C.R.,
Shape Variations under Oxygen Adsorption
Surface Science **417** (1998) 350 – 360.

Greely, J. and Mavrikakis, M.,
Methanol Decomposition on Cu(111): A DFT Study
Journal of Catalysis **208** (2002a) 291 – 300.

Greely, J. and Mavrikakis, M.,
A First Principles Study of Methanol Decomposition on Pt(111)
Journal of the American Chemical Society **124** (2002b) 7193 – 7201.

Grönbeck, H. and Andreoni, W.,
Gold and Platinum Microclusters and their Anions: Comparison of Structural and Electronic Properties
Chemical Physics **262** (2000) 1 – 14.

Grönbeck, H. and Rosén, A.,
Investigation of Niobium Clusters: Bare and CO-Adsorption
Physical Review B **54** (1996) 159 – 1552.

Guest, M.F., van Lenthe, J.H., Kendrick, J., Schoffel, K. and Sherwood, P., with contributions from Amos, R.D., Buenker, R.J., van Dam, H.J.J., Dupuis, M., Handy, N.C., Hillier, I.H., Knowles, P.J., Bonacic-Koutecky, V., von Niessen, W., Harrison, R.J., Rendell, A.P., Saunders, V.R., Stone, A.J., Tozer, D.J. and de Vries, A.H. The package is derived from the original GAMESS code: Dupuis, M., Spangler, D. and Wendoloski, J., *NRCC Software catalog, Vol. 1,* Program No. QG01(GAMESS), 1980.

Gupta, N.M. and Tripathi, A.K.,
The Role of Nanosized Gold Particles in Adsorption and Oxidation of Carbon Monoxide over Au/Fe_2O_3 Catalyst
Gold Bulletin **34:4** (2001) 120 – 128.

Guzman, J. and Gates, B.C.,
Catalysis by Supported Gold: Correlation Between Catalytic Activity for CO Oxidation and Oxidation States of Gold
Journal of the American Chemical Society **126** (2004) 2672 – 2673.

Guzman, J. and Gates, B.C.,
Gold Nanoclusters Supported on MgO: Synthesis, Characterization, and Evidence of Au_6
Nano Letters **1** (2001) 689 – 692.

Häberlen, O.D., Chung, S.-C., Stener, M. and Rösch, N.,
From Clusters to Bulk: A relativistic Density Functional Investigation on a Series of Gold Clusters Au_n, n= 6, …,147
Journal of Chemical Physics **106** (1997) 5189 – 5201.

Häkkinnen, H. J. and Landman, U.,
Structural, Electronic and Imprity-Doping Effects in Catalytically Active Gold Nanoclusters and Nanostructures,
Presented at the Gold2003 Conference: New Industrial Applications for Gold, September 28 – October 1, 2003, Vancouver, Canada.

Häkkinen, H. and Landman, U.,
Gold Clusters (Au_N, $2 \leq N \leq 10$) and Their Anions
Physical Review B **62** (2000) R2287 – R2290.

Halgren, T.A. and Lipscomb, W.N.,
The Synchronous-Transit Method for Determining Reaction Pathways and Locating Molecular Transition States
Chemical Physics Letters **49** (1977) 225 – 232.

Hammer, B., and Nørskov, J.L.,
Why Gold is the Noblest of All the Metals
Nature **376** (1995) 238 – 240.

Hammer, B., Jacobsen, K.W., Nørskov, J.L.,
Role of Nonlocal Exchange Correlation in Activated Adsorption
Physical Review Letters **70** (1993) 3971 – 3974.

Hamprecht, F.H., Cohen, A.J., Tozer, D.J. and Handy, N.C.,
Development and Assessment of New Exchange-Correlation Functionals
Journal of Chemical Physics **109** (1998) 6264 – 6270.

Hao, Z., Fen, L., Lu, G.Q., Liu, J., An, L. and Wang, H.,
In Situ Electron Paramagnetic Resonance (EPR) Study of Surface Oxygen Species on Au/ZnO Catalyst for Low-Temperature Carbon Monoxide Oxidation
Applied Catalysis A: General **213** (2001) 173 – 177.

Haruta, M.,
Size- and Support-Dependency in the Catalysis of Gold
Catalysis Today **36** (1997) 153 – 166.

Haruta, M., Tsubota, S., Kobayashi, T., Kageyama, H., Genet, M.J. and Delmon, B.,
Low-Temperature Oxidation of CO over Gold Supported on TiO_2, α-Fe_2O_3 and Co_3O_4
Journal of Catalysis **144** (1993) 175 – 192.

Haruta, M., Yamada, N., Kobayashi, T. and Iijima, S.,

Gold Catalysts Prepared by Coprecipitation for Low-Temperature Oxidation of Hydrogen and of Carbon Monoxide
Journal of Catalysis **115** (1989) 310 – 309.

Haruta, M., Kobayashi, T., Sano, H. and Yamada, N.,
Novel Gold Catalysts for the Oxidation of Carbon Monoxide at a Temperature far Below 0°C
Chemistry Letters (1987) 405 – 408.

Heiz, U. and Schneider, W-D.,
Nanoassembled Model Catalysts
Journal of Physics D: Applied Physics **33** (2000) R85 – R102.

Heiz, U., Sanchez, A., Abbet, S. and Schneider, W.-D.,
Tuning the Oxidation of Carbon Monoxide using Nanoassembled Model Catalysts
Chemical Physics **262** (2000) 189 – 200.

Hodge, N.A., Kiely, C.J., Whyman, R., Siddiqui, M.R.H., Hutchings, G.J., Pankhurst, Q.A., Wagner, F.E., Rajaram, R.R. and Golunski, S.E.,
Microstructural Comparison of Calcined and Uncalcined Gold/Iron Oxide Catalysts for Low-Temperature CO Oxidation
Catalysis Today **72** (2002) 133 – 144.

Hoffmann, R.,
Extented Hückel Theory I: Hydrocarbons
Journal of Chemical Physics **39** (1963) 1397 – 1412.

Holmgren, L., Grönbeck, H., Andersson, M. and Rosén, A.,
CO on Copper Clusters: Orbital Symmetry Rules
Physical Review B **53** (1996) 16644 – 16651.

Hu, Z.-H. and Nakatsuji, H.,
Active Sites for Methanol Synthesis on a Zn/Cu(100) Catalyst
Chemical Physics Letters **313** (1999) 14 – 18.

Huber, K.P. and G. Hertzberg, G.,
Molecular Spectra and Molecular Structure, vol. IV, Constants of Diatomic Molecules, van Nostrand, New York, 1979.

Hutchings, G.J.,
Gold Catalysis in Chemical Processing
Catalysis Today **72** (2002) 11 – 17.

Idriss, H. and Seebauer, E.G.,
Reactions of Ethanol over Metal Oxides
Journal of Molecular Catalysis A: Chemical **152** (2000) 201 – 212.

Ilieva, L.I., Andreeva, D.H. and Andreev, A.A.,
TPR and TPD Investigation of Au/α-Fe_2O_3
Themochimica Acta **292** (1997) 169 – 174.

Illas, F., Sousa, C., Gomes, J.R.B., Clotet, A. and Ricart, J.M.,
Elementary Steps of Catalytic Processes on Metallic and Bimetallic Surfaces, *in* "Theoretical Aspects of Heterogeneous Catalysis",
Progress in Theoretical Chemistry and Physics. Vol. 8, Editor: Chaer-Nascimento, M.A., Kluwer Academic Publishers, Dordrecht, 2001,149 – 182.

Jiang, Q., Li, J.C. and Chi, B.Q.,
Size-dependent Cohesive Energy of Nanocrystals
Chemical Physics Letters **366** (2002) 551 – 554.

Johnston, S.M., Mulligan, A., Dhanak, V. and Kadodwala, M.,
The Structure of Methanol and Methoxy on Cu(1 1 1)
Surface Science **530** (2003) 111 – 119.

Jonnard, P., Hombourger, C., Vergand, F., Bonnelle, C., Ealet, B., Renou, A. and Gillet, E.,
Comparison of Cu-MgO Interfaces Studied by EXES and XPS
Surface Review and Letters **5:1** (1998) 369 – 373.

Jugnet, Y., Cadete Santos Aires, F.J., Deranlot, C., Piccolo, L. and Bertolini, J.C.,
CO Chemisorption on Au (110) Investigated Under Elevated Pressures by Polarized Reflection Absorption Infrared Spectroscopy and Scanning Tunneling Microscopy
Surface Science **521** (2002) L639 – L644.

Kakumoto, T. and Watanabe, T.,
A Theoretical Study for Methanol Synthesis by CO_2 Hydrogenation
Catalysis Today **36** (1997) 39 – 44.

Kandoi, S., Gokhale, A.A., Grabow, L.C., Dumesic, J.A. and Mavrikakis, M.,
Why Au and Cu are More Selective Than Pt for Preferential Oxidation of CO at Low Temperature
Catalysis Letters **93** (2004) 93 – 100.

Koslowski, B., Boyen, H.-G., Wilderotter, C., Kästle, G., Ziemann, P., Wahrenberg, R. and Oelhafen, P.,
Oxidation of Preferentially (111)-Oriented Au Films in an Oxygen Plasma Investigated by Scanning Tunneling Microscopy and Photoelectron Spectroscopy
Surface Science **475** (2001) 1 – 10.

Kulkarni, G.U. and Rao, C.N.R.,
EXAFS and XPS Investigations of Cu/ZnO Catalysts and their Interaction with CO and Methanol
Topics in Catalysis **22** (2003) 183 – 189.

Kubo, M., Stirling, A., Miura, R., Yamauchi, R. and Miyamoto, A.,
Molecular Dynamics Simulation for Ultrafine Gold Particles Deposited on Metal Oxides
Catalysis Today **36** (1997) 143 – 151.

Laasonen, K., Pasquarello, A., Lee, C. and Vanderbilt, D.,
Car-Parrinello Molecular Dynamics with Vanderbilt Ultrasoft Pseudopotentials
Physical Review B **47** (1993) 10142 – 10153.

Landrum, G.A. and Glassey, W.V.,
bind (ver 3.0), 2001. **bind** is distributed as part of the YAeHMOP extended Huckel molecular orbital package and is freely available on the WWW at URL; *http://sourceforge.net/projects/yaehmop/*

Leach, A.R.,
Molecular Modelling: Principles and Applications
2nd Edition, Pearson Education, England, 2001.

Li, J., Li, X., Zhai, H-J. and Wang, L-S.,
Au_{20}: A Tetrahedral Cluster
Science **299** (2003) 864 – 866.

Liang, B. and Andrews, L.,
Reactions of Laser-Ablated Ag and Au atoms with Carbon Monoxide: Matrix Infrared Spectra and Density Functional Calculations on $Ag(CO)_n$ (n=2,3), $Au(CO)_n$ (n=1,2) and $M(CO)_n^+$ (n=1-4; M=Ag, Au)

Journal of Physical Chemistry A **104** (2000) 9156 – 9164.

Lide, D.R. (editor-in-chief),
CRC Handbook of Chemistry and Physics, 73rd ed., (CRC Press, Inc., 1992). Experimental bond energies that are reported at 298K have been extrapolated to 0K using the recommended factor (3/2)RT, which is about 0.04 eV.

Liu, Z-P., Gong, X-Q., Kohanoff, J., Sanchez, C. and Hu, P.,
Catalytic Role of Metal Oxides in Gold-Based Catalysts: A First Principles Study of CO Oxidation on TiO_2 Supported Au
Physical Review Letters **91** (2003) 2661021 – 2661024.

Liu, Z-P., Hu, P. and Alavi, A.,
Catalytic Role of Gold in Gold-Based Catalysts: A Density Functional Theory Study on the CO Oxidation on Gold
Journal of the American Chemical Society **124** (2002) 14770 – 14779.

Lopez, N. and Nørskov, J.K.,
Theoretical Study of the Au/TiO_2(110) Interface
Surface Science **515** (2002a) 175 – 186.

Lopez, N. and Nørskov, J.K.,
Catalytic CO Oxidation by a Gold Nanoparticle: A Density Functional Study
Journal of the American Chemical Society **124** (2002b) 11262 – 11263.

Maeland, A.J. and Flanagan, T.B.,
Canadian Journal of Physics **42** (1964) 2364.

Mainardi, D.S. and Balbuena, P.B.,
Hydrogen and Oxygen Adsorption on Rh_n(n=1-6) Clusters
Journal of Physical Chemistry A **107** (2003) 10370 – 10380.

Margitfalvi, J.L., Fási, A., Hegedüs, M., Lónyi, F., Göbölös, S. and Bogdanchikova, N., Au/MgO Catalysts Modified with Ascorbic Acid for Low Temperature CO Oxidation Catalysis Today **72** (2002) 157 – 169.

Mavrikakis, M., Stoltze, P. and Nørskov, J.K.,
Making Gold Less Noble
Catalysis Letters **64** (2000) 101 – 106.

McElhiney, G. and Pritchard, J.,
The Adsorption of Xe and CO on Au (100)
Surface Science **60** (1976) 397 – 410.

Mealli, C., Proserpio, D. and Ienco, A.,
Computer Aided Composition of Atomic Orbitals
PC Beta-Version 5.0, Istituto per lo Studio della Stereochimica ed Energetica dei Composti di Coordinazione, Italy, 1998.

Meier, D.C. and Goodman, D.W.,
The Influence of Metal Cluster Size on Adsorption Energies: CO Adsorbed on Au Clusters Supported on TiO_2
Journal of the American Chemical Society **126** (2004) 1892 – 1899.

Mendizabal, F.,
Theoretical Study of Gold-Carbonyls Interaction in $Au(CO)_n$ (n=1-3) Complexes
Organometallics **20** (2001) 261 – 265.

Minicò, S., Scirè, S., Crisafulli, C. and Galvagno, S.,
Influence of Catalyst Pretreatments on Volatile Organic Compounds Oxidation over Gold/Iron Oxide
Applied Catalysis B: Environmental **34** (2001) 277 – 285.

Minicò, S., Scirè, S., Crisafulli, C., Maggiore, R. and Galvagno, S.,
Catalytic Combustion of Volatile Organic Compounds on Gold/Iron Oxide Catalysts
Applied Catalysis B: Environmental **28** (2000) 245 – 251.

Minicó, S., Scirè, S., Crisafulli, C., Visco, A.M. and Galvagno, S.,
FT-IR Study of Au/Fe_2O_3 Catalysts for CO Oxidation at Low Temperature
Catalysis Letters **47** (1997) 273 – 276.

Molina, L.M. and Hammer, B.,
Active Role of Oxide Support During CO Oxidation at Au/MgO
Physical Review Letters **90** (2003) 2061021 – 2061024.

Molina, L.M. and Hammer, B.,
Theoretical Studies of Thiol-Induced Reconstructions on the Au(111) Surface
Chemical Physics Letters **360** (2002) 264 – 271.

Monkhorst, H.J. and Pack, J.D.,
Special Points for Brillouin-zone Integrations
Physical Review B **13** (1976) 5188 – 5192.

Morikawa,Y., Iwata, K., and Terakura, K.,
Theoretical Study of Hydrogenation Process of Formate on Clean and Zn deposited Cu(1 1 1) Surfaces
Applied Surface Science **169 – 170** (2001) 11 – 15.

Musolino, V., Selloni, A. and Car, R.,
Atomic and Electronic Structure of Cu Clusters on MgO
Surface Science **402-404** (1998) 413 – 417.

Nakatsuji, H., Hu, Z.. -M., Nakai, H. and Ikeda, K.,
Activation of O_2 on Cu, Ag and Au Surfaces for the Epoxidation of Ethylene: Dipped Adcluster Model Study
Surface Science **387** (1997) 328 – 341.

Nasluzov, V.A., Ivanova, E.A., Shor, A.M., Vayssilov, G.N., Birkenheuer, U. and Rösch, N.,
Elastic Polarizable Environment Cluster Embeding Approach for Covalent Oxides and Zeolites Based on a Density Functional Method
Journal of Physical Chemistry B **107** (2003) 228 – 241.

Nasluzov, V.A., Rivanekov, V.V., Gordienko, A.B., Neyman, K.M., Birkenheuer, U. and Rösch, N.,
Cluster Embedding in an Elastic Polarizable Environment: Density Functional Study of Pd Atoms Adsorbed at Oxygen Vacancies of MgO(001)
Journal of Chemical Physics **115** (2001) 8157 – 8171.

Nijhuis, T.A., Huizinga, B.J., Makkee, M. and Moulijn, J.A.,
Direct Epoxidation of Propene Using Gold Dispersed on TS-1 and Other Titanium-Containing Supports
Industrial Engineering and Chemistry Research **38:3** (1999) 884 – 89.

Noguera, C.,
Polar Oxide Surfaces
Journal of Physics: Condensed Matter **12** (2000) R367 – R410.

Olivera, P.P., Patrito, E.M. and Sellers, H.,
Hydrogen Peroxide Synthesis over Metallic Catalysts
Surface Science **313** (1994) 25 – 40.

Okumura, M., Kitagawa, Y., Haruta, M. and Yamaguchi, K.,
DFT Studies of Interaction Between O_2 and Au Clusters. The Role of Anionic Surface Au Atoms on Au Clusters for Catalysed Oxygenation
Chemical Physics Letters **346** (2001) 163 – 168.

Park, E.D. and Lee, J.S.,
Effects of Pretreatment Conditions on CO Oxidation over Supported Au Catalysts
Journal of Catalysis **186** (1999) 1 – 11.

Parravano, G.,
Surface Reactivity of Supported Gold II. Hydrogen Transfer Between Benzene and Cyclohexane
Journal of Catalysis **18** (1970) 320 – 328.

Perdew, J.P. and Wang, Y.,
Accurate and Simple Analytic Representation of the Electron-Gas Correlation Energy
Physical Review B **45** (1992)13244 – 13249.

Phala, N.S., van Steen, E., Klatt, G., Koch, K.R. and Fletcher, J.C.Q.,
Computational Study on Reaction Intermediates in Gold Catalysed Methanol Synthesis
Submitted to Catalysis Letters, 2003.

Pyykkö, P. and Desclaux, J.-P.,
Relativity and the Periodic System of Elements
Accounts of Chemical Research **12** (1979) 276 – 281.

Pyykkö, P. and Runeberg, N.,
Calculated Properties of the 'Empty' $[AuPH_3]_4^{2+}$ and Related Systems. Rôle of Covalent and Correlation Contributions
Chemical Communications (1993) 1812 - 1813.

Rhodes, C., Hutchings, G.J. and Ward, A.M.,
Water-Gas Shift Reaction: Finding the Mechanistic Boundary
Catalysis Today **23** (1995) 43 – 58.

Rogan, J., Ramírez, R., Romero, A.H. and Kiwi, M.,
Rearrangement Collisions Between Gold Clusters
The European Physical Journal D **28** (2004) 219 – 228.

Rouabah, D. and Fraissard, J.,
Pt-Au/Al_2O_3 Catalysts: Preparation, Characterization, and Dehydrogenation Activity
Journal of Catalysis **144** (1993) 30 – 37.

Roques, J., Lacaza-Dufaure, C. and Mijoule, C.,
Comparison Between Some Properties of Small Clusters and the (111) Surface of Palladium: A Density-Functional Approach
Surface Science **479** (2001) 231 – 240.

Ruban, A., Hammer, B., Stoltze, P., Skriver, H.L. and Nørskov, J.L.,
Surface Electronic Structure and Reactivity of Transition and Noble Metals
Journal of Molecular Catalysis A: Chemical **115** (1997) 421 – 429.

Ruggiero, C. and Hollins, P.,
Adsorption of Carbon Monoxide on the Gold (332) Surface
Journal of the Chemical Society, Faraday Transactions **92:2** (1996) 4829 – 4834.

Sakurai, H., Ueda, A., Kobayashi, T. and Haruta, M.,
Low-Temperature Water-Gas Shift Reaction over Gold Deposited on TiO_2
Chemical Communications (1997) 271 – 272.

Sakurai, H. and Haruta, M.
Synergism in Methanol Synthesis from Carbon Dioxide over Gold Catalysts Supported on Metal Oxides
Catalysis Today **29** (1996) 361 – 365.

Sakurai, H. and Haruta., M.
Carbon Dioxide and Carbon Monoxide Hydrogenation over Gold Supported on Titanium, Iron, and Zinc Oxides
Applied Catalysis A: General **127** (1995) 93 – 105.

Sakurai, H., Tsubota, S. and Haruta, M.
Hydrogenation of CO_2 over Gold Supported on Metal Oxides
Applied Catalysis A: General **102** (1993) 125 – 136.

Salama, T.M., Ohnishi, R., Shido, T. and Ichikawa, M.,
Highly Selective Catalytic Reduction of NO by H_2 over Au^0 and Au(I) Impregnated in NaY Zeolite Catalysts
Journal of Catalysis **162** (1996) 169 – 178.

Schewikhard, L., Hansen, K., Herlet, A., Herráiz, M.D., Marx, G., and Vogel, M.,
Recent Gold Cluster Studies in a Penning Trap
International Journal of Mass Spectrometry **219** (2002) 363 – 371.

Schmidt, M.W., Baldridge, K.K., Boatz, J.A., Elbert, S.T., Gordon, M.S., Jensen, J.H., Koseki, S., Matsunaga, N., Nguyen, K.A., Su, J.S., Windus, T.L., Dupuis, M. and Montgomery, J.A.,
General Atomic, Molecular and Electronic Structure System
Journal of Computational Chemistry **14** (1993) 1347 – 1363.

Scirè, S., Minicò, S., Crisafulli, C. and Galvagno, S.,
Catalytic Combustion of Volatile Organic Compounds on Gold/Cerium Oxide Catalysts

Applied Catalysis B: Environmental **40** (2003) 43 – 49.

Scirè, S., Minicò, S., Crisafulli, C. and Galvagno, S.,
Catalytic Combustion of Volatile Organic Compounds over Group IB Metal Catalysts
Catalysis Communications **2** (2001) 229 – 232.

Segall, M.D., Lindan, P.L.D., Probert, M.J., Pickard, C.J., Hasnip, P.J., Clark, S.J. and Payne, M.C.,
First-Principles Simulation: Ideas, Illustrations and The CASTEP Code
Journal of Physics: Condensed Matter **14** (2002) 2717 – 2743. CASTEP and DMol^3 are available as part of Materials Studio^{TM} Version 2.2 from Accelrys, Inc. ©2001 – 2003.

Sellers, H.,
The Generalized UBI-QEP Method for Modeling The Energetics of Reactions on Transition Metal Surfaces
Surface Science **524** (2003) 29 – 39.

Shaw, E.A., Walker, A.P., Rayment, T. and Lambert, R.M.
Methanol Synthesis Activity of Au/CeO_2 Catalysts Derived from a $CeAu_2$ Alloy Precursor: Do Schottky Barriers Matter?
Journal of Catalysis **134** (1992) 747 – 750.

Sherwood, P., de Vries, A.H., Guest, M.F., Schreckenback, G., Catlow, C.R.A., French, S.A., Sokol, A.A., Bromley, S.T., Thiel, W., Turner, A.J., Billeter, S., Terstegen, F., Thiel, S., Kendrich, J., Rogers, S.C., Casci, J., Watson, M., King, F., Karlsen, E., Sjøvll, M., Fahmi, A., Schäfer A. and Lennartz, C.,
QUASI:A General Purpose Implementation of the QM/MM Approach and Its Application to Problems in Catalysis
Journal of Molecular Structure (Theochem) **632** (2003) 1 – 28.

Sherwood, P., de Vries, A.H., Collins, S.J., Greatbanks, S.P., Burton, N.A., Vincent, M.A. and Hillier, I.H.,
Computer Simulation of Zeolite Structure and Reactivity using Embedded Cluster Methods
Journal of Chemical Society Faraday Transaction **106** (1997) 79 – 92.

Shustorovich, E.,
Chemisorption Phenomena: Analytic Modeling Based on Perturbation Theory and Bond-Order Conservation
Surface Science Reports **6** (1986) 1 – 63.

Sokol, A.A., Bromley, S.T., French, S.A., Catlow, C.R.A. and Sherwood, P.,
A Hybrid QM/MM Embedding Approach for the Treatment of Localised Surface States in Ionic Materials
Submitted to International Journal of Quantum Chemistry, 2003.

Spencer, M.S.,
The Reactions of Carbon Dioxide with the Copper Metal Surface in a $Cu/ZnO/Al_2O_3$ Catalyst
Surface Science **339** (1995) L897 – L901.

Stangland, E.E., Stavens, K.B., Andres, R.P. and Delgass, W.N.,
Propylene Epoxidation over Gold-Titania Catalysts
Studies in Surface Science and Catalysis **130** (2000) 827 – 832.

Stobiński, L., Nowakowski, R. and Dus, R.,
Atomic Hydrogen Adsorption on Thin Discontinuous and Continuous Gold Films – Similarities and Differences
Vacuum **48** (1997) 203 – 207.

Stobiński, L.,
Molecular and Atomic Deuterium Chemisorption on Thin Gold Films at 78K:An Isotope Effect
Applied Surface Science **103** (1996) 503 – 508.

Stolcic, D., Fischer, M., Ganteför, G., Kim, Y.D., Sun, Q. and Jena, P.,
Direct Observation of Key Reaction Intermediates on Gold Clusters
Journal of the American Chemical Society **125** (2003) 2848 – 2849.

Sun, Q., Wang, Y., Fan, F., and Deng, J.,
Ab Initio Pseudopotential Study of Dehydrogenation of Methanol on Oxygen Modified Ag(110) Surface
Surface Science **459** (2000) 213 – 222.

Sung, S. and Hoffmann, R.,
How Carbon Monoxide Bonds to Metal Surfaces
Journal of the American Chemical Society **107** (1985) 578 – 584.

Tabakova, T., Idakiev, V., Andreeva, D. and Mitov, I.,
Influence of the Microscopic Properties of the Support on the Catalytic Activity of Au/ZnO, Au/ZrO_2, Au/Fe_2O_3, Au/Fe_2O_3-ZnO, Au/Fe_2O_3-ZrO_2 Catalysts for the WGS Reaction
Applied Catalysis A: General **202** (2000) 91 – 97.

Taylor, K.J., Jin, C., Conceicao, J., Wang, L.-S., Cheshnovsky, O., Johnson, B.R., Nordlander, P.J., and Smalley, R.E.,
Vibrational Autodetachment Spectroscopy of Au_6^-: Image-Charge-Bound States of a Gold Ring
Journal of Chemical Physics **93** (1990) 7515 – 7518.

Triguero, L., Wahlgren, U., Bousard, P. and Siegbahn, P.,
Calculations of Hydrogen Chemisorption Energies on Optimized Copper Clusters
Chemical Physics Letters **237** (1995) 550 – 559.

Ueda, A. and Haruta, M.,
Nitric Oxide Reduction with Hydrogen, Carbon Monoxide, and Hydrocarbons over Gold Catalysts
Gold Bulletin **32:1** (1999) 3 – 11.

Uphade, B.S., Yamada, N., Akita, T., Nakamura, T. and Haruta, M.,
Synthesis and Characterization of Ti-MCM-41 and Vapor-Phase Epoxidation of Propylene using H_2 and O_2 over Au/Ti-MCM-41
Applied Catalysis A: General **215** (2001) 137 – 148.

Uphade, B.S., Okumura, M., Yamada, N., Tsubota, S. and Haruta, M.,
Vapor-Phase Epoxidation of Propene using H_2 and O_2 over Au/Ti-MCM-41 and Au/Ti-MCM-48
Studies in Surface Science and Catalysis **130** (2000) 833 – 838.

Valden, M., Lai, X., Goodman, D.W.,
Onset of Catalytic Activity of Gold Clusters on Titania with the Appearance of Nonmetallic Properties
Science **281** (1998) 1647 – 1650.

Van Hardeveld, R. and Hartog, F.,
The Statistics of Surface Atoms and Surface Sites on Metal Crystals
Surface Science **15** (1969) 189 – 230.

van Santen, R.A. and Neurock, M.,
Concepts in Theoretical Heterogeneous Catalytic Reactivity
Catalysis Reviews: Science and Engineering **37** (1995) 557 – 698.

Vittadini, A. and Selloni, A.,
Small Gold Clusters on Stoichiometric and Defected TiO_2 anatase (101) and Their Interaction with CO: A Density Functional Study
Journal of Chemical Physics **117** (2002) 353 – 361.

Vogel, M., Herlet, A. and Schweikhard, L.,
Photodissociation of Small Group-11 Metal Cluster Ins: Fragmentation Pathways and Photoabsorption Cross Sections
Journal of the American Society of Mass Spectrometry **14** (2003) 614-621. and references therein.

Wahlström, E., Vestergaard, E.K., Schaub, R., Rønnau, A., Vestergaard, M., Lægsgaard, E., Stensgaard, I. And Besenbacher, F.,
Electron Transfer – Induced Dynamics of Oxygen Molecules on the TiO_2(110) Surface
Science **303** (2004) 511 – 513.

Wahlström, E., Lopez, N., Schaub, R., Thostrup, P., Rønnau, A., Africh, C., Lægsgard, E., Nørskov, J.K. and Basenbacher, F.,
Bonding of Gold Nanoclusters to Oxygen Vacancies on Rutile TiO_2(110)
Physical Review Letters **90** (2003) 261011 – 261014.

Wallace, W.T. and Whetten, R.L.,
Coadsorption of CO and O_2 on Selected Gold Clusters: Evidence for Efficient Room-Temperature CO_2 Generation
Journal of the American Chemical Society **124** (2002) 7499 – 7505.

Wallace, W.T. and Whetten, R.L.,
Carbon Monoxide Adsorption on Selected Gold Clusters: Highly Size-Dependent Activity and Saturation Compositions
Journal of Physical Chemistry B **104** (2000) 10964 – 10968.

Wander, A. and Harrison, N.M.,

The Stability of Polar Oxide Surfaces: The Interaction of H_2O with ZnO(0001) and ZnO($000\bar{1}$)

Journal of Chemical Physics **115** (2001) 2312 – 2316.

Wang, G.Y., Zhang, W.X., Lian, H.L., Jiang, D.Z. and Wu, T.H.,

Effect of Calcination Temperatures and Precipitant on the Catalytic Performance of Au/ZnO Catalysts for CO Oxidation at Ambient Temperature and in Humid Circumstances

Applied Catalysis A: General **239** (2003) 1 – 10.

Wang, J., Wang, G. and Zhao, J.,

Density-Functional Study of Au_n (n=2-20) Clusters: Lowest-Energy Structures and Electronic Properties

Physical Review B **66** (2002) 354181 – 354186.

Waters, R.D., Weimer, J.J. and Smith, J.E.,

An Investigation of the Activity of Coprecipitated Gold Catalysts for Methane Oxidation,

Catalysis Letters **30** (1995) 181 – 188.

Watson, G.W., Wells, R.P.K., Willock, D.J. and Hutchings, G.J.,

A Comparison of the Adsorption and Diffusion of Hydrogen on the {111} Surfaces of Ni, Pd, and Pt From Density Functional Theory Calculations

Journal of Physical Chemistry B **105** (2001) 4889 – 4894.

Whitmore, L., Sokol, A.A. and Catlow, C.R.A.,

Surface Structure of Zinc Oxide ($10\bar{1}0$), Using an Atomistic, Semi-infinite Treatment

Surface Science **498** (2002) 135 – 146.

Wimmer, E. and Freeman, J.A.,
Fundamentals of the Electronic Structure of Surfaces
in Handbook of Surface Science, Vol.2 Electronic Structure, Volume Editors: Horn, K. and Scheffler, M., Series Editors: Richardson, N.V., and Holloway, S., Elsevier, Amsterdam, 1-92, 2000.

Wu, X., Senapati, L., Nayak, S.K., Selloni, A. and Hajaligol, M.,
A Density Functional Study of Carbon Monoxide Adsorption on Small Cationic, Neutral, and Anionic Gold Clusters
Journal of Chemical Physics **117** (2002) 4010 – 4015.

Xu, Y. and Mavrikakis, M.,
Adsorption and Dissociation of O_2 on Gold Surfaces: Effect of Steps and Strain
Journal of Physical Chemistry B **107** (2003) 9298 – 9307.

Yoon, B., Häkkinen, H. and Landman, U.,
Interaction of O_2 with Gold Clusters: Molecular and Dissociative Adsorption
Journal of Physical Chemistry A **107** (2003) 4066 – 4071.

Zhang, J., Wang, Y., Chen, B., Li, C. and Wu, D.,
Selective Oxidation of CO in Hydrogen Rich Gas over Platinum–Gold Catalyst Supported on Zinc Oxide for Potential Application in Fuel Cell
Energy Conversion and Management **44** (2003) 1805 – 1815.

Zheng, C., Apeloig, Y. and Hoffmann, R.,
Bonding and Coupling of C_1 Fragments on Metal Surfaces
Journal of the American Chemical Society **110** (1988) 749 – 774.

APPENDIX

A1. List of Publications

N. S. Phala, G. Klatt and E. van Steen
Elementary Steps in CO_x (x=1,2) Hydrogenation to Methanol on a Gold Surface: Periodic and Cluster DFT Studies
Submitted to Journal of the Physical Chemistry B, Feb 2004.

N.S. Phala, G. Klatt and E. van Steen
A DFT Study of Hydrogen and Carbon Monoxide Chemisorption onto Small Gold Clusters
Submitted to Chemical Physics Letters, Feb 2004.

S.A. French, P. Sherwood, P., C.R.A. Catlow, A.A. Sokol, S.T. Bromley, N.S. Phala, G. Klatt and E. van Steen
The Nature of the Oxidation States of Au on ZnO
Manuscript in preparation

N.S. Phala, G. Klatt and E. van Steen
Gold Catalysed Syngas Conversion: Pathways and Size Effects
Proceedings of the Gold2003 Conference: New Industrial Applications for Gold, September 28 – October 1, 2003, Vancouver, Canada

N.S. Phala, E. van Steen, and G. Klatt
Non-dispersion Size Effects in Au/Me_xO_y Catalyst: A DFT Electronic Structure Study
Oral presentation at the Catalysis Society of South Africa (CATSA) Conference, Cape Town, South Africa, November 2002.

N.S. Phala, E. van Steen, and G. Klatt

Interaction of CO and H_2 with Au_2 and $(OH)_2Au_2O$ Clusters Studied by DFT

Poster presentation at the Catalysis Society of South Africa (CATSA) Conference, Cape Town, South Africa, November 2002.

N.S. Phala, E. van Steen, and G. Klatt

A Quantum Chemical Study of Small Gold Clusters

Oral presentation at the 7^{TH} Annual Materials Modelling Meeting, University of the North, Limpopo Province, South Africa, March 2003.

N.S. Phala, A.A. Sokol, S.A. French, C.R.A. Catlow, P. Sherwood, G. Klatt, and E. van Steen

A QM/MM Study of the Au-Support Interaction in Au/ZnO Catalysts

Oral presentation at the 8^{TH} Annual Materials Modelling Meeting, University of the North, Limpopo Province, South Africa, March 2004.

N.S. Phala, E. van Steen, and G. Klatt

Hydrogen and Carbon Monoxide Chemisorption onto Gold Nanoparticles: A Computational Study

Oral presentation at the Nano Africa I: A conference organized by the South African Nanotechnology Initiative and hosted by UNESCO Associated Centre for Macromolecules and Materials, University of Stellenbosch, Stellenbosch, South Africa, April 2004.

A2. Total CASTEP Pseudo Atomic Energies (PW91-GGA and Ultrasoft Pseudopotentials)

Hydrogen $1s^1$ Total energy = -12.102842 eV

Carbon $2s^2\ 2p^2$ Total energy = -145.311283 eV

Oxygen $2s^2\ 2p^4$ Total energy = -427.946725 eV

Gold $5d^{10}\ 6s^1$ Total energy = -911.783593 eV

A3. Specifications for Basis Sets in DMol^3 Calculations

These are atomic parameters for the double-numerical basis set, with polarization (DNP). For the gold atom, a 60-electron ECP was employed.

Atomic cutoff radius = 10.39 au (5.5 Å)

Hydrogen z = 1; 3 radial functions; rcore = 0.00; zval= 1.

n=1 L=0 occ= 1.00 e=-0.240212Ha -6.5365eV
n=1 L=0 occ= 0.00 e=-0.845000Ha -22.9936eV
n=2 L=1 occ= 0.00 e=-2.000000Ha -54.4228eV

Carbon z = 6; 7 radial functions; rcore = 0.00; zval= 6.

n=1 L=0 occ= 2.00 e=-10.052779Ha -273.5502eV
n=2 L=0 occ= 2.00 e=-0.505759Ha -13.7624eV
n=2 L=1 occ= 2.00 e=-0.195589Ha -5.3223eV
n=2 L=0 occ= 0.00 e=-1.485570Ha -40.4244eV
n=2 L=1 occ= 0.00 e=-1.170076Ha -31.8394eV
n=3 L=2 occ= 0.00 e=-2.722222Ha -74.0755eV
n=3 L=2 occ= 0.00 e=-1.388886Ha -37.7935eV

Oxygen z= 8; 7 radial functions; rcore = 0.00; zval= 8.

n=1 L=0 occ= 2.00 e=-18.913267Ha -514.6564eV
n=2 L=0 occ= 2.00 e=-0.880420Ha -23.9575eV
n=2 L=1 occ= 4.00 e=-0.334992Ha -9.1156eV
n=2 L=0 occ= 0.00 e=-2.144815Ha -58.3634eV
n=2 L=1 occ= 0.00 e=-1.593916Ha -43.3727eV
n=3 L=2 occ= 0.00 e=-2.722222Ha -74.0755eV
n=3 L=2 occ= 0.00 e=-1.388886Ha -37.7935eV

Gold z= 79; 7 radial functions; rcore= 3.66 zval= 19.

Au ECP ECP60MWB : 60 3 32

n=5 L=0 occ= 2.00 e=-3.985190Ha -108.4426eV

n=5 L=1 occ= 6.00 e=-2.199741Ha -59.8580eV

n=5 L=2 occ=10.00 e=-0.255568Ha -6.9544eV

n=6 L=0 occ= 1.00 e=-0.211112Ha -5.7446eV

n=5 L=2 occ= 0.00 e=-1.008880Ha -27.4530eV

n=6 L=0 occ= 0.00 e=-0.836704Ha -22.7679eV

n=6 L=1 occ= 0.00 e=-0.540440Ha -14.7061eV

A4. Additional Information for QM/MM Calculations

A4.1. Construction of the Oxide Surface Model

- The molecular mechanics (MM) software, GULP is used to carry out a 3D periodic calculation of bulk ZnO.
- A second MM software, MARVIN, is used to cut and relax the surface of interest (e.g. ZnO(0001)).
- An active site is chosen, and a hemispherical cluster (~1000 – 3000 atoms) is cut from this active site based on a cutoff radius.
- Atomic centres within the hemispherical cluster are labeled for QM/MM calculations. Atoms that are to be treated at a QM level of theory are identified. At this stage, modifications to the surface, e.g. vacancies, defects and any adsorbates, can be made.
- A utility called Construct, provided with Chemshell, is run. This will define fully a multi-region hybrid QM/MM model, with fitted point charges to simulate the Madelung field of the crystal remainder, based on a system of cut-off radii.

At this point the model will be ready for QM/MM Chemshell calculations using the Hybrid procedure and specifying the QM and MM software to be employed. Parameters to be used in the QM and MM codes can be specified within Chemshell.

A4.2. Pseudopotentials for Au and Zn Atoms

The pseudopotentials are of the semi-local type, and their form is that advanced by Andrae et al., *Theor. Chim. Acta.* **77** (1990) 123, and Hay and Wadt, *J. Chem. Phys.* **82** (1985) 270. For each term, the three numbers represent the power of r, the coefficient and the exponent respectively. lmax is the maximum angular momentum.

Zinc

Effective core charge = 2.0 and lmax = 3

term l+1	2	0.00000000	1.00000000
term |s><s|	2	14.93680000	1.50000000
	2	-2.62660000	0.75000000
term |p><p|	2	11.43290000	1.50000000
	2	-1.49390000	0.75000000
term |d><d|	2	1.16900000	0.75000000
	2	0.37070000	0.37500000

Gold

Effective core charge = 19.0 and lmax = 4

term l+1	2	0.00000000	1.00000000
term |s><s|	2	426.70984000	13.20510000
	2	35.93882400	6.60255000
term |p><p|	2	261.16102300	10.45202000
	2	26.62628400	5.22601000
term |d><d|	2	124.75683100	7.85110000
	2	15.77226000	3.92555000
term |f><f|	2	30.56847500	4.78980000
	2	5.18377400	2.39491000

A4.3. Basis Sets for Atoms Included in the QM Calculations

O1 and O2 represent the oxygen atoms for adsorbates (e.g CO) and the ZnO surface respectively.

H {5s2p/3s2p}

S

0.02549380	33.8650000
0.19037300	5.0947900
0.85216100	1.1587900

S

1.00000000	0.3258400

S

1.00000000	0.1027410

P

1.00000000	1.5000000

P

1.00000000	0.3750000

O1 {12s7p2d/6s4p1d}

S

0.000217263025	27032.3826
0.00168386622	4052.38714
0.00873956163	922.327227
0.0352399688	261.240710
0.111535191	85.3546414
0.255889540	31.0350352

S

0.402992100	12.2434900
0.247605000	4.9798140

S

1.000000000 1.1620200

S

1.000000000 0.4248607

S

1.000000000 0.1563954

S

1.000000000 0.06255816

P

0.006439951 62.1198500

0.043726060 14.4356400

0.167061000 4.4037520

0.373299200 1.4927610

P

1.000000000 0.4860210

P

1.000000000 0.1546932

P

1.000000000 0.06187728

D

0.107507353 1.579323610

0.703501500 0.341495254

C {11s6p3d/5s3p2d}

S

0.00022246 13575.3496820

0.00172327 2035.2333680

0.00892557 463.22562359

0.03572798 131.20019598

0.11076260 42.85301589

0.24295628 15.58418577

S

0.41440263 6.20671385
0.23744969 2.57648965
S
1.00000000 0.57696339
S
1.00000000 0.22972831
S
1.00000000 0.09516444
P
0.00533337 34.69723224
0.03586411 7.95826228
0.14215873 2.37808269
0.34270472 0.81433209
P
1.00000000 0.28887547
P
1.00000000 0.10056824
D
0.26285000 1.20670000
0.80430000 0.38550000
D
0.65350000 0.12190000

Cl {15s10p4d/6s5p2d}
S
0.00054315 69507.99094500
0.00419905 10426.15688000
0.02159214 2373.23340610
0.08459885 671.56420071
0.24757250 218.41999790

0.47016930 77.57224971
0.37436371 28.88881528
S
0.02518217 127.10527185
0.10786112 39.33958296
-0.27408822 7.67406800
S
1.32138750 3.87456276
0.68636955 1.83858326
S
1.00000000 0.50229058
S
1.00000000 0.17962723
S
1.00000000 0.06960000
P
0.00236327 666.50423284
0.01887930 157.64241690
0.08720634 50.26252098
0.25285613 18.53607811
0.43507155 7.29405328
0.35026513 2.94332490
P
1.00000000 1.04049708
P
1.00000000 0.38456415
P
1.00000000 0.13069643
P
1.00000000 0.04360000
D

0.28530000 0.95280000
0.81690000 0.35800000
D
0.10130000 0.12500000
0.04300000 0.04360000

O2 {11s6p2d/4s3p1d}

S
0.000217263025 27032.3826
0.00168386622 4052.38714
0.00873956163 922.327227
0.0352399688 261.240710
0.111535191 85.3546414
0.255889540 31.0350352
0.402992100 12.2434900
0.247605000 4.9798140
S
1.000000000 1.1620200
S
1.000000000 0.4248607
S
1.000000000 0.1563954
P
0.006439951 62.1198500
0.043726060 14.4356400
0.167061000 4.4037520
0.373299200 1.4927610
P
1.000000000 0.4860210
P

1.000000000 0.1546932

D

0.107507353 1.579323610

0.703501500 0.341495254

Zn {4s1p/3s1p}

S

0.247432220 2.034397290

-1.049453166 1.002428075

S

1.000000000 0.277518273

S

1.000000000 0.102997914

P

1.000000000 0.170822458

Au {7s6p5d1f/6s3p3d1f}

S

-0.15910719389 20.115299000

0.79105526778 12.193477000

S

1.0000000000 6.0735294368

S

1.0000000000 1.3174451569

S

1.0000000000 0.58596768244

S

1.0000000000 0.13875427354

S

1.0000000000 0.48876985527E-01

P

0.50053018599 8.6096650000
-0.72681584494 7.3353260000
0.57315511417 1.6575296365
0.49579068859 0.78159310216
P
1.0000000000 0.32384840661
P
1.0000000000 0.0540
D
-0.37099566643 4.1439490000
0.40197233762 3.5682570000
0.46001988624 1.2345757130
D
1.0000000000 0.48190232338
D
1.0000000000 0.16490636769
F
1.0000000000 1.05626245

A4.4. Forms of the MM Potentials

The potentials that were used together for the MM calculations had the following forms (see Whitmore et.al., *Surface Science* **498** (2002) 135. for parameters and cutoff radii):

Buckingham:

$E = A \exp(-r/\rho) - C/r^6$

Lennard-Jones:

$E = A/r^{12} - C/r^6$

Spring (core-shell interaction on the oxygen atom):

$E = (1/2)(k^2r^2 + k^4r^4)$. Ionic charges were +2 for Zn, +1.754415 for the oxygen core, and -3.754415 for the oxygen shell.

Polynomial:

$E = C_0 + C_1r + C_2r^2 + C_3r^3 + C_4r^4 + C_5r^5$

Coulomb:

$E = q_1q_2/r$